

# **Stony Brook University**



OFFICIAL COPY

**The official electronic file of this thesis or dissertation is maintained by the University Libraries on behalf of The Graduate School at Stony Brook University.**

**© All Rights Reserved by Author.**

**Mechanism and Inhibition Studies of MenE MbtI and MenF Three  
Potential Drug Targets  
against *Mycobacterium Tuberculosis* and *Staphylococcus aureus***

A Dissertation Presented

by

**Rong Zhou**

To

The Graduate School

in Partial Fulfillment of the

Requirements

for the Degree of

Doctor of Philosophy

In

**Chemistry**

Stony Brook University

**August 2010**

**Stony Brook University**

The Graduate School

**Rong Zhou**

We, the dissertation committee for the above candidate for the

Doctor of Philosophy degree, hereby recommend

Acceptance of this dissertation

Peter J. Tonge – Dissertation Advisor

Professor of Chemistry Department

Dale G. Drueckhammer – Chairperson of Defense

Professor of Chemistry Department

Daniel P. Raleigh – Committee Member of Defense

Professor of Chemistry Department

Subramanyam Swaminathan – External Committee Member of Defense

Principle Investigator of the Structural Genomics Initiative of the BNL  
Biology

This dissertation is accepted by the Graduate School

Lawrence Martin

Dean of the Graduate School

## Abstract of the Dissertation

Mechanism and Inhibition Studies of MenE MbtI and MenF Three  
Potential

Drug Targets

against *Mycobacterium Tuberculosis* and *Staphylococcus aureus*

by

Rong Zhou

Doctor of Philosophy

in

Chemistry

Stony Brook University

2010

A detailed understanding of the catalytic mechanism of enzyme drug targets is required to guide structure-based drug discovery. In my thesis research I have primarily focused on the catalytic mechanism and inhibition of MenE the OSB-CoA synthetase from three different organisms: *M. tuberculosis*, *S. aureus* and *E. coli*. MenE catalyzes the formation of OSB-CoA through a two step reaction that proceeds via acyl adenylate intermediate and utilizes ATP and CoA as cofactors. In chapter 2, I discuss the catalytic mechanism of MenE from *S. aureus* (saMenE) where steady state kinetics coupled with site-directed mutagenesis has been used to identify key catalytic residues in the

active site of MenE and to elucidate the molecular details of each half reaction. In chapter 3, I present data on the inhibition of saMenE as well as the enzymes from *M. tuberculosis* (tbMenE) and *E. coli* (ecMenE). These studies have focused on a series of OSB-AMP intermediate analogs synthesized by our collaborator Dr. Tan at Memorial Sloan-Kettering Cancer Center. The most potent compound inhibits MenE with a  $K_{id}$  value of  $11.2 \pm 0.9$  nM. While the majority of my work has focused on MenE, I have also undertaken kinetic studies of the chorismate-dependent enzymes Men from *E. coli* and MbtI from *M. tuberculosis* (chapter 4). These enzymes catalyze the initial reaction in menaquinone biosynthetic pathway and mycobactin biosynthetic pathway, respectively. Interestingly, in the absence of  $Mg^{2+}$ , MenF and MbtI show chorismate mutase activity, although these enzymes have no similarity to the AroQ/H chorismate mutase. Because tbEntC, which is annotated as isochorismate synthase in *M. tuberculosis* menaquinone pathway, cannot yet be well expressed by using a heterologous *E. coli* expression system, I propose that MbtI might have a dual function and produce isochorismate for menaquinone *in vitro*.

## Table of Contents

List of Figures.....	x
List of Tables.....	xiii
List of Abbreviations and Symbols.....	xiv
Chapter I: Introduction of Drug Resistance Bacteria and Two Biosynthetic Pathways as Potent Drug Target.....	1
1.1 Search For Novel Drugs Towards The Treatment of Drug Resistance .....	1
1.2 Mycobacterium Tuberculosis.....	2
1.2.1 Nonreplicating Persistence And Latency of Tuberculosis .....	5
1.2.2 Current Treatment of Tuberculosis.....	6
1.3 Small Colony Variants of <i>Staphylococcus aureus</i> .....	9
1.4 Potential Drug Targets for Drug-resistance Organisms .....	10
1.4.1 The Menaquinone Biosynthetic Pathway.....	12
1.4.2 The Mycobactin Biosynthetic Pathway .....	15
1.6 Objectives of My Research.....	18
Reference .....	20

Chapter II: Overexpression, Purification, and Characterization of MenE,  
an o-Succinylbenzoyl-Coenzyme A Synthetase from *Staphylococcus*

<b>aureus</b> .....	29
<b>2.1 Introduction</b> .....	29
<b>2.2 Materials and Methods</b> .....	32
<i>Materials and Substrates</i> .....	32
<i>Synthesis of o-succinylbenzoic acid (OSB)</i> .....	32
<i>Cloning, Expression and Purification of saMenE</i> .....	33
<i>Reaction of OSB-CoA Synthetase with o-succinylbenzoic Acid</i> .....	36
<i>Steady-state Kinetic Assay</i> .....	36
<i>Product Inhibition Study</i> .....	37
<i>Direct Binding Fluorescence Titrations</i> .....	38
<i>Kinetic Inhibition Assay</i> .....	39
<b>2.3 Experimental Results</b> .....	40
<i>Overexpression and purification of saMenE</i> .....	40
<i>pH Optimum</i> .....	41
<i>Kinetics Constants of Enzymes and Mutants</i> .....	42
<i>The OSB-CoA Synthetase Kinetic Mechanism</i> .....	42
<i>Product Inhibition Studies</i> .....	46
<i>Direct Binding of ATP with saMenE</i> .....	48
<i>Identification of Key Active Site Residues Identified From</i>	
<i>Steady-state Kinetic Analysis of Site-directed Mutants</i> .....	49
<i>Inhibition Study of saMenE with OSB-AMP Intermediate Analogues</i> .....	57
<b>2.4 Discussion</b> .....	61

<i>Bi uni uni Bi Ping-Pong Kinetic Mechanism</i> .....	61
<i>Sequence alignment</i> .....	63
<i>Analysis of the Substrate Binding Pocket</i> .....	65
<i>Domain Alternation and the Adenylate-forming Family of Enzymes</i> .....	68
<i>Essential Residues as Functional Anchors in Active Site Architecture</i> .....	73
<b>2.5 Conclusion</b> .....	77
<b>Reference</b> .....	78
<b>Chapter III: Inhibition Studies of MenE, an o-Succinylbenzoyl-Coenzyme</b>	
<b>A Synthetase from <i>Mycobacterium tuberculosis</i></b> .....	85
<b>3.1 Introduction</b> .....	85
<b>3.2 Materials and methods</b> .....	88
<i>Materials and Substrates</i> .....	88
<i>Cloning, Expression and Purification of tbMenE</i> .....	88
<i>Reaction of OSB-CoA Synthetase with O-succinylbenzoic Acid</i> .....	90
<i>Steady-state Kinetic Assay</i> .....	90
<i>pH Optimum</i> .....	95
<i>Kinetics Constants of Enzymes</i> .....	95
<i>IC<sub>50</sub> values of tbMenE with OSB-AMP intermediate analogs</i> .....	96
<i>Inhibition Kinetics of Sulfamate OSB-AMS</i> .....	100
<b>3.4 Discussion</b> .....	111
<i>Expression of tbMenE</i> .....	111
<i>Design of Mechanism-based Bisubstrate Inhibitors</i> .....	112



<i>Steady-State Kinetic Mechanism</i> .....	115
<b>3.5 Conclusion</b> .....	117
<b>Reference</b> .....	119
<b>Chapter IV: MbtI Catalyze Chorismate Isomerization and Isochorismate</b>	
<b>Elimination</b> .....	123
<b>4.1 Background</b> .....	123
<i>Mycobactin Biosynthetic Pathway</i> .....	123
<i>Family of Chorismate-utilizing Enzymes</i> .....	124
<b>4.2 Materials and Methods</b> .....	127
<i>Materials and Substrates</i> .....	127
<i>Cloning of menF and mbtI</i> .....	127
<i>Overexpression and Purification of MbtI (Salicylic Synthase)</i> .....	128
<i>Mutagenesis</i> .....	129
<i>Enzyme Assays</i> .....	130
<i>Kinetic Analysis</i> .....	132
<i>Crystallization of MenF and MbtI</i> .....	135
<sup>1</sup> H NMR study.....	136
<i>Liquid Chromatography-mass Spectrometry Analysis (LC/MS)</i> .....	136
<b>4.3 Results</b> .....	138
<i>Overexpression and Purification of MenF from E. coli</i> .....	138
<i>Overexpression and Purification of MbtI from M. tuberculosis</i> .....	139
<i>pH Optimum</i> .....	140

<i>Kinetics Constants of Enzymes and Mutants</i> .....	140
<i>Kinetic Mechanism for MenF and MbtI</i> .....	142
<i>Products Characterization of MbtI Reaction in Response to Changes in pH Using LC/MS and NMR</i> .....	149
<b>4.4 Discussion</b> .....	153
<i>Sequence Comparison</i> .....	153
<i>Pyruvate Elimination Selectivity</i> .....	157
<i>Enzyme Activities Affecting End Product Distribution in Response to Changes in Ion Concentration</i> .....	160
<b>4.5 Conclusion</b> .....	164
<b>Reference</b> .....	167

## List of Figures

Figure 1- 1: Complex cell wall of <i>M. tuberculosis</i> .....	4
Figure 1- 2: Structures of five front-line anti-TB drugs .....	8
Figure 1- 3: Overview of menaquinone biosynthetic pathways in <i>E. coli</i> .....	14
Figure 1- 4: Selected menaquinone biosynthesis inhibitors for MenA and MenD.....	15
Figure 1- 5: The cell-associated and water-soluble mycobactins.....	16
Figure 1- 6: The molecular structure of mycobactin from <i>M. tuberculosis</i> .....	17
Figure 2- 1: Adenylation-Ligation reaction catalyzed by MenE. ....	29
Figure 2- 2: <sup>1</sup> H NMR spectrum of OSB .....	33
Figure 2- 3: 15% SDS-PAGE analysis of the fractions from purification of wild-type saMenE.....	40
Figure 2- 4: OSB-CoA synthetase kinetic mechanism .....	45
Figure 2- 5: The Bi uni uni Bi Ping-Pong mechanism for saMenE .....	47
Figure 2- 6: AMP product inhibition assay.....	48
Figure 2- 7: Direct binding of ATP with saMenE in the presence of magnesium.....	49
Figure 2- 8: Crystal structures of enzymes belonging to the adenylyate-forming enzymes superfamily .....	50
Figure 2- 9: Insight view of overlaid CBAL ligands bound structures .....	57
Figure 2- 10: Two types of Ping-Pong mechanisms for the three-substrate, three-product reaction .....	63

Figure 2- 12: CBAL is composed of two structural domains .....	73
Figure 2- 13: A comparison of the active sites of bacterial MenE and CBAL .....	74
Figure 2- 14: Proposed saMenE mechanism .....	77
Figure 3- 1: Inhibitors of aryl acid adenylation enzymes. ....	86
Figure 3- 2: 15% SDS-PAGE analysis of the fractions from purification of wild-type tbMenE.....	94
Figure 3- 3: The bisubstrate inhibitors .....	97
Figure 3- 4: Morrison analysis of tight-binding inhibition of tbMenE by sulfamate OSB-AMS inhibitor .....	102
Figure 3- 5: Morrison analysis of tight-binding inhibitor sulfamate OSB-AMS against tbMenE .....	106
Figure 3- 6: A plot of $K_i^{app}$ vs substrate concentration can reveal the binding modality for the tight-binding inhibitor .....	107
Figure 3- 7: $K_i^{app}$ values of inhibitor sulfamate OSB-AMS against ecMenE. ....	110
Figure 3- 8: Scaffold of OSB-AMP intermediate analogues .....	113
Figure 4- 1: Summarization of mycobactin biosynthetic pathway .....	124
Figure 4- 2: Chorismate is an important starting material .....	126
Figure 4- 3: Summarization of enzyme assays .....	132
Figure 4- 4: Ternary random mechanism .....	134
Figure 4- 5: 15% SDS-PAGE analysis of the fractions from purification of	

wild-type MenF .....	138
Figure 4- 6: 15% SDS-PAGE analysis of the fractions from purification of wild-type MenF .....	139
Figure 4- 7: Kinetics of Mg <sup>2+</sup> activation of MenF at 37°C, pH 7.5.....	143
Figure 4- 8: Kinetics of Mg <sup>2+</sup> activation of MbtI at 37°C, pH 7.5.....	144
Figure 4- 9: UV-vis absorption spectroscopy and HPLC analysis of MbtI reaction mixtures at pH 7.5 .....	147
Figure 4- 10: UV-vis absorption spectroscopy and HPLC analysis of MbtI reaction mixtures at pH 8.0 .....	148
Figure 4- 11: The nonenzymatic degradation of isochorismate.....	149
Figure 4- 12: The characterization of MbtI reaction products in pD 7.5 buffer.....	151
Figure 4- 13: The characterization of MenF reaction products in pD 8.0 buffer .....	152
Figure 4- 14: The characterization of MbtI reaction products in pD 8.0 buffer .....	153
Figure 4- 15: The alignment above explores sequence conservation in the TrpE <i>Serratia marcescens</i> 1I7Q structure with bound Mg <sup>2+</sup> , benzoate and pyruvate .....	157
Figure 4- 16: Proposed intramolecular mechanism catalyzed elimination mechanism for MbtI.....	159
Figure 4- 17: The model of twisted boat conformation built by PyMOL.....	160
Figure 4- 18: The proposed mechanism for substrate activation via Mg <sup>2+</sup> .....	163

## List of Tables

Table 2- 1: The primers for site-directed mutagenesis of saMenE enzyme .....	35
Table 2- 2: The steady-state kinetic constants for saMenE .....	52
Table 2- 3: Inhibition constant of OSB-AMP intermediate analogs.....	59
Table 2- 4: Sequence comparison of CBAL and saMenE .....	66
Table 2- 5: Sequence comparison of CBAL and saMenE .....	70
Talbe 3- 1: IC <sub>50</sub> values of tbMenE, saMenE and ecMenE against designed bisubstrate inhibitors .....	98
Talbe 3- 2: Inhibitory parameters against OSB for tbMenE and ecMenE.....	117
Table 4- 1: Kinetic evaluation of wtMbtI and mutant MbtI enzymes of chorismate mutase activity .....	142
Table 4- 2: Kinetic evaluation of wtMenF, wtMbtI and mutant MbtI enzymes of ternary mechanism.....	145

## List of Abbreviations

ACS	Acetyl-CoA synthetase
AMP	Adenosine monophosphate
ATP	Adenosine triphosphate
BME	$\beta$ -mercaptoethanol
CoA	Coenzyme A
DHNA	Dihydroxynaphthoic acid
<i>E. coli</i>	<i>Escherichia coli</i>
EntB	Enterobactin synthetase from <i>Escherichia coli</i>
ESI	Electrospray ionization
ecMenE	MenE from <i>Escherichia coli</i>
ICS	Isochorismate synthase
INH	Isoniazid
IPTG	isopropyl-1-thio- $\beta$ -D-thiogalactopyranoside
LC-FACS	Long chain fatty acid CoA synthetase
LC/MS	Liquid chromatography/mass spectrometry
LDH	Lactate dehydrogenase
<i>M. tuberculosis</i>	<i>Mycobacterium tuberculosis</i>
MbtI	Salicylate synthase
MDR-TB	Multidrug-resistant tuberculosis
MenB	1, 4-dihydroxy-2naphthoyl-CoA synthase
MenE	OSB-CoA synthase

MenF	Isochorismate synthase
MRSA	Methicillin-resistant <i>Staphylococcus aureus</i>
NAD <sup>+</sup>	Nicotinamide adenine dinucleotide, oxidized
form	
NADH	Nicotinamide adenine dinucleotide, reduced
form	
NMR	Nuclear magnetic resonance
NRPS	Nonribosomal polyketide synthase
O.D.	Optical density
ORF	Open reading frame
OSB	<i>o</i> -succinylbenzoic acid
PCR	Polymerase chain reaction
PPi	Pyrophosphate
<i>S. aureus</i>	<i>Staphylococcus aureus</i>
saMenE	MenE from <i>Staphylococcus aureus</i>
SCVs	Small-colony variants
SDS-PAGE	Sodium dodecyl sulfate-polyacrylamide gel electrophoresis
SEPHCHC	2-succinyl-5-enolpyruvyl-6-hydroxy- 3-cyclohexene-1-carboxylate
SHCHC	2-succinyl-6-hydroxy-2, 4-cyclohexadiene-1- Carboxylate



SS	Salicylate synthase
TB	Tuberculosis
tbEntC	EntC from <i>Mycobacterium tuberculosis</i>
tbMenE	MenE from <i>Mycobacterium tuberculosis</i>
VRSA	Vancomycin-resistant <i>Staphylococcus aureus</i>
WHO	World health organization
WT	Wild type
XDR-TB	Extensively drug-resistant tuberculosis

## **Acknowledgement**

This is a great honor to express my respect to a great many people who have contributed to this dissertation.

I would like to gratefully and sincerely thank my advisor Prof. Peter J. Tonge, who has not only provided great support and advice but also given me the opportunity to explore my own research interests. His mentorship was paramount in providing a well rounded supervision consistent with my long-term career goals. Thanks very much for his great help so far and I will miss him after I leave.

I would like to thank Prof. Dale G. Drueckhammer and Prof. Daniel P. Raleigh for teaching me and helping through all my academic meetings and reports. Thanks very much for your time and help. I would also like to thank Prof. Subramanyam Swaminathan for being my outside member of my dissertation. It is my honor and pleasure to collaborate with his group. I hope that the relationship between our two labs will go well in the future.

I would like to thank my labmates in Tonge Group, who shared a lot of happy time with me and gave a lot of good memories here. I would also like to thank my friends in Stony Brook, who supported me a lot during all these years.

The last but not least, I thank my parents. Without your love I cannot go this far.

## **Chapter I: Introduction of Drug Resistance Bacteria and Two Biosynthetic Pathways as Potent Drug Target**

### **1.1 Search For Novel Drugs Towards The Treatment of Drug Resistance**

Antimicrobial resistance of pathogens is a global problem. Each year worldwide, more than 11 million people died of infectious diseases alone, far more than the number killed in the natural or man-made catastrophes. The increasing drug resistance among Gram-positive bacteria is a significant problem because they are responsible for one-third of nosocomial infections; drug resistances in Gram-positive organisms have achieved prominence in the past 15 years (1). Currently, tuberculosis, which affects 1.7 billion people per year in the world, is the primary cause of death from a single infectious agent. The World Health Organization report from 2008 indicated that there were an estimated 9.2 million new active cases of tuberculosis reported worldwide in 2006, 8% of which were in HIV-positive individuals (2). Multi-drug resistant *Mycobacterium tuberculosis* strains are being reported in increasing numbers and the emergence of multidrug-resistant strains of *M. tuberculosis* (MDR-TB) seriously threatens TB control and prevention efforts. In addition to tuberculosis, methicillin-resistant *Staphylococcus aureus* (MRSA) is one of most frequent nosocomial pathogens in developed countries. Therefore, identification of new molecular targets through the identification of essential ubiquitous bacterial genes in pathogens that are not present in eukaryotes s

holds the promise for the development of novel therapies that circumvent existing drug resistant mechanisms. (3-4)

The “Golden era” of antibiotic discovery was from 1940-1960, during which most of the currently used molecules were identified and characterized (5). However, only very few new drugs have been introduced into the drug market since then. Hence, there is an urgent need to develop new chemotherapeutics to combat these serious infectious agents.

## **1.2 Mycobacterium Tuberculosis**

*Mycobacterium tuberculosis*, which is the causative agent of the disease tuberculosis, is the world’s most successful pathogen, infecting one third of the population and killing two million people annually (6-7). There are over 3 million people who have died from the disease every year. Recent comparative genomic analysis shows that modern *M. tuberculosis* existed at least 35,000 years ago, with human pathogen ancestors possibly dating back to 3,000,000 years ago (8). Currently, the global number of tuberculosis cases is rising at a rate of 2% per year (World Health Organization tuberculosis fact sheet: <http://www.stoptb.org>) (9)

*M. tuberculosis* is an obligate aerobe growing most successfully in tissues with high oxygen content, such as the lungs. It is classified as a Gram-resistant bacterium, which can be defined as neither Gram-positive nor Gram-negative, due to the high lipid content in its cell wall, which makes it

hard to retain any bacteriological stain. Ziehl-Neelsen staining, or acid-fast staining, is used in general. Since mycobacteria do not retain the crystal violet stain compared to the other standard Gram-positive bacteria, they are also classified as acid-fast due to their lack of a phospholipid outer cell membrane (10).

The growth of *M. tuberculosis* is extremely slow compared to other bacteria. While *Escherichia coli* dividing every 20 minutes, *M. tuberculosis* divide every 16-20 hours. It is a small bacillus that can withstand weak disinfectants and can survive in a dry state for many weeks. The components of the *M. tuberculosis* cell wall are atypical, and are rich in lipids such as mycolic acid and glycolipid. This waxy cell wall (**Fig. 1-1**) is likely responsible for drug resistance and is a key virulence factor (8).

Several antibiotics for the treatment of *M. tuberculosis* were discovered and developed in the past sixty years and the incidence of the disease then declined, particularly in developed countries. However, in the last twenty years, this trend has been reversed. The tuberculosis infection can arise after immune suppression by HIV. Consequently, the co-infection with TB and HIV doubles the risk of the death of a person infected with HIV alone.

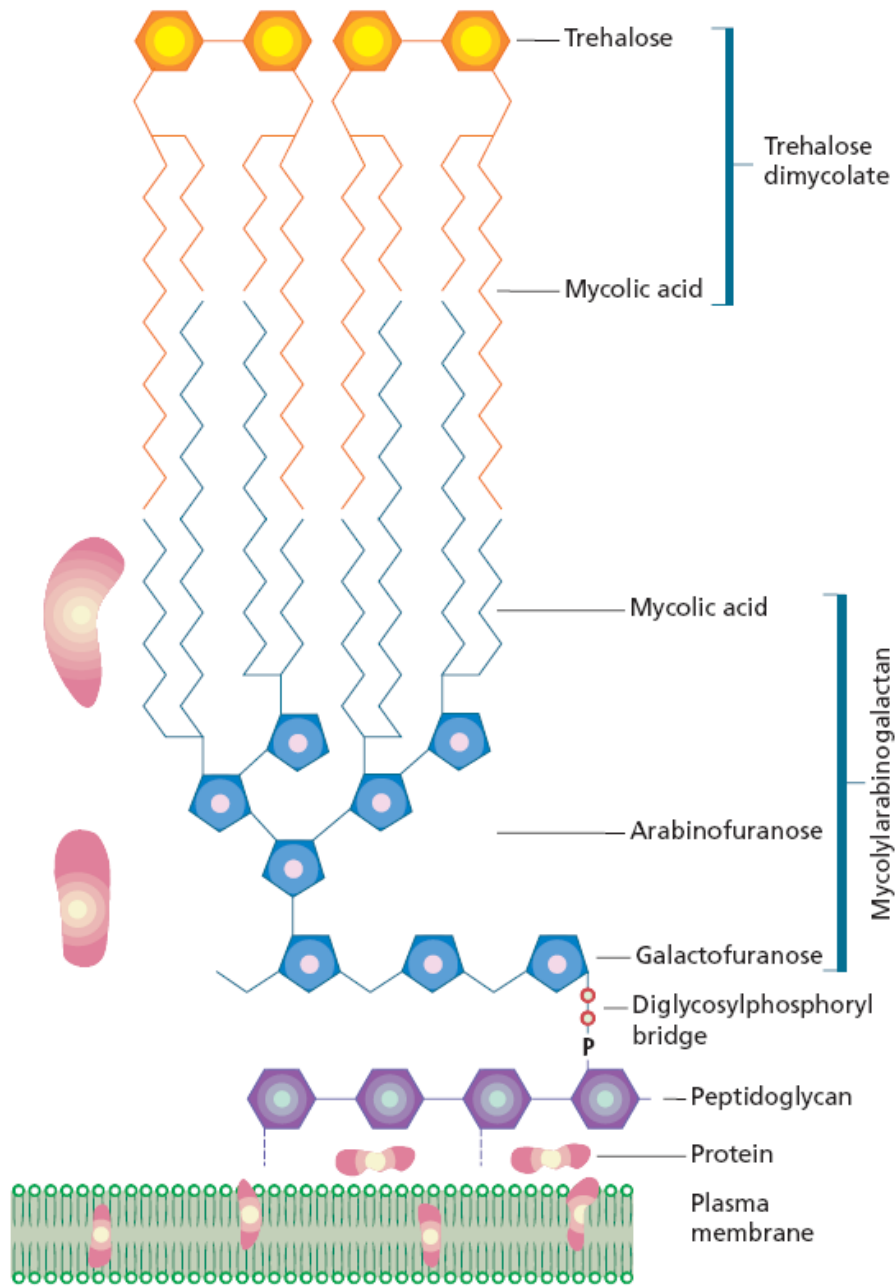


**Figure 1- 1: Complex cell wall of *M. tuberculosis*. Attached to the plasma membrane is a net work of glycolipids and proteins that protects against environmental and chemical threats and modulates the host immune response (10).**

### **1.2.1 Nonreplicating Persistence And Latency of Tuberculosis**

Tuberculosis is spread through the air, when people who have the disease cough, sneeze, or spit. Most infections in human beings will result in asymptomatic, latent infection, and about one in ten latent infections will eventually progress to active disease, which, if left untreated, kills more than half of its victims. The classic symptoms of tuberculosis are a chronic cough with blood-tinged sputum, fever, night sweats, and weight loss. Infection of other organs causes a wide range of symptoms (11-12).

Primary tuberculosis disease occurs immediately after the host is infected and *M. tuberculosis* replication overcomes the immune system. Upon initial infection there are three possible clinical outcomes, which are the eradication of the bacillus, the development of the active tuberculosis and the development of an asymptomatic latent infection with the potential for subsequent reactivity. The mechanisms of the three clinical outcomes are not fully understood so far, due to the complicated interactions between the host and pathogen (12).

When infected, *M. tuberculosis* is phagocytosed into alveolar macrophages and then replicates as an intracellular pathogen, attracting activated macrophages as part of larger cell mediated immune response, eventually leading to granuloma formation, which contain T lymphocytes, B lymphocytes, neutrophils, fibroblasts, dendritic cells and extracellular matrix

components. This granuloma provides a proper local environment for communication of cells in the immune system. According to the latent *M. tuberculosis* infection, the present hypothesis is that within these granulomas, *M. tuberculosis* can keep asymptomatic for a long time (13-14).

However there remain debates as to the best experimental models for understanding the mechanism of human *M. tuberculosis* latent infection (15). One simple and pioneering *in vitro* model has been developed by Wayne and Hayes. This model is thought to mimic the events in the lung, which occur during the immunological response to infection in the patient. Their work also suggested that *in vitro* grown non-replicating tubercle bacilli have less susceptibility to the activity of TB drugs. However, besides the Wayne-Hayes model, nitrous oxide is also thought to induce latency. Differentiations of TB drug susceptibilities between oxygen depletion and nitrous oxide induced dormancy have also been identified (16-18).

It is still not obvious which model best mirrors the *in vivo* conditions. The mechanism of the persistence to *M. tuberculosis* is also poorly understood, which becomes a big challenge when developing TB drugs against nonreplicating bacilli.

### **1.2.2 Current Treatment of Tuberculosis**

Treatment for tuberculosis uses antibiotics to kill the bacteria. The two



antibiotics most commonly used are rifampicin and isoniazid. However, instead of the short course of antibiotics typically used to cure other bacterial infections, tuberculosis requires much longer periods of treatment (about 6 to 12 months) to entirely eliminate mycobacteria from the patient (19-21). Latent tuberculosis treatment usually uses a single antibiotic, while active tuberculosis disease is best treated with combinations of several antibiotics, to reduce the risk of the bacteria developing antibiotic resistance. Patients with latent tuberculosis infections are treated to prevent them from progressing to active tuberculosis disease later in life. However, treatment using rifampicin and pyrazinamide has their own risks. The Centers for Disease Control and Prevention (CDC) notified healthcare professionals of revised recommendations against the use of rifampin plus pyrazinamide for treatment of latent tuberculosis infection, due to high rates of hospitalization and death from liver injury associated with the combined use of these drugs (22-24). Structures of five commonly used front-line anti-TB drugs are shown in **Fig. 1-2**.

Drug resistant tuberculosis is transmitted in the same way as regular tuberculosis. Primary resistance occurs in patients who are infected with a resistant strain of tuberculosis. A patient with fully susceptible tuberculosis develops secondary resistance (acquired resistance) during tuberculosis therapy because of inadequate treatment, such as not taking the prescribed regimen appropriately, or using low quality medication. Drug-resistant

tuberculosis is a public health issue in many developing countries, since the treatment is longer and requires more expensive drugs. Multi-drug-resistant tuberculosis (MDR-TB) is defined as resistance to the two most effective front-line TB drugs: rifampicin and isoniazid. Extensively drug-resistant TB (XDR-TB) is defined as resistance to three or even more of the six classes of second-line drugs (25). The DOTS (Directly Observed Treatment Short-course) strategy of tuberculosis treatment based on clinical trials done in the 1970s by Tuberculosis Research Centre, Chennai, India, focusing on a neglected area of infectious disease control is now showing promising results in effectively treating all tuberculosis cases in the community (26-29).

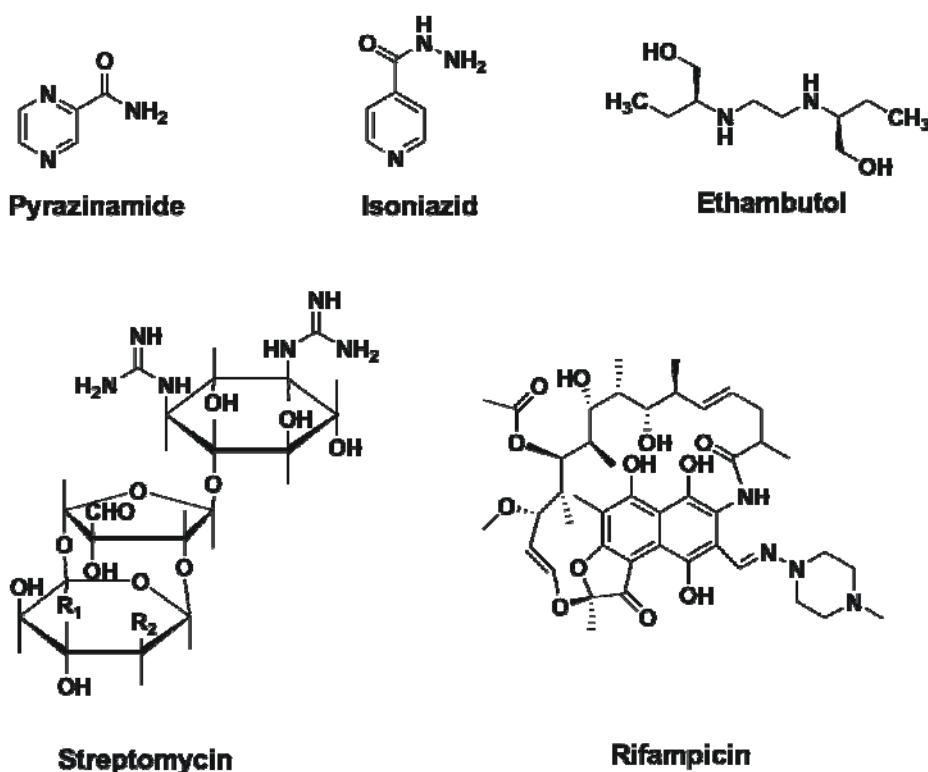


Figure 1- 2: Structures of five front-line anti-TB drugs: Pyrazinamide, Isoniazid, Ethambutol, Streptomycin and Rifampicin.

One significant advance in the treatment of latent tuberculosis was made by Boshof and coworkers in 2004. They used groupings of DNA microarray profiles to analyze the response of *M. tuberculosis* to a variety of chemical and environmental conditions (30). The mechanisms of some known drugs were accurately predicted based on this new technique. In addition, the type II NADH menaquinone oxidoreductase was isolated by its identification as the target of a novel class of phenothiazines (31). According to Boshof and coworkers' contribution, both the duration and cost of *M. tuberculosis* treatment could possibly be shortened due to the exploration of these novel targets.

### **1.3 Small Colony Variants of *Staphylococcus aureus***

*Staphylococcus aureus* is a Gram-positive bacterium, which was first discovered in Aberdeen, Scotland in 1880 (32). *S. aureus* is one of the most common causative agents of hospital-acquired infectious, including superficial skin lesions and even more severe infections. Spread of *S. aureus* is through human-to-human contact, although recently some vets have discovered that the infection can be spread through pets. The community-acquired staphylococcal infections have been increasing during the last thirty years (33).

*S. aureus* infection that is not antibiotic resistant can be treated in about a

month using antibiotics. However it has become resistant to many commonly used antibiotics today, such as penicillin, methicillin and vancomycin. The first case of methicillin-resistant *S. aureus* (MRSA) was reported in England in 1961, while the first case of vancomycin-resistant *S. aureus* (VRSA) was reported in Japan in 1996. Eleven cases of VRSA infection have been reported in the United States until 2010. (34-35)

Bacterial small colony variants (SCVs) were first reported in 1910. The variant strain has been described in *S. aureus* in 1995. There are two types of SCVs in *S. aureus*, which are consistently recovered from clinical specimens: electron-transport defective SCVs and thymidine-defective SCVs. Many studies suggest that the SCV strains can escape from host defense, and are responsible for recurrent and persistent infections. Additionally, it has been reported that SCVs cannot be treated by traditional approaches. Hence, the novel therapies are urgently required. (36-37)

#### **1.4 Potential Drug Targets for Drug-resistance Organisms**

No new antibiotics against tuberculosis have been developed in the past thirty years. Hence, an urgent call of developing new antibiotics against tuberculosis is widely acknowledged and a Global Alliance for TB Drug Development ([www.tballiance.org](http://www.tballiance.org)) has been established with goals to accelerate the discovery and development of new TB drugs that will shorten

treatment, be effective against susceptible and resistant strains, be compatible with antiretroviral therapies for those HIV-TB patients currently on such therapies, and improve treatment of latent infection. So far, there have been four new drugs that are applied in clinical trials and more successes are expected in the future (38-39).

MRSA stands for methicillin-resistant *S. aureus* bacteria. This organism is thought to cause skin infections. Although *S. aureus* has been causing infections (Staph infections) probably as long as the human race has existed, MRSA has a relatively short history. MRSA was first noted in 1961, about two years after the antibiotic methicillin was initially used to treat *S. aureus* and other infectious bacteria (40). The resistance to methicillin was due to a penicillin-binding protein coded for by a mobile genetic element termed the methicillin-resistant gene (*mecA*). In recent years, the gene has continued to evolve so that many MRSA strains are currently resistant to several different antibiotics such as penicillin, oxacillin, and amoxicillin (Amoxil, Dispermox, and Trimox) (41-42). In 2009, research showed that many antibiotic-resistant genes and toxins are bundled and transferred together to other bacteria, which speed the development of toxic and resistant strains of MRSA (40, 43). In addition, HIV infected patients also are at high risk for MRSA. Several reports have indicated the high prevalence in this population, with one report that it is 18 times more prevalent than among those who are not HIV infected (44-45).

Many of the potential new drug targets are classic biosynthetic enzymes,

which are composed in the different biosynthetic pathways. The genome-wide transposon mutagenesis study and microarray study identified a large number of genes that are essential for the growth of *M. tuberculosis* and *S. aureus* *in vitro*. Many of these genes correspond to biosynthetic proteins but some have completely unknown functions. These biosynthetic proteins become major candidates for developing new drugs because of their potential importance in *M. tuberculosis* and *S. aureus* growth.

#### **1.4.1 The Menaquinone Biosynthetic Pathway**

Menaquinone, which can not be synthesized by humans, is essential for electron transport and ATP synthesis in aerobic bacteria. Enzymes in the menaquinone biosynthetic may consequently be novel targets for antibacterial drug development. Menaquinone in *E. coli* is thought to be synthesized through a biosynthetic pathway which is composed of up to seven menaquinone specific genes (*menA-menH*) (46-47). These enzymes are encoded by 2 clusters of genes. The *men* gene cluster consists of the *menB*, *C*, *D*, *E*, *F* and a separate cluster composed of *menA* and *menG*.

The initial reaction of the pathway is carried out by an isochorismate synthase annotated as MenF. Interestingly in the *M. tuberculosis* H37Rv genome there is no annotated *menF* gene. Instead located more than one million bp from a cluster of other men genes, there is an isochorismate

synthase annotated as EntC. There are also three other genes with homology to the *E. coli menF* gene that includes *mbtl*, *pabB*, and *trpE* (48-49). The proposed biosynthetic pathway in *E. coli* is summarized in **Fig 1-3**.

MenF, an isochorismate synthase, is the first enzyme to catalyze the reaction of chorismate, derived from shikimate pathway, to isochorismate. The condensation reaction of isochorismate with  $\alpha$ -ketoglutarate to form SEPHCHC is catalyzed by MenD, followed with YfbB to eliminate the pyruvate side chain. MenC catalyzes the dehydration reaction from SHCHC to *o*-succinyl benzoic acid (OSB). MenE, an OSB-CoA synthetase, is an enzyme that catalyzes a two step reaction, in which OSB is converted into the aliphatic mono-CoA thioester (OSB-CoA) by adenylation and thioesterification half reactions which require ATP and CoA as the two cofactors. MenB catalyzes the cyclization reaction to form DHNA-CoA, and following the hydrolysis of DHNA-CoA to form DHNA, MenA catalyzes the decarboxylation reaction and attachment of the prenyl side chain on DHNA. Finally, MenG (UbiE) catalyzes the methylation of the naphthoquinone nucleus. Menaquinones are known to have side chains of different sizes in different organisms or even within the same organisms. The most commonly used menaquinones contain 7, 8 and 9 isoprene units. MK-7 is the major menaquinone component in many Gram-positive bacteria, MK-8 is in *E. coli* or *S. aureus* and MK-9 is in *M. tuberculosis*.

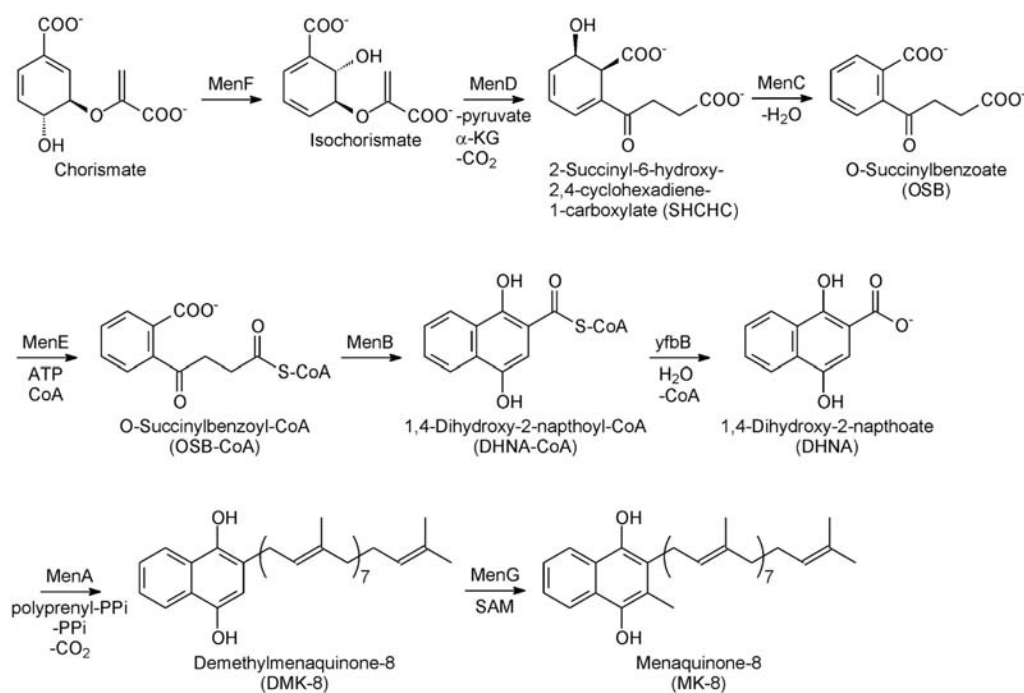


**Figure 1- 3: Overview of menaquinone biosynthetic pathways in *E. coli*.**

(50)

**o-succinyl benzoyl-CoA (OSB-CoA) synthetase encoded by menE gene;**  
**1,4-dihydroxy-2-naphthoyl- CoA (DHNA-CoA) synthetase encoded by**  
**menB gene..**

Menaquinone is an essential component of the electron transport system in Gram-positive organisms, and importantly it has been shown that inhibitors of MenA can act as selective antibacterial agents against organisms such as MRSA. And M tuberculosis (51), indicating that menaquinone synthesis is a valid new drug target in Gram-positive organisms. In addition to MenA, inhibitor discovery efforts have also focused on MenD (SHCHC synthase) and MenB (DHNA-CoA synthase) (52). The structures of the current menaquinone biosynthesis inhibitors are shown in **figure 1-4**.



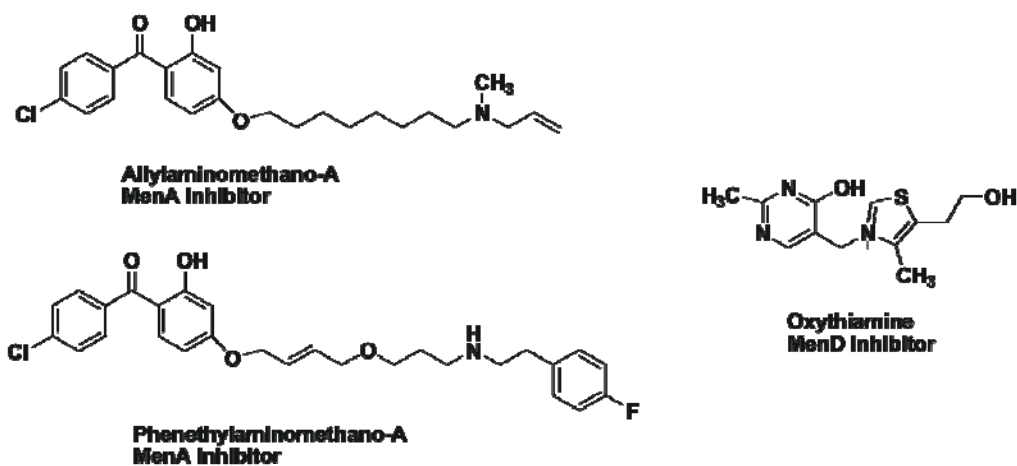


Figure 1- 4: Selected menaquinone biosynthesis inhibitors for MenA and MenD.

#### 1.4.2 The Mycobactin Biosynthetic Pathway

Iron, an essential element for growth of pathogenic bacteria, is scavenged from human hosts by iron chelators known as siderophores, especially in iron-limited extracellular spaces. In order to take up ferric iron through the bacterial cell wall, *M. tuberculosis* produces the siderophore mycobactin that differ in the nature of group R<sub>1</sub> and R<sub>2</sub>. The proposed mechanism for uptake of iron has been reviewed by C. Ratledge in 2004 (53-54). The core structures of these two siderophores are highly related and vary mainly in their fatty acid substituent. Comparing with the water-soluble carboxymycobactins, which have a short unsaturated sidechain, the lipid-soluble mycobactins have longer saturated sidechain (55). Mycobactin is now generally identified among large number of mycobacteria. The molecular structures of mycobactin from *M.*

*tuberculosis* are shown in Fig. 1-5.

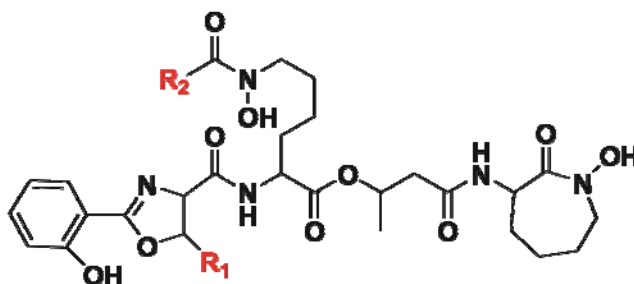


Figure 1- 5: The cell-associated and water-soluble mycobactins from *M. tuberculosis*.

Cell-associated mycobactins:  $R_1=H$ ;  $R_2 = (CH_2)_{16-19}CH_3$ ,

$(CH_2)_nCH=CH(CH_2)_mCH_3$ ,  $(n + m) = 14-17$ . Water-soluble mycobactins:

$R_1=H, Me$ ;  $R_2=(CH_2)_{1-7}COOCH_3$ ,  $(CH_2)_{1-7}COOH$ ,

$(CH_2)_nCH=CH(CH_2)_mCOOCH_3$ ,  $(CH_2)_nCH=CH(CH_2)_mCOOH$ ,  $(n + m) = 1-5$ .

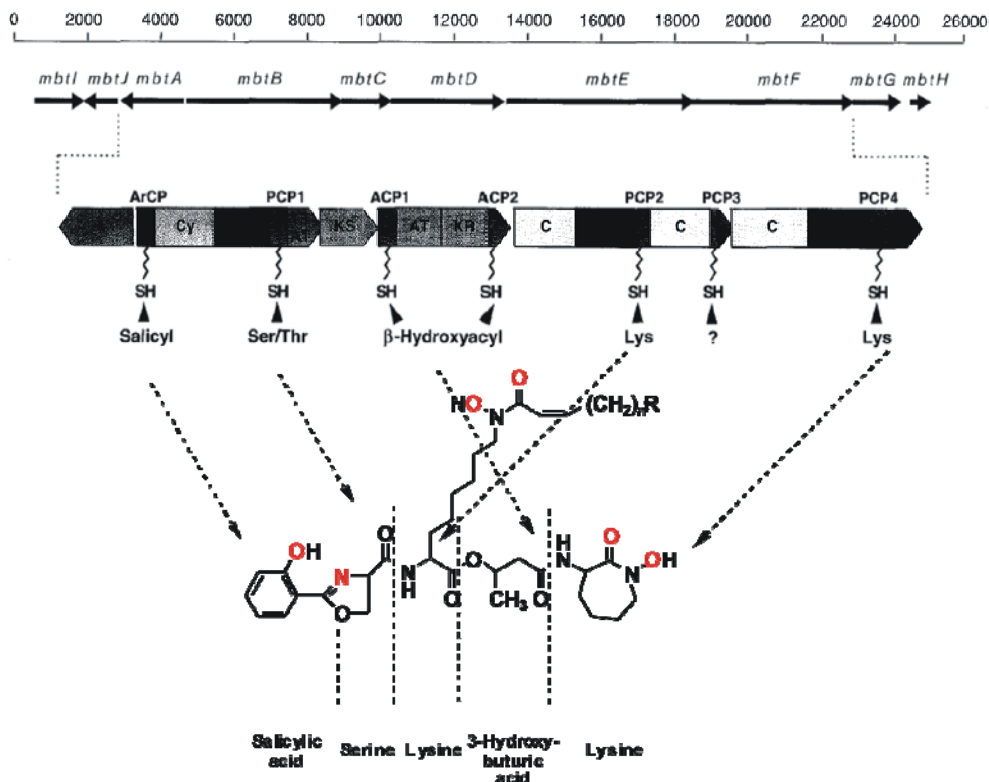


**Figure 1- 6: The molecular structure of mycobactin from *M. tuberculosis* (Cited from Chemistry & Biology 1998, Vol5 No 11)**

Salicylic acid is synthesized by a salicylate synthase annotated as MbtI, which is the first enzyme involved in the mycobactin biosynthetic pathway. Sequencing of the H37Rv genome, there is a cluster of 10 genes (*mbtA-J*) starting with *mbtI*, which is proposed to encode enzymes in the mycobactin pathway. Particularly, the six genes *mbtA* to *mbtF* consists of a genomic sequence for producing of a 20-domain assembly line, which could manufacture the portions needed for mycobactin shown in **Fig 1-6**. Three chelating groups responsible for the binding of ferric iron are highlighted in red. The mycobactin biosynthetic pathway has been reviewed in detail by C.T. Walsh in 2002 (56). Since iron uptake is essential for bacterial growth, the

biosynthesis of siderophores is thought to be a novel target for drug discovery.

### **1.6 Objectives of My Research**

A detailed understanding of the catalytic mechanism of enzyme drug targets is required to guide structure-based drug discovery. In my thesis research I have primarily focused on the catalytic mechanism and inhibition of MenE the OSB-CoA synthetase from three different organisms: *M. tuberculosis*, *S. aureus* and *E. coli*. MenE catalyzes the formation of OSB-CoA through a two step reaction that proceeds via acyl adenylate intermediate and utilizes ATP and CoA as cofactors. In chapter 2, I discuss the catalytic mechanism of MenE from *S. aureus* (saMenE) where steady state kinetics coupled with site-directed mutagenesis has been used to identify key catalytic residues in the active site of MenE and to elucidate the molecular details of each half reaction. In chapter 3, I present data on the inhibition of saMenE as well as the enzymes from *M. tuberculosis* (tbMenE) and *E. coli* (ecMenE). These studies have focused on a series of OSB-AMP intermediate analogs synthesized by our collaborator Dr. Tan at Memorial Sloan-Kettering Cancer Center. The most potent compound inhibits MenE with a  $K_{id}$  value of  $11.2 \pm 0.9$  nM. While the majority of my work has focused on MenE, I have also undertaken kinetic studies of the charismata-dependent enzymes Men from *E. coli* and MbtI from *M. tuberculosis* (chapter 4). These enzymes catalyze the initial reaction in menaquinone biosynthetic pathway and mycobactin biosynthetic pathway, respectively. Interestingly, in

the absence of Mg<sup>2+</sup>, MenF and MbtI show chorismate mutase activity, although these enzymes have no similarity to the AroQ/H chorismate mutase. Because tbEntC, which is annotated as isochorismate synthase in *M. tuberculosis* menaquinone pathway, cannot yet be well expressed by using a heterologous *E. coli* expression system, I propose that MbtI might have a dual function and produce isochorismate for menaquinone *in vitro*.

## Reference

1. Grenet, K., Guillemot, D., Jarlier, V., Moreau, B., Dubourdiou, S., Ruimy, R., Armand-Lefevre, L., Bau, P., and Andreumont, A. (2004) Antibacterial resistance, Wayampis Amerindians, French Guyana, *Emerg Infect Dis* 10, 1150-1153.
2. Zarocostas, J. (2008) WHO urges action on drug resistant tuberculosis, *BMJ* 336, 465.
3. N'Guessan J, D., Coulibaly, A., Ramanou, A. A., Okou, O. C., Djaman, A. J., and Guede-Guina, F. (2007) Antibacterial activity of *Thonningia sanguinea* against some multi-drug resistant strains of *Salmonella enterica*, *Afr Health Sci* 7, 155-158.
4. Haddadin, A. S., Fappiano, S. A., and Lipsett, P. A. (2002) Methicillin resistant *Staphylococcus aureus* (MRSA) in the intensive care unit, *Postgrad Med J* 78, 385-392.
5. Wright, G. D. (2007) The antibiotic resistome: the nexus of chemical and genetic diversity, *Nat Rev Microbiol* 5, 175-186.
6. Corbett, E. L. (2003) HIV and tuberculosis: surveillance revisited, *Int J Tuberc Lung Dis* 7, 709.
7. Corbett, E. L., Watt, C. J., Walker, N., Maher, D., Williams, B. G., Raviglione, M. C., and Dye, C. (2003) The growing burden of tuberculosis: global trends and interactions with the HIV epidemic, *Arch Intern Med* 163, 1009-1021.

8. Gutierrez, M. C., Brisse, S., Brosch, R., Fabre, M., Omais, B., Marmiesse, M., Supply, P., and Vincent, V. (2005) Ancient origin and gene mosaicism of the progenitor of *Mycobacterium tuberculosis*, *PLoS Pathog* 1, e5.
9. (2010) Global tuberculosis control: key findings from the December 2009 WHO report, *Wkly Epidemiol Rec* 85, 69-80.
10. Tonge, P. J. (2000) Another brick in the wall, *Nat Struct Biol* 7, 94-96.
11. Tupasi, T. E., Radhakrishna, S., Quelapio, M. I., Villa, M. L., Pascual, M. L., Rivera, A. B., Sarmiento, A., Co, V. M., Sarol, J. N., Beltran, G., Legaspi, J. D., Mangubat, N. V., Reyes, A. C., Solon, M., Solon, F. S., Burton, L., and Mantala, M. J. (2000) Tuberculosis in the urban poor settlements in the Philippines, *Int J Tuberc Lung Dis* 4, 4-11.
12. Rose, C., Auxenfants, E., Noel, M. P., Mahieu, M., Demory, J. L., Croxo, C., Wallaert, B., and Bauters, F. (1997) [Tuberculosis, mycobacterium infection and hairy cell leukemia], *Presse Med* 26, 110-114.
13. Parrish, N. M., Dick, J. D., and Bishai, W. R. (1998) Mechanisms of latency in *Mycobacterium tuberculosis*, *Trends Microbiol* 6, 107-112.
14. Bishai, W. R., Dannenberg, A. M., Jr., Parrish, N., Ruiz, R., Chen, P., Zook, B. C., Johnson, W., Boles, J. W., and Pitt, M. L. (1999) Virulence of *Mycobacterium tuberculosis* CDC1551 and H37Rv in rabbits evaluated by Lurie's pulmonary tubercle count method, *Infect Immun* 67, 4931-4934.

15. Tufariello, J. M., Chan, J., and Flynn, J. L. (2003) Latent tuberculosis: mechanisms of host and bacillus that contribute to persistent infection, *Lancet Infect Dis* 3, 578-590.
16. Gardam, M., and Iverson, K. (2003) Rheumatoid arthritis and tuberculosis: time to take notice, *J Rheumatol* 30, 1397-1399.
17. Long, R., and Gardam, M. (2003) Tumour necrosis factor-alpha inhibitors and the reactivation of latent tuberculosis infection, *CMAJ* 168, 1153-1156.
18. Gardam, M. A., Keystone, E. C., Menzies, R., Manners, S., Skamene, E., Long, R., and Vinh, D. C. (2003) Anti-tumour necrosis factor agents and tuberculosis risk: mechanisms of action and clinical management, *Lancet Infect Dis* 3, 148-155.
19. Amaral, L., Viveiros, M., and Kristiansen, J. E. (2001) Phenothiazines: potential alternatives for the management of antibiotic resistant infections of tuberculosis and malaria in developing countries, *Trop Med Int Health* 6, 1016-1022.
20. Amaral, L., Kristiansen, J. E., Viveiros, M., and Atouguia, J. (2001) Activity of phenothiazines against antibiotic-resistant Mycobacterium tuberculosis: a review supporting further studies that may elucidate the potential use of thioridazine as anti-tuberculosis therapy, *J Antimicrob Chemother* 47, 505-511.
21. Viveiros, M., and Amaral, L. (2001) Enhancement of antibiotic activity



against poly-drug resistant *Mycobacterium tuberculosis* by phenothiazines, *Int J Antimicrob Agents* 17, 225-228.

22. Bonhoeffer, S., Lipsitch, M., and Levin, B. R. (1997) Evaluating treatment protocols to prevent antibiotic resistance, *Proc Natl Acad Sci U S A* 94, 12106-12111.
23. Bonhoeffer, S., Coffin, J. M., and Nowak, M. A. (1997) Human immunodeficiency virus drug therapy and virus load, *J Virol* 71, 3275-3278.
24. Nowak, M. A., Bonhoeffer, S., Shaw, G. M., and May, R. M. (1997) Anti-viral drug treatment: dynamics of resistance in free virus and infected cell populations, *J Theor Biol* 184, 203-217.
25. Gandhi, N. R., Moll, A., Sturm, A. W., Pawinski, R., Govender, T., Lalloo, U., Zeller, K., Andrews, J., and Friedland, G. (2006) Extensively drug-resistant tuberculosis as a cause of death in patients co-infected with tuberculosis and HIV in a rural area of South Africa, *Lancet* 368, 1575-1580.
26. Frieden, T. R. (1996) The phylogeny of *Mycobacterium tuberculosis*, *Tuber Lung Dis* 77, 291.
27. Washko, R. M., and Frieden, T. R. (1996) Tuberculosis surveillance using death certificate data, New York City, 1992, *Public Health Rep* 111, 251-255.
28. Kaye, K., and Frieden, T. R. (1996) Tuberculosis control: the relevance

of classic principles in an era of acquired immunodeficiency syndrome and multidrug resistance, *Epidemiol Rev* 18, 52-63.

29. Frieden, T. R. (1996) Clarifying the issues in tuberculosis control, *Am J Public Health* 86, 267-268.
30. Boshoff, H. I., Myers, T. G., Copp, B. R., McNeil, M. R., Wilson, M. A., and Barry, C. E., 3rd. (2004) The transcriptional responses of *Mycobacterium tuberculosis* to inhibitors of metabolism: novel insights into drug mechanisms of action, *J Biol Chem* 279, 40174-40184.
31. Barczak, A. K., Domenech, P., Boshoff, H. I., Reed, M. B., Manca, C., Kaplan, G., and Barry, C. E., 3rd. (2005) In vivo phenotypic dominance in mouse mixed infections with *Mycobacterium tuberculosis* clinical isolates, *J Infect Dis* 192, 600-606.
32. (1984) Classics in infectious diseases. "On abscesses". Alexander Ogston (1844-1929), *Rev Infect Dis* 6, 122-128.
33. McGregor, J. C., Dumyati, G., Casiano-Colon, A. E., Chang, P. J., and Klevens, R. M. (2009) Usefulness of antibiogram surveillance for methicillin-resistant *Staphylococcus aureus* in outpatient pediatric populations, *Diagn Microbiol Infect Dis* 64, 70-75.
34. Panlilio, A. L., Culver, D. H., Gaynes, R. P., Banerjee, S., Henderson, T. S., Tolson, J. S., and Martone, W. J. (1992) Methicillin-resistant *Staphylococcus aureus* in U.S. hospitals, 1975-1991, *Infect Control Hosp Epidemiol* 13, 582-586.

35. Eady, E. A., and Cove, J. H. (2003) Staphylococcal resistance revisited: community-acquired methicillin resistant *Staphylococcus aureus*--an emerging problem for the management of skin and soft tissue infections, *Curr Opin Infect Dis* 16, 103-124.
36. Baumert, N., von Eiff, C., Schaaff, F., Peters, G., Proctor, R. A., and Sahl, H. G. (2002) Physiology and antibiotic susceptibility of *Staphylococcus aureus* small colony variants, *Microb Drug Resist* 8, 253-260.
37. Brouillette, E., Martinez, A., Boyll, B. J., Allen, N. E., and Malouin, F. (2004) Persistence of a *Staphylococcus aureus* small-colony variant under antibiotic pressure in vivo, *FEMS Immunol Med Microbiol* 41, 35-41.
38. Ma, Z., Lienhardt, C., McIlleron, H., Nunn, A. J., and Wang, X. (2010) Global tuberculosis drug development pipeline: the need and the reality, *Lancet* 375, 2100-2109.
39. Lienhardt, C., Vernon, A., and Raviglione, M. C. (2010) New drugs and new regimens for the treatment of tuberculosis: review of the drug development pipeline and implications for national programmes, *Curr Opin Pulm Med* 16, 186-193.
40. Thompson, D. (2010) Hospital infection control and the reduction in intensive care unit-acquired MRSA between 1996 and 2009, *J Hosp Infect.*

41. Cavaco, L. M., Hasman, H., Stegger, M., Andersen, P. S., Skov, R., Fluit, A. C., Ito, T., and Aarestrup, F. M. (2010) Cloning and occurrence of *czrC*, a gene conferring cadmium and zinc resistance in MRSA CC398, *Antimicrob Agents Chemother*.
42. Naimi, T. S., LeDell, K. H., Como-Sabetti, K., Borchardt, S. M., Boxrud, D. J., Etienne, J., Johnson, S. K., Vandenesch, F., Fridkin, S., O'Boyle, C., Danila, R. N., and Lynfield, R. (2003) Comparison of community- and health care-associated methicillin-resistant *Staphylococcus aureus* infection, *JAMA* 290, 2976-2984.
43. Perencevich, E. N., and Diekema, D. J. (2010) Decline in invasive MRSA infection: where to go from here?, *JAMA* 304, 687-689.
44. Skiest, D., Brown, K., Hester, J., Moore, T., Crosby, C., Mussa, H. R., Hoffman-Roberts, H., and Cooper, T. (2006) Community-onset methicillin-resistant *Staphylococcus aureus* in an urban HIV clinic, *HIV Med* 7, 361-368.
45. Cohen, P. R., and Grossman, M. E. (2004) Management of cutaneous lesions associated with an emerging epidemic: community-acquired methicillin-resistant *Staphylococcus aureus* skin infections, *J Am Acad Dermatol* 51, 132-135.
46. Shaw, D. J., Guest, J. R., Meganathan, R., and Bentley, R. (1982) Characterization of *Escherichia coli* men mutants defective in conversion of o-succinylbenzoate to 1,4-dihydroxy-2-naphthoate, *J*

*Bacteriol* 152, 1132-1137.

47. Bentley, R., and Meganathan, R. (1982) Biosynthesis of vitamin K (menaquinone) in bacteria, *Microbiol Rev* 46, 241-280.
48. Kolappan, S., Zwahlen, J., Zhou, R., Truglio, J. J., Tonge, P. J., and Kisker, C. (2007) Lysine 190 is the catalytic base in MenF, the menaquinone-specific isochorismate synthase from *Escherichia coli*: implications for an enzyme family, *Biochemistry* 46, 946-953.
49. Zwahlen, J., Kolappan, S., Zhou, R., Kisker, C., and Tonge, P. J. (2007) Structure and mechanism of MbtI, the salicylate synthase from *Mycobacterium tuberculosis*, *Biochemistry* 46, 954-964.
50. Truglio, J. J., Theis, K., Feng, Y., Gajda, R., Machutta, C., Tonge, P. J., and Kisker, C. (2003) Crystal structure of *Mycobacterium tuberculosis* MenB, a key enzyme in vitamin K<sub>2</sub> biosynthesis, *J Biol Chem* 278, 42352-42360.
51. Kurosu, M., Narayanasamy, P., Biswas, K., Dhiman, R., and Crick, D. C. (2007) Discovery of 1,4-dihydroxy-2-naphthoate [corrected] prenyltransferase inhibitors: new drug leads for multidrug-resistant gram-positive pathogens, *J Med Chem* 50, 3973-3975.
52. Kurosu, M., and Begari, E. (2010) Vitamin K<sub>2</sub> in electron transport system: are enzymes involved in vitamin K<sub>2</sub> biosynthesis promising drug targets?, *Molecules* 15, 1531-1553.
53. Dhungana, S., Ratledge, C., and Crumbliss, A. L. (2004) Iron chelation

properties of an extracellular siderophore exochelin MS, *Inorg Chem* 43, 6274-6283.

54. Ratledge, C. (2004) Iron, mycobacteria and tuberculosis, *Tuberculosis (Edinb)* 84, 110-130.
55. Ferreras, J. A., Ryu, J. S., Di Lello, F., Tan, D. S., and Quadri, L. E. (2005) Small-molecule inhibition of siderophore biosynthesis in *Mycobacterium tuberculosis* and *Yersinia pestis*, *Nat Chem Biol* 1, 29-32.
56. Crosa, J. H., and Walsh, C. T. (2002) Genetics and assembly line enzymology of siderophore biosynthesis in bacteria, *Microbiol Mol Biol Rev* 66, 223-249.

## Chapter II: Overexpression, Purification, and Characterization of MenE, an o-Succinylbenzoyl-Coenzyme A Synthetase from *Staphylococcus aureus*

### 2.1 Introduction

Vitamin K2 (menaquinone) is derived from the shikimate pathway and plays an essential role in the electron transport pathway of many Gram positive aerobic bacteria including *Staphylococcus aureus* (1). The biosynthesis pathway of menaquinone has been reviewed recently (2-4), and there are at least eight enzymes involved in converting chorismate into the prenylated naphthoquinone final product. One of the major reactions in the biosynthetic pathway is the formation of the bicyclic aromatic compound 1,4-dihydroxyl-2-naphthoic acid (DHNA) from the benzenoid compound o-succinylbenzoic acid (OSB), which requires the activation of the OSB carboxylate via the formation of o-succinylbenzoyl coenzyme A (OSB-CoA) (5-6). Formation of OSB-CoA is catalyzed by OSB-CoA synthetase, in a reaction that and requires the presence of ATP and CoA in addition to OSB (7). The two-step reaction catalyzed by saMenE is summarized in **Figure 2-1**.

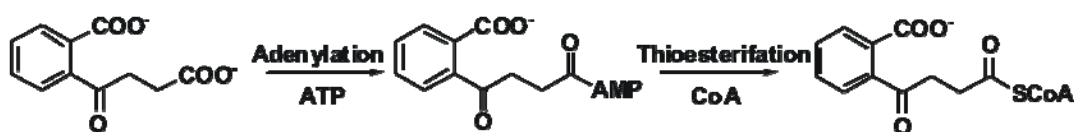


**Figure 2- 1: Adenylation-Ligation Reaction Catalyzed by MenE.**

*S. aureus* infection can cause scalded skin syndrome, a severe staphylococcal disease which is extremely prevalent in atopic dermatitis patients who are less resistant to it than other people (8). *S. aureus* infection that is not drug resistant can be treated in about a month using antibiotics (9-10). However, currently there are many strains of *S. aureus* that are resistant to many of the commonly used antibiotics, such as penicillin, methicillin, and vancomycin. The first case of methicillin-resistant *S. aureus* (MRSA) was reported in England in 1961, while the first case of vancomycin-intermediate *S. aureus* (VRSA) was reported in Japan in 1996. Eleven cases of VRSA infection have been reported in the United States as of 2010 (11-13). The spread of *S. aureus* (including MRSA) is through human-to-human contact, although recently some vets have discovered that the infection can be spread through pets, with environmental contamination thought to play a relatively unimportant part (14). Hence, *S. aureus* infections are widely found in hospitals and an urgent requirement of infection control is recommended (7, 9).

Enzymes that catalyze the adenylation of the carboxylic acid reactant by ATP, followed by displacement of the adenylate by the thiol coreactant, belong to the adenylate-forming superfamily (PFAM00501). This large adenylate-forming enzyme superfamily is composed of three subfamilies: acyl-CoA synthetases, firefly luciferase and the adenylation domains of nonribosomal peptide synthetases (NRPSs) (10, 15-16). Despite the low



sequence identity, members of the superfamily exhibit very similar structural elements, folding into a large N-terminal domain and a small C-terminal domain with the active site at the interface between the two domains. X-ray structural data are currently available for members of the adenylate-forming superfamily. Five different conformations have been identified that are associated with different stages of the reaction according to the mechanistic diversity of the superfamily. The movement of small C-terminal domain, induced by the rotation of a solvent peptide linker, is reported to play an essential role in the catalytic mechanism of acyl-CoA synthetases (17).

In this chapter, the gene encoding OSB-CoA synthetase (*menE*) has been cloned from *S. aureus*. The MenE enzyme has been overexpressed, purified and biochemically characterized. Here we used steady-state kinetic assay to determine the kinetic mechanism of this enzyme. In addition, to understand the mechanistic features that distinguish among members of the adenylate-forming superfamily, we have determined steady-state kinetic results for a series of MenE active site mutants.

## **2.2 Materials and Methods**

### *Materials and Substrates*

ATP, Coenzyme A and isopropyl- $\beta$ -D-thiogalactopyranosid (IPTG) were purchased from Sigma. Restriction enzymes, DNA ligase, pfu DNA polymerase and DpnI were from stratagene (LA Jolla, CA). Primers were ordered from IDT. Ni-NTA metal affinity chromatography and His-bind metal affinity chromatography resins were from Novagen. Sephadex<sup>TM</sup> G-25 resin was purchased from Amersham Biosciences. Millipore centriplus YM-30 was from Fisher. All other chemical reagents were purchased from Sigma

### *Synthesis of o-succinylbenzoic acid (OSB)*

Fifty g of succinic acid (0.4 mol) was heated in a three-neck round bottom flask to 200°C until it melted. Subsequently, 40.0 g of phthalic anhydride (0.3 mol) and 21.8 g sodium acetate (0.3 mol) were added to the succinic acid. The reaction mixture was then refluxed at the 200°C for 40 min after which it was extracted with boiling water four times (4 x100 mL). The water is evaporated using rotovap. 13.3 g (0.04 mol, yield 27%) pure spirodilactone was obtained after recrystallization with MeOH. The spirodilactone (0.04 mol) was refluxed in 500 mL of 1.5 M NaOH solution for 30 min, after which the solution was cooled and the pH adjusted to 1.5 with HCl. The product was extracted with 100 mL ethyl acetate three times and the organic solvent was removed under

the vacuum giving 14.0 g of OSB (0.04 mol, yield 95%) as a white powder. The

$^1\text{H}$  NMR spectra of OSB is shown in **Figure 2-2**.

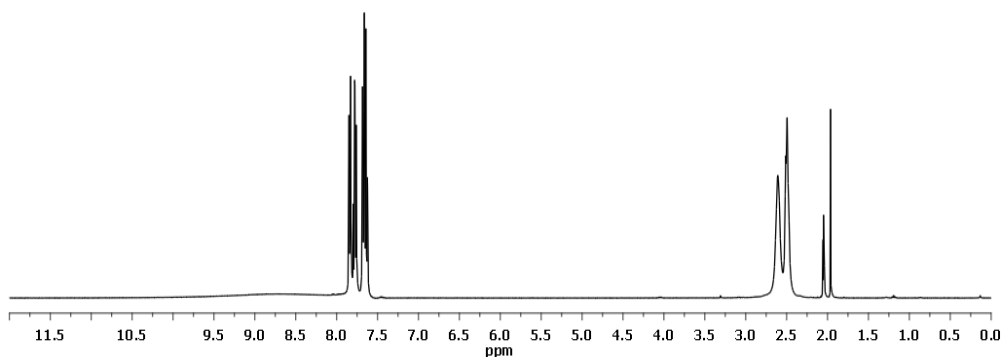


**Figure 2- 2:**  $^1\text{H}$  NMR spectrum of OSB

#### *Cloning, Expression and Purification of saMenE*

The *menE* gene from *S. aureus* NCTC 8325 strain was amplified using the forward primer 5'-GGAATTCCATATGATGGACTTTTGGTTATATAAA-3' and reverse primer 5'-CGCGGATCCTCATCCTCTATACAACTT-3' and cloned into pET 15b vector (Novagen) using the 5' NdeI and 3'BamHI restriction enzymes (sites underlined) so that a His6-tag was encoded at the N-terminus. The plasmid, pET15bSaMenE, was transformed into XL1Blue cells (Stratagene) and, following growth on media X supplemented with antibiotic y, plasmid was isolated using a DNA purification and gel extraction kit from Qiagen Inc. The correct sequence of the construct was verified by ABI DNA sequencing.

Protein expression was performed by transforming the pET15bsaMenE plasmid into *E. coli* BL21(DE3)pLysS cells which were grown in 10 mL of Luria Broth (LB) media containing 1 mM ampicillin in a 50 mL falcon tube at 37°C

overnight. The overnight culture was used to inoculate 500 mL of LB media containing 1 mM ampicillin which was then shaken (250 rpm) at 37°C until the optical density at 600 nm (OD<sub>600</sub>) reached 0.8-1.0. Induction of protein expression was initiated by adding 1 mM IPTG and the culture was then incubated with shaking for an additional 20 h at 25°C. Cells were harvested by centrifugation at 5,000 rpm for 20 min at 4°C. The cell pellet was resuspended in 30 mL of His-binding buffer (5 mM imidazole, 0.5 M NaCl, 20 mM Tris-HCl, pH 7.9) and the bacteria were disrupted by three passages through a French Press cell (1000 psi). Cell debris was removed by centrifugation at 33,000 rpm for 90 min at 4°C and the clear supernatant was loaded onto a His-bind column (1.5 cm x 15 cm) containing 4 mL His-bind resin (Novagen) that had been charged with 10mL of charge buffer (Ni<sup>2+</sup>). The protein was eluted from the column using the standard His-bind purification procedure using a gradient of 30 mL elute buffer and 30 mL binding buffer mixture. The eluted fractions, which contained the protein, were loaded onto a Sephadex G-25 column (1.5 cm x 55 cm) and eluted using 20 mM Tris-HCl, 0.15M NaCl at pH 7.5 in order to remove imidazole. The protein that eluted from the G-25 column was concentrated at 5,000 rpm for 2h using Millipore centriplus YM-30 and 10% glycerol was added during the concentration in order to prevent protein precipitation. The purity of saMenE was determined by 15% SDS-PAGE gel which gave an apparent molecular weight for the protein consistent with the known MW of 52kDa. The final concentration of protein was determined by

measuring the absorption at 280 nm and using a calculated extinction coefficient of 40,480 M<sup>-1</sup>cm<sup>-1</sup>. The protein was stored at -80°C.

*Site-Directed Mutagenesis, Expression and Purification of saMenE Mutants.*

The MenE mutants Thr169Ala, His213Ala, Thr306Ala, Arg394Ala, Lys396Ala, Ser401Ala, Gly403Leu, Glu404Ala, and Lys483Ala were constructed using the QuikChange site-directed mutagenesis kit from Stratagene, following by purification using the same procedure as that described above for the wild type plasmid. The results of the mutagenesis reaction were confirmed by ABI sequencing. The primers designed for site-directed mutagenesis are listed in **Table 2-1**.

<b>Table 2- 1: The primers for site-directed mutagenesis of saMenE enzyme</b>	
Mutants	Primer sequence (forward only, reverse primer is complementary)
MenE T169A	GCATCGATTATGTTT <u>GCTTC</u> AGGG
MenE H213A	GTCTTGCCGATTTAT <u>GCT</u> ATTTTCG
MenE T306A	AATTCATTTGGTATG <u>GCCG</u> AGACA
MenE R394A	GTCATGATTTATGAC <u>GCCCGTAA</u> GATTTAATT
MenE K396A	ATTTATGACCGACGT <u>GCA</u> GATTTAATTATTAGT
MenE S401A	AAAGATTTAATTATT <u>GCT</u> GGCGGTGAAAATATT
MenE E404A	ATTATTAGTGGCGGT <u>GCCA</u> ATATTTATCCATAT
MenE K483A	TATACATCAACAGGT <u>GCA</u> TTACAA

### *Reaction of OSB-CoA Synthetase with o-succinylbenzoic Acid*

saMenE OSB-CoA synthetase activity was monitored according to a previously reported assay in which the reaction was coupled to the formation of DHNA-CoA catalyzed by tbMenB (18). In order to determine the activity, saMenE and tbMenB were incubated with OSB, baselined from 220-400 nm and scans incrementally taken over this wavelength range. Reaction mixtures contained 500 nM saMenE and 2  $\mu$ M tbMenB, and were performed at 25°C in 20 mM Tris-HCl, 150 mM NaCl, 1 mM  $Mg^{2+}$  at pH 7.5 by varying the concentration of OSB. Formation of DHNA-CoA was monitored by following the increase in the absorbance at 392 nm using an extinction coefficient of 4000  $M^{-1}cm^{-1}$ . A Varian 300-Cary UV-Vis spectrophotometer was used for all reactions.

### *Steady-state Kinetic Assay*

In order to determine the kinetic mechanism, three sets of kinetic data were obtained in which OSB, ATP and CoA were each varied at fixed concentrations of the other substrates. The first sets of kinetic data were measured by varying the concentration of OSB (15-75 $\mu$ M) at different fixed ATP (240 $\mu$ M) and CoA (60-360 $\mu$ M) concentrations. The second sets of kinetic data were measured by varying the ATP (60-480 $\mu$ M) concentration at different fixed OSB (240 $\mu$ M) and CoA (60-360 $\mu$ M) concentrations. The third sets of kinetic data were measured by varying the OSB (2-20 $\mu$ M) concentration at

different fixed CoA (1mM) and ATP (60-360 $\mu$ M) concentrations. Individual data sets were then fit to the Michaelis-Menten equation (**Eq. 2-1**) using Grafit 4.0.

$$v = V_{\max} [S] / (K_m + [S]) \quad \text{Equation 2-1}$$

The kinetic data sets were then plotted in a double reciprocal pattern to differentiate between the Ping-Pong mechanism or ternary-complex mechanism. Finally the kinetic data were globally fitted to the equation for steady-state Bi Bi ping pong mechanism (**Eq. 2-2**) to determine the  $K_m$  values for OSB, ATP and CoA .

$$v = (V_{\max} [A][B] / K_{iA} K_B + K_B [A] + K_A [B] + [A][B] ) \quad \text{Equation 2-2}$$

In equation 2-2,  $v$  is the initial velocity,  $V_{\max}$  is the maximum rate,  $[A]$  and  $[B]$  are the concentration of substrates,  $K_A$  and  $K_B$  are the Michaelis constants for A and B respectively,  $K_{iA}$  is the dissociation constant for A. Grafit 4.0 was used for the data fitting.

### *Product Inhibition Study*

The product inhibition studies were performed with AMP. The effects of the inhibitor on reaction rates was studied by varying the concentration of one product inhibitor and one substrate while keeping the other two substrates at constant saturating concentrations. The concentration of AMP (0-480 $\mu$ M) was varied at a concentration of ATP 120 $\mu$ M and a concentration of OSB 3 $\mu$ M. In another case, the concentration of AMP (0-480 $\mu$ M) was varied at a concentration of OSB 3 $\mu$ M and a concentration of CoA 25 $\mu$ M. The type of

inhibition in each case was subsequently determined using a Lineweaver-Burk plot. The experimental data were then fit to **Eqs 2-3-1 to 2-3-4** by nonlinear regression analysis to obtain the relevant kinetic parameters.

$$v = V_{max}/[1+(K_m/[S])(1+ [I]/K_i)] \quad \text{competitive inhibition} \quad \text{Eq 2-3-1}$$

$$v = V_{max}/(1+[I]/K_i+K_m/[S]) \quad \text{uncompetitive inhibition} \quad \text{Eq 2-3-2}$$

$$v = V_{max}/[(K_m/[S])(1+[I]/K_i)+1+ [I]/\alpha K_i] \quad \text{mixed-type inhibition} \quad \text{Eq 2-3-3}$$

$$v = V_{max}/[(1+[I]/K_i)(1+ K_m/[S])] \quad \text{noncompetitive inhibition} \quad \text{Eq}$$

#### **2-3-4**

In each of the equations,  $v$  is the reaction rate,  $V_{max}$  is the maximum velocity of the reaction,  $[S]$  is the substrate S concentration,  $[I]$  is the inhibitor I concentration,  $K_m$  is the Michaelis-Menten constant for substrate S,  $K_i$  is the dissociation constant of the inhibitor I to free enzyme E, and  $\alpha K_i$  is the dissociation constant for inhibitor I to ES complex. Grafit 4.0 was used for the data fitting.

#### *Direct Binding Fluorescence Titrations*

ATP binding was quantitated in the presence of  $Mg^{2+}$  by monitoring the intrinsic tryptophan fluorescence of saMenE using a Quanta Master fluorimeter (Photon Technology International). Excitation and emission wavelengths were 280 and 334 nm with an excitation slit width of 4.0 nm and an emission slit width of 8.0 nm. ATP stock in buffer (20mM Tris-HCl pH 7.5)



was titrated into the enzyme in the same buffer. The concentration of enzyme in the direct binding measurements was 1.3  $\mu\text{M}$  in all cases. All stock solutions were filtered and equilibrated to 25°C. Titration curves were corrected for inner filter effects and  $K_d$  values were calculated using the Scatchard equation. Grafit 4.0 was used for the data fitting.

#### *Kinetic Inhibition Assay*

Reactions were performed in 20mM Tris-HCl, 150mM NaCl and 1mM  $\text{MgCl}_2^+$  buffer at pH 7.5. 50nM of saMenE was incubated with inhibitor (0-500 $\mu\text{M}$ ) providing from Dr. Tan's group, ATP (240 $\mu\text{M}$ ) and CoA (240 $\mu\text{M}$ ) followed by addition of tbMenB (4 $\mu\text{M}$ ) and OSB (20 $\mu\text{M}$ ). The formation of DHNA-CoA was monitored at 392 nm and initial velocities were determined using an extinction coefficient of 4,000  $\text{M}^{-1}\text{cm}^{-1}$ .  $\text{IC}_{50}$  values were calculated by fitting the initial velocity data using Grafit 4.0.

## **2.3 Experimental Results**

### *Overexpression and purification of saMenE*

Overexpression strain pLysS was grown and saMenE was induced and purified as described before. The purity of saMenE during various stages of purification was determined by 15% SDS-PAGE gel, which is shown in **Figure 2-3**.

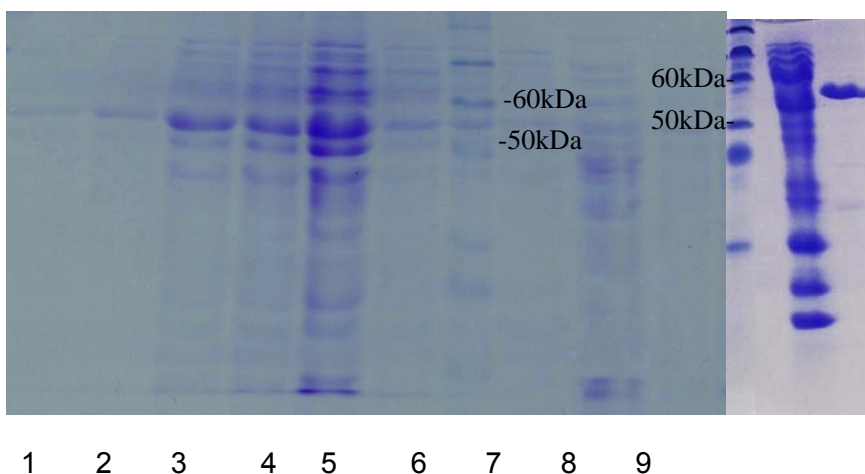


**Figure 2- 3: 15% SDS-PAGE analysis of the fractions from purification of wild-type saMenE before (left) and after (right) AKTA chromatography. Lane 1-4, G-25 purified fractions; Lane 5-6, Ni-NTA metal affinity chromatography purified fractions; Lane 7, protein ladder; Lane 8, wash solution; Lane 9 flow through solution.**

After the purification of saMenE from Ni-NTA metal affinity chromatography, the concentrated fractions were reloaded onto AKTA

purification system and further purified to remove impurities observed on SDS-PAGE gel.

Since saMenE rapidly lost kinetic activity at 4°C, it was concentrated to 10mg/mL and stored at -80°C immediately. The concentration of saMenE was determined by UV absorbance at 280nm ( $\epsilon = 40480 \text{ M}^{-1} \text{ cm}^{-1}$ ).

The purified saMenE was shown to catalyze the adenylation and thioesterification of OSB with CoA and ATP as cofactors. No activity was observed in the absence of  $\text{Mg}^{2+}$ . Because His-tagged saMenE precipitated rapidly, N-terminal His-tags were cleaved by thrombin after purification. However the cleaved protein was also unstable and also showed extremely low catalytic activity. Hence, we use His-tagged saMenE for all the kinetic experiments.

#### *pH Optimum*

The pH optimum was determined by monitoring activity over the pH range of 6.5 to 8.5 in 20mM Tris-HCl, 150mM NaCl and 1mM  $\text{MgCl}_2$  buffer. For saMenE, the enzyme exhibited optimum OSB-CoA synthetase activity between pH 7.0 and pH 8.5, while at pH 6.5 the enzyme activity decreased significantly. There were no differences in the activity whether Tris-HCl or phosphate buffer was used in the assay.

### *Kinetics Constants of Enzymes and Mutants*

*In vitro*, saMenE exhibited OSB-CoA synthetase activity which was  $Mg^{2+}$  dependent. The kinetic data were analyzed using the Michaelis-Menten equation giving an apparent  $K_m$  of  $6.1 \pm 0.9 \mu M$  and  $k_{cat}$  value of  $3.8 \pm 0.4 \text{ min}^{-1}$ . Since the kinetic constants were determined using the coupled reaction with MenB, which converts OSB-CoA to DHNA-CoA, the preincubation control experiment was designed to ensure the rate limiting reaction was carried out by saMenE in the assay. It is observed that an apparent  $K_m$  of  $4.2 \pm 2.1 \mu M$ ;  $k_{cat}$  value of  $3.6 \pm 0.7 \text{ min}^{-1}$ . The two sets of Michaelis constant were comparable with each other.

Site directed mutants T169A , H213A, T306A, R394A, K396A, S401A, E404A, and K483A were constructed using site directed mutagenesis. All mutants still exhibited OSB-CoA synthetase activity in the presence of  $Mg^{2+}$  with different decreasing folds comparing with the wild-type saMenE. The  $k_{cat}$  and  $K_m$  values are given in **Table 2-2**.

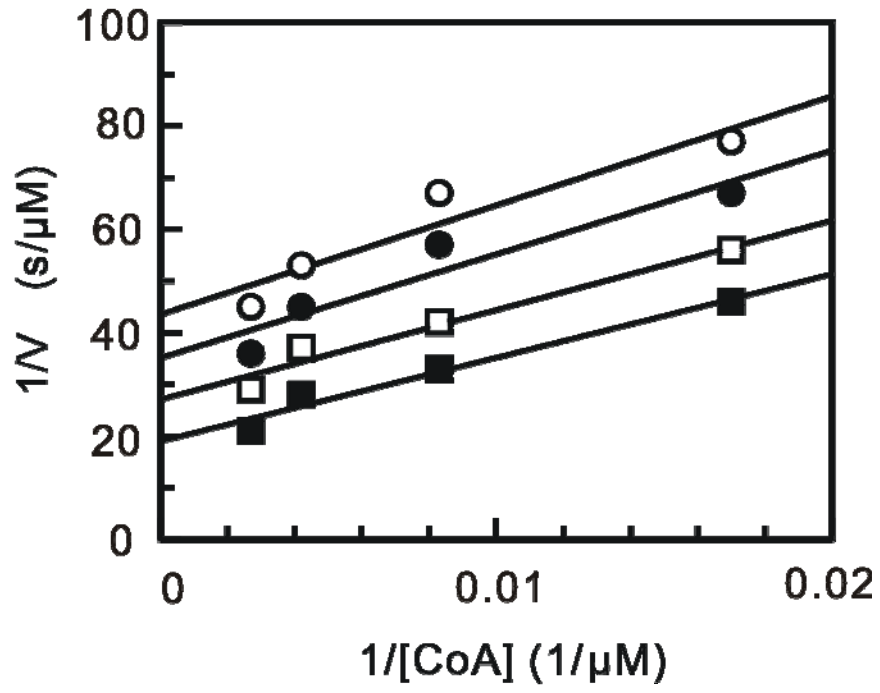
### *The OSB-CoA Synthetase Kinetic Mechanism*

saMenE is  $Mg^{2+}$  dependent enzyme. In order to determine the kinetic mechanism for saMenE, a full matrix of initial rates was determined with the concentration of one substrate being varied and the concentrations of the other two substrates being held constantly. The kinetic data were replotted in the form of double reciprocal plots in **Figure 2-4**. The parameters in **equation**

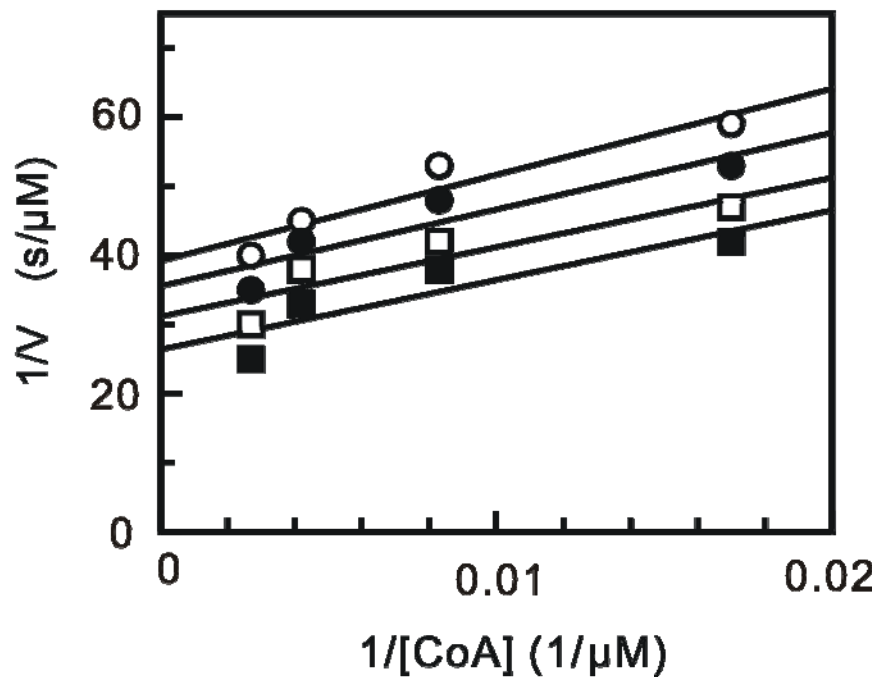
**2-2** were determined by simultaneously fitting the data using Grafit 4.0 (19).

When the concentration of OSB was varied (15-75 $\mu$ M) at a fixed saturating concentration of ATP (240 $\mu$ M) and at several fixed concentrations of CoA (36-360 $\mu$ M) the the double reciprocal plot of the data gave parallel lines (**Figure 2-4A**). This was also observed when the CoA concentration was varied at a fixed saturating concentration of ATP and at several fixed OSB concentrations (**Figure 2-4B**). However, intersecting lines were observed in the double reciprocal plot when the concentration of ATP was varied at several fixed concentrations of OSB and a single saturating concentration of CoA (**Figure 2-4C**). These kinetic plots are consistent with a Bi Bi Ping-Pong kinetic mechanism. The Michaelis-Menten constants for saMenE obtained from these experiments are given in Table summarized in **Figure 2-4**. This should be a table. The measured  $k_{cat}$ ,  $K_{m, OSB}$ ,  $K_{m, ATP}$  and  $K_{m, CoA}$  values were  $5.3 \pm 0.2 \text{ min}^{-1}$ ,  $6.2 \pm 0.9 \mu\text{M}$ ,  $180 \pm 22 \mu\text{M}$  and  $50 \pm 3 \mu\text{M}$ , respectively. This result is consistent with the previous reports for other enzymes in this family including acetyl-CoA synthetase (16), propionyl-CoA synthetase (17) and 4-chlorobenzoate-CoA synthetase (20).

A



B



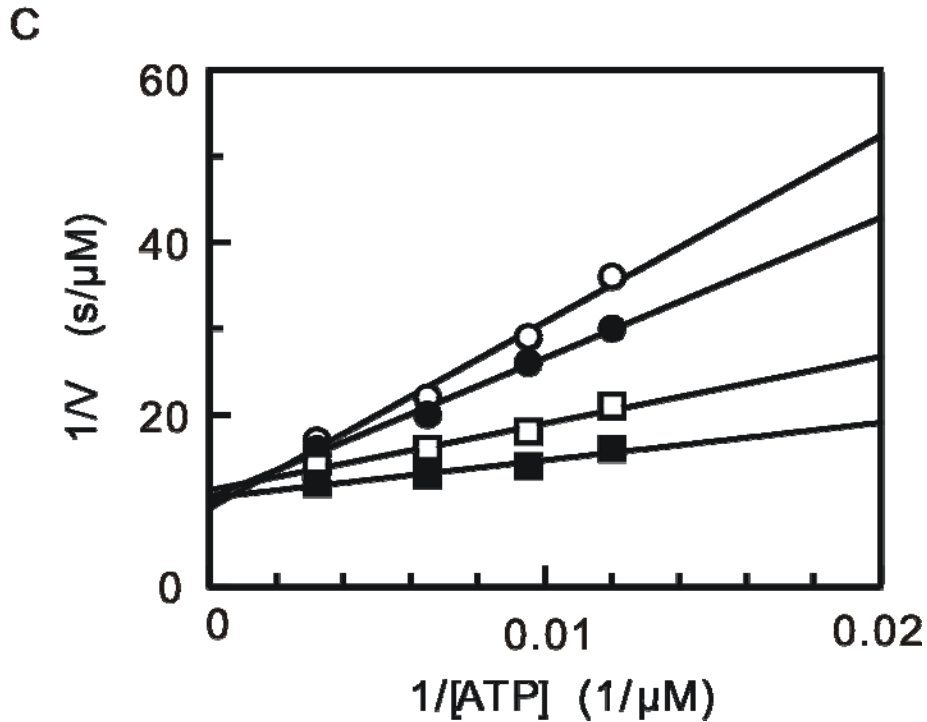


Figure 2- 4: OSB-CoA synthetase kinetic mechanism. (A) Plots of  $1/V$  vs  $1/[CoA]$  at various concentrations of OSB and at a concentration of ATP  $240\mu M$ . OSB concentrations are  $15$  (○),  $30$  (●),  $60$  (□),  $75$  (■)  $\mu M$ . (B) Plots of  $1/V$  vs  $1/[CoA]$  at various concentrations of ATP and at a concentration of OSB  $240\mu M$ . ATP concentrations are  $60$  (○),  $120$  (●),  $240$  (□),  $480$  (■)  $\mu M$ . (C) Plots of  $1/V$  vs  $1/[ATP]$  at various concentrations of OSB and at a concentration of CoA  $1mM$ . OSB concentrations are  $2$  (○),  $5$  (●),  $10$  (□),  $20$  (■)  $\mu M$ . The data were fitted into equation 2 and the apparent values for kinetic constants are  $K_m(OSB)=6.2\pm 0.9\mu M$   $K_m(CoA)=50\pm 3\mu M$ ,  $K_m(ATP)=180\pm 22\mu M$ ,  $k_{cat} = 5.3\pm 0.2 \text{ min}^{-1}$

### *Product Inhibition Studies*

To differentiate between the Bi Bi uni uni Ping-Pong and the Bi uni uni Bi Ping-Pong mechanism and to study the order of product release, we performed product inhibition studies. Nonlinear regression was performed on the experimental data using **eqs 2-3**. When the ATP concentration was varied at fixed concentrations of AMP with both OSB and CoA concentrations fixed at subsaturating levels, the data was fit to **eq 2-3-1**. A Lineweaver-Burk plot of the data produced a series of lines that converged on the y-axis (**Figure 2-6B**), indicating AMP is a competitive inhibitor of ATP. When the concentration of CoA was varied at fixed concentrations of AMP with both OSB and ATP kept at subsaturating levels, the data was fit to **eq 2-3-2** and the Lineweaver-Burk plot produced a series of parallel lines (**Figure 2-6A**), indicating that AMP is an uncompetitive inhibitor of CoA. This result is consistent with a Bi uni uni Bi Ping-Pong mechanism and rules out the Bi Bi uni uni ping-pong mechanism (**Figure 2-5**). In addition, the formation of OSB-AMP is proposed based on the Bi uni uni Bi Ping-Pong mechanism. A series of OSB-AMP intermediate inhibitors were designed and analyzed, which is discussed in the later part of this chapter.



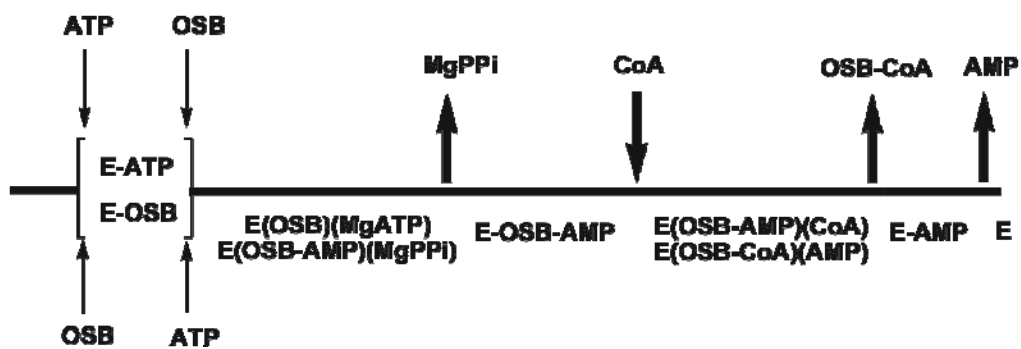
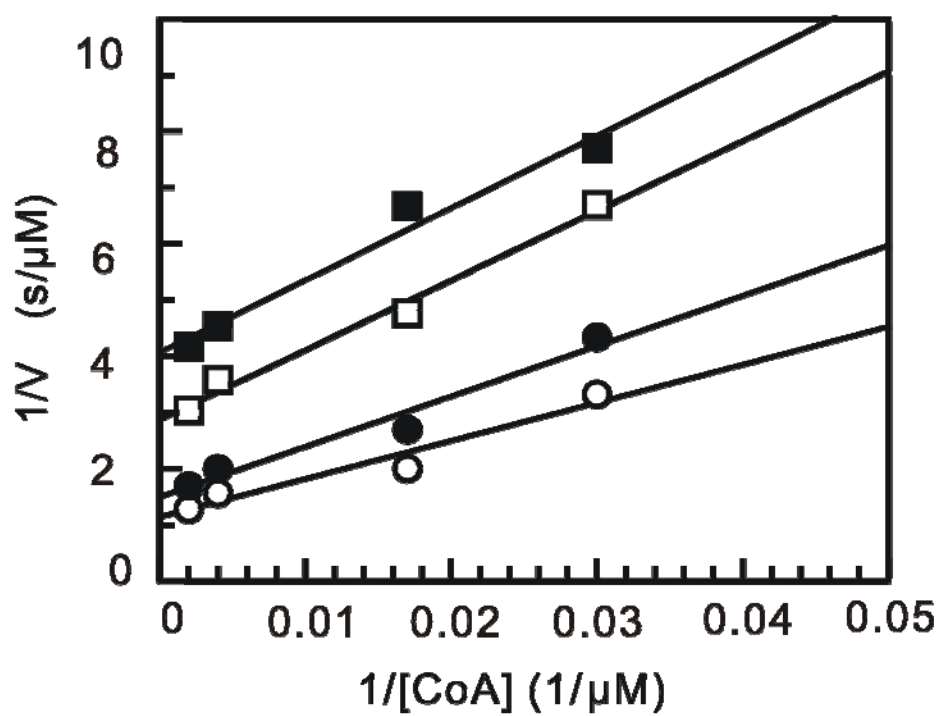
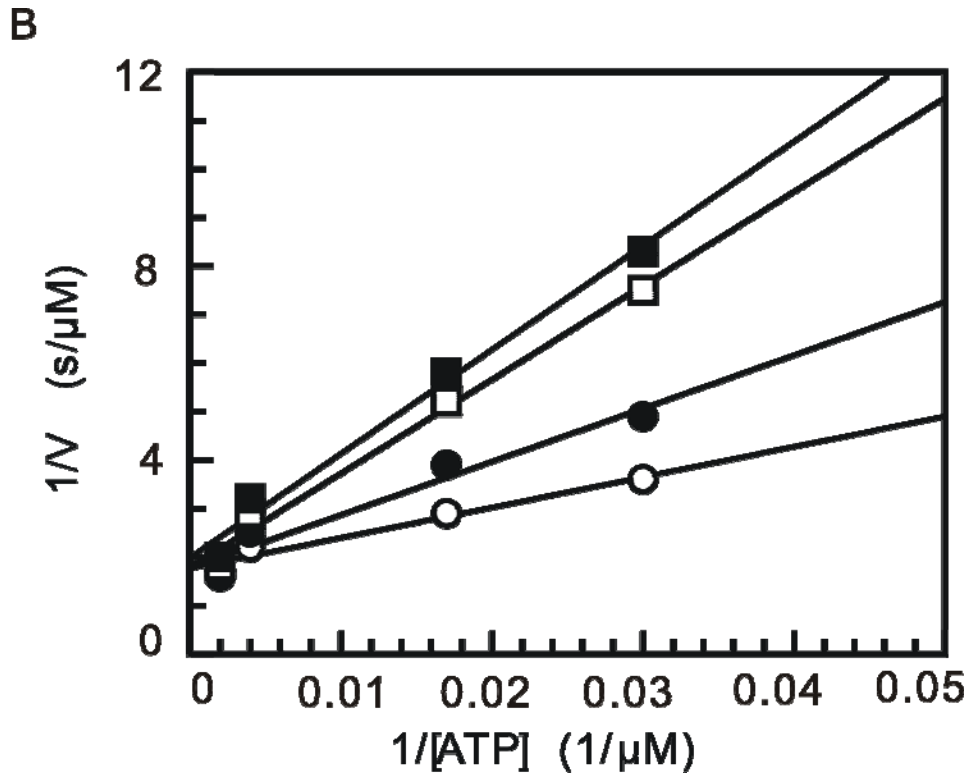


Figure 2- 5: The Bi uni uni Bi Ping-Pong mechanism for saMenE

A





**Figure 2- 6: AMP product inhibition assay. (A) Plots of  $1/V$  vs  $1/[\text{CoA}]$  at various concentrations of AMP and at a concentration of ATP  $120\mu\text{M}$  and a concentration of OSB  $3\mu\text{M}$ . AMP concentrations are  $30$  ( $\circ$ ),  $60$  ( $\bullet$ ),  $240$  ( $\square$ ),  $480$  ( $\blacksquare$ )  $\mu\text{M}$ . (B) Plots of  $1/V$  vs  $1/[\text{ATP}]$  at various concentrations of AMP and at a concentration of OSB  $3\mu\text{M}$  and a concentration of CoA  $25\mu\text{M}$ . AMP concentrations are  $30$  ( $\circ$ ),  $60$  ( $\bullet$ ),  $240$  ( $\square$ ),  $480$  ( $\blacksquare$ )  $\mu\text{M}$ .**

#### *Direct Binding of ATP with saMenE*

The interaction of ATP with saMenE was examined using a direct binding experiment in which the intrinsic tryptophan fluorescence of saMenE was used to measure the binding affinity of ATP to saMenE. The interaction of ATP with free saMenE in the presence of  $\text{Mg}^{2+}$  resulted in a rapid decrease in fluorescence. After correction of the data for the inner filter effect, the

fluorescence titrations yielded a  $K_d$  value of  $243.2 \pm 5.0 \mu\text{M}$  for the interaction of ATP with the free enzyme (**Figure 2-7**).

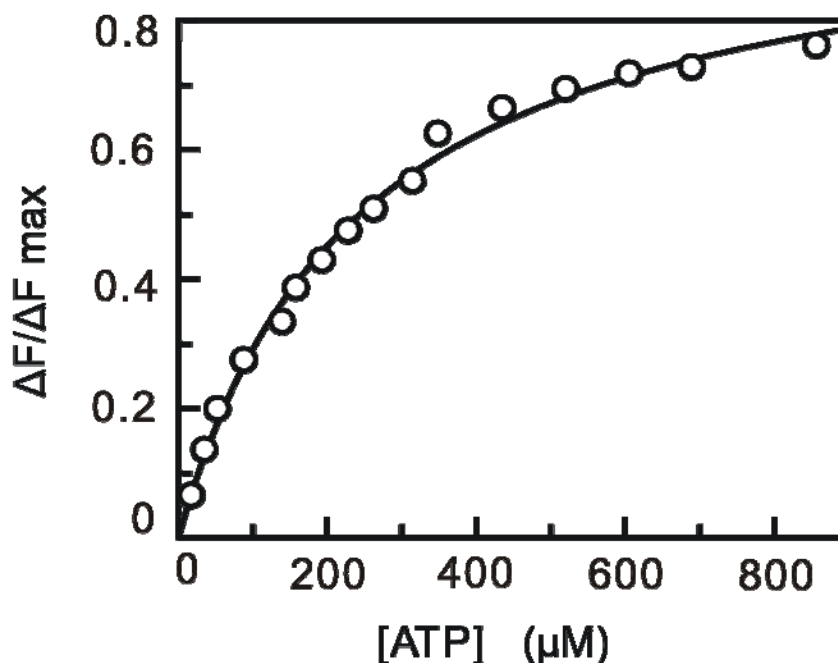


**Figure 2- 7: Direct binding of ATP with saMenE in the presence of magnesium**

*Identification of Key Active Site Residues Identified From Steady-state Kinetic Analysis of Site-directed Mutants*

An alignment was performed using the primary sequence of enzymes belonging to the adenylate-forming superfamily. This included 4-chlorobenzoate CoA synthetase (CBAL), acetyl-CoA synthetase (ACS), long-chain fatty acid CoA synthetase (LC FACS), the NRPS A-domains of DhbE and PheA and firefly luciferase (LUCF) (**Fig. 2-8**). The X-ray structures of these enzymes with or without bound ligand are available in PDB. The sequence alignment result indicated that although the enzymes have

functional diversity, they may maintain common active site residues.

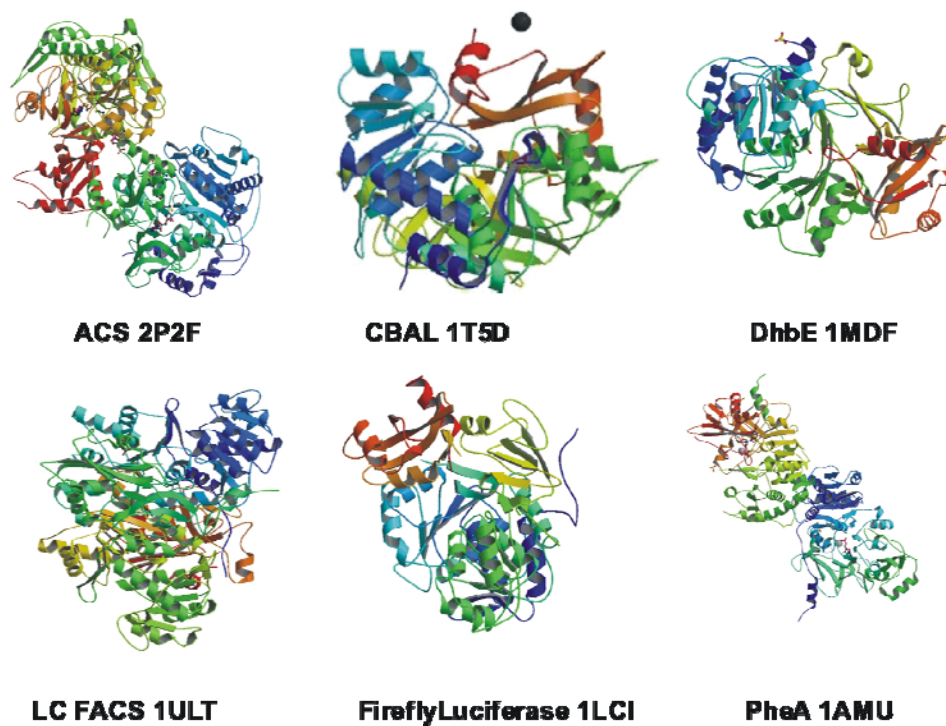


**Figure 2- 8: Crystal structures of enzymes belonging to the adenylate-forming enzymes superfamily; 4-chlorobenzoate CoA synthetase (CBAL), acetyl-CoA synthetase (ACS), long-chain fatty acid CoA synthetase (LC FACS), NRPS A-domains (DhbE and PheA) and firefly luciferase (LUCF).**

In order to determine the functional anchors for substrates in the active site of saMenE, a series of active site residues were mutated and steady-state kinetic analysis was used to assess the impact of the mutagenesis on catalysis.

**Table 2-2** lists the kinetic parameters for wild-type enzyme and the saMenE mutants. In some cases the difference in the wild-type and mutant saMenE  $k_{cat}/K_m$  values exceeded 50-fold indicating that the mutated residue was important for catalysis. Below we present data for individual mutants.

<b>Table 2- 2: The steady-state kinetic constants for saMenE (* Apparent kcat/Km)</b>					
Enzyme	Substrate	$K_m$ ( $\mu\text{M}$ )	$k_{\text{cat}}$ ( $\text{min}^{-1}$ )	$k_{\text{cat}}/K_m$ ( $\text{min}^{-1}\mu\text{M}^{-1}$ )	Decrease in $k_{\text{cat}}/K_m$
WT	OSB	6.2±0.9	5.3±0.2	0.85±0.22	
	ATP	180±22	5.3±0.2	0.03±0.009	
	CoA	50±3.0	5.3±0.2	0.10 ± 0.06	
Thr169A	OSB	64.1±3.2	0.10±0.002	0.0017±0.00072	500
	ATP	1858.9±93.4	0.11±0.001	0.00006±0.00002	500
His213A	OSB	95.6±7.8	0.27±0.006	0.0028 ± 0.00081	300
	ATP	411.8±33.9	0.24±0.003	0.0006 ± 0.0001	45
Thr306A	OSB	26.9±2.6	0.23±0.01	0.0085 ± 0.0043	100
	ATP	215.8±20.6	0.22±0.008	0.001 ± 0.0004	28
Lys483A	OSB	73.6±5.1	0.25±0.004	0.0034 ± 0.00074	250
	ATP	419.8±28.7	0.25±0.003	0.0006 ± 0.0001	45
Arg394A	OSB	17.3±3.8	0.15±0.01	0.0085 ± 0.0034	100
	CoA*	N/A	N/A	0.00004±0.000001	250
Lys396A	OSB	8.4±1.2	1.4±0.06	0.17±0.051	5
	CoA	122.4±23.3	1.2±0.07	0.01 ± 0.003	10
Ser401A	OSB	4.8±1.4	0.82±0.01	0.17 ± 0.0039	5
	CoA*	N/A	N/A	0.00004±0.00001	250
Glu404A	OSB	9.4±1.1	0.05±0.002	0.0056 ± 0.0019	150
	CoA	583.3±21.3	0.07±0.001	0.00012±0.000047	800

### **His213**

In 4-chlorobenzoate CoA synthetase (CBAL), the side chain of His207 blocks access to the active site by the pantetheine portion of CoA when 4-chlorobenzoic acid is bound to the enzyme. Wu and coworkers have proposed that His207 must move in order for CoA to bind and in agreement with this hypothesis replacement of this residue with an Ala results in a 500-fold decrease in  $k_{\text{cat}}/K_m$  for chlorobenzoic acid and a smaller effect on  $k_{\text{cat}}/K_m$  for ATP (20). In the case of saMenE, replacement of His213 with Ala causes a 300 fold reduction in the OSB  $k_{\text{cat}}/K_m$  value and a smaller (45-fold) effect on  $k_{\text{cat}}/K_m$  for ATP. These data strongly suggest that His213 in saMenE plays a similar role to the corresponding residue in CBAL.

### **Lys483**

In the structures of CBAL and acetyl-CoA synthetase (ACS), a strictly conserved lysine residue (Lys492 in CBAL) is observed to interact with the substrate carboxylate group. Movement of this lysine side is essential for the catalysis and adenylation of the substrate carboxylate is thought to break the interaction with Lys492 allowing the enzyme to move between conformation A and B (15, 20). For saMenE, replacement of the homologous residue Lys483 with Ala resulted in a significant (250-fold) decrease in the  $k_{\text{cat}}/K_m$  value. It indicated that Lys483 had a great impact in enzyme catalysis and the conformation of Lys483 might even affect the stabilization of OSB-AMP

intermediate based on the ligand bound crystal structure of CBAL.

### **Thr306 and Thr169**

The Thr306Ala mutant displayed a 100-fold decrease in the  $k_{cat}/K_m$  value for OSB. The corresponding threonine was observed in the acetyl-CoA synthetase from *Salmonella enterica* to establish the hydrogen bond with the  $\alpha$ -phosphate of AMP (21). Correspondingly, Thr306Ala mutant had a 28-fold decrease of  $k_{cat}/K_m$  value with ATP as the substrate.

The phosphate-binding loop, called “P-loop”, commonly exists through the adenylate-forming enzyme superfamily (9, 11, 15, 21). Thr169 is the first residue of the P-loop. If it is replaced by Ala, the  $k_{cat}/K_m$  values decrease by 500-fold with OSB or ATP as the varied substrates. This indicates that Thr169 plays an essential role in enzyme catalysis, in both OSB binding and ATP delivery. Another mutant saMenE that we assayed was Thr173Ala. It didn't show a great change of  $k_{cat}/K_m$  value as Thr169Ala mutant. However the importance of the P-loop in catalysis of the first adenylation reaction was proved by many published works (20, 22).

### **Ser401 and Glu404**

In addition to ATP, CoA is also required for the reaction catalyzed by saMenE. Based on the structural data a series of residues surround the CoA ligand and form hydrogen bonds between the main chain carbonyls and the



amide NHs of the CoA pantetheine ligand (20, 23). In addition the side chain of a serine (Ser401 in saMenE) is also within hydrogen bonding distance of the CoA. Hence, Ser401Ala mutant was generated and assayed with OSB and CoA as the varied substrates. Although the effect on this mutation in the  $k_{\text{cat}}/K_m$  value with OSB is modest, a 250-fold decrease of  $k_{\text{cat}}/K_m$  value with CoA was observed. This is consistent with our hypothesis that Ser401 is important for CoA binding.

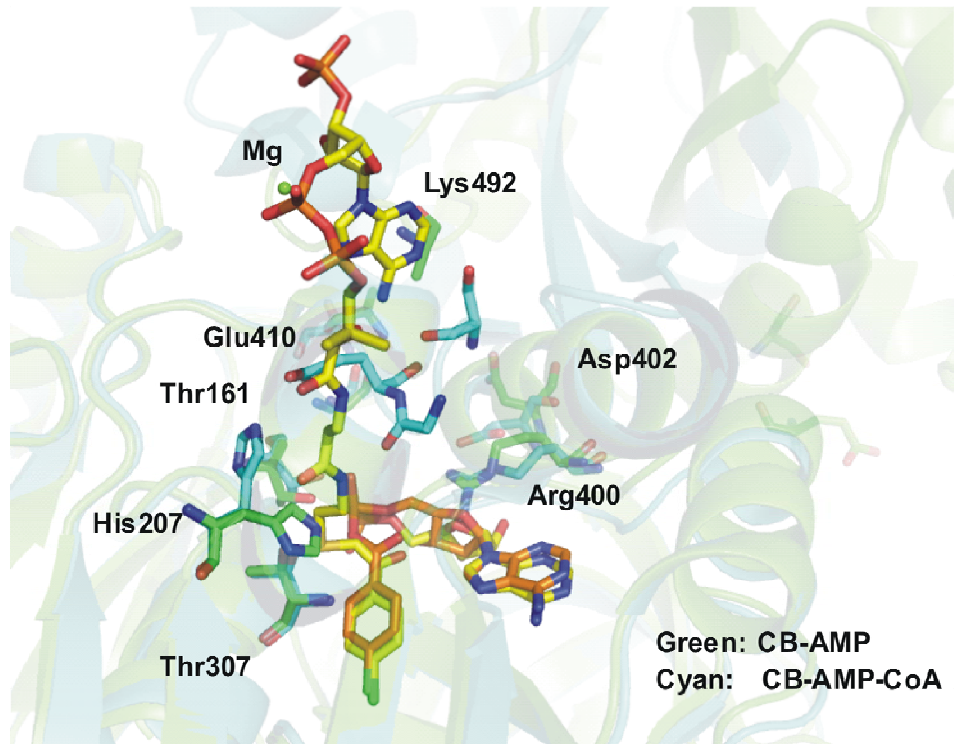
Another mutant of saMenE that was observed to have a significant effect on the CoA  $k_{\text{cat}}/K_m$  value was Glu404Ala. This residue is strictly conserved through the adenylate-forming enzyme superfamily. However in the crystal structure of CBAL, it does not directly interact with the CoA ligand and instead it is coordinated to the histidine side chain which is part of the 4-chlorobenzoate binding pocket. Here we report that the Glu404Ala has a  $k_{\text{cat}}/K_m$  value for CoA that is 800-fold lower than the value for the wild-type enzyme. This observation is interesting and needs further discussion once we could obtain the ligand bound crystal structure of saMenE.

### **Arg394 and Lys396**

All enzymes belonging to the adenylate-forming enzyme superfamily are composed of a large N-terminal domain and a small C-terminal domain that are connected by a peptide linker, which is called the hinge motif or L motif (22-25). During the two step catalytic reaction, the C-terminal domain adopts a

second conformation for the thioesterification reaction. Consequently, we chose to alter the first residue in this hinge motif which is Arg394. In the Arg394AIA mutant the  $k_{cat}/K_m$  value for CoA is reduced 250-fold compared to the value for the wild-type enzyme. These data suggest that saMenE might also experience a domain movement after the first adenylation reaction. However if we pick another residue Lys396, which is not strictly conserved through the superfamily, the mutant didn't show a big change in the value of  $k_{cat}/K_m$ .

The active site residues of overlaid CBAL ligands bound structures used as a parent model were summarized in **Figure 2-9**.

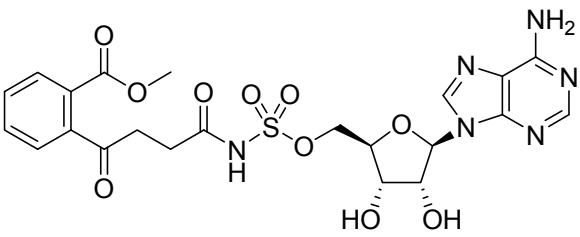
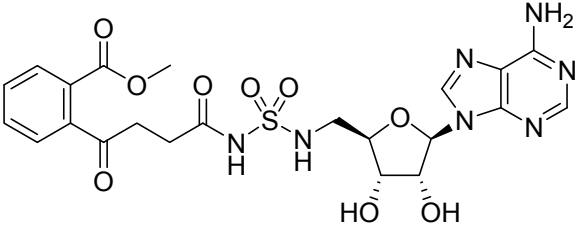
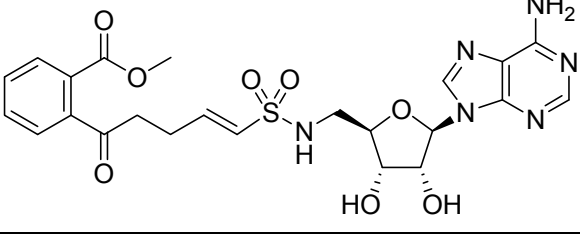
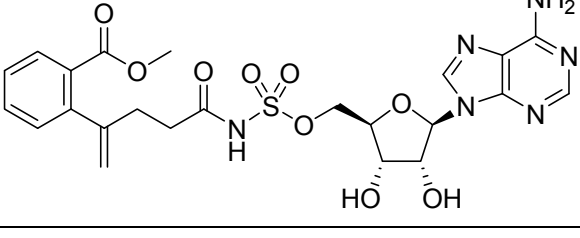
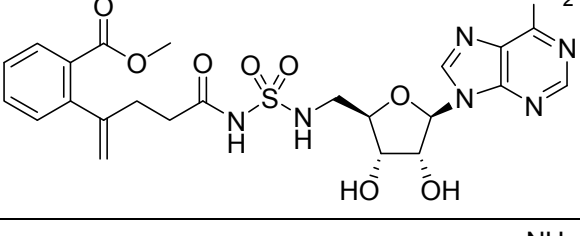
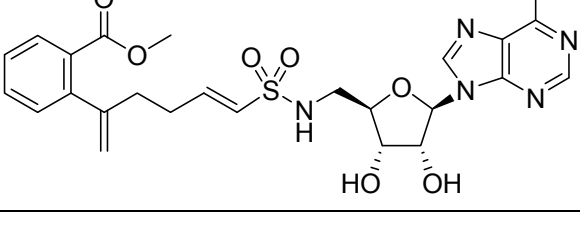


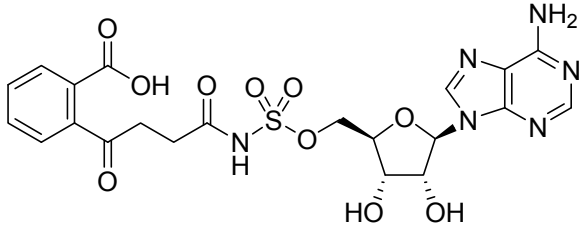
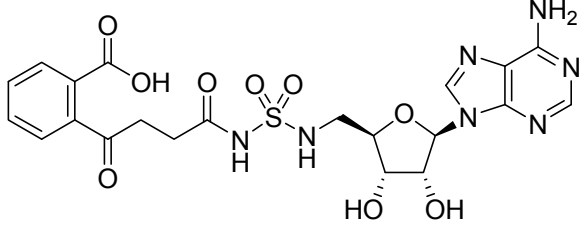
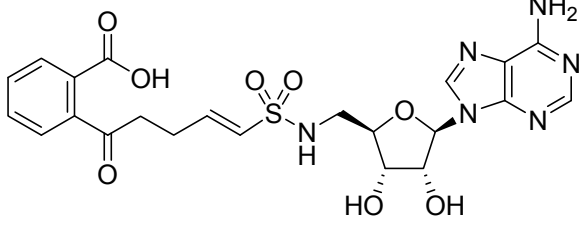
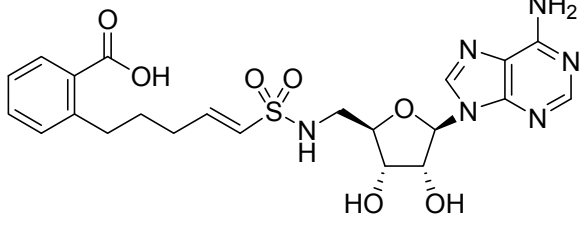
**Figure 2- 9: Insight view of overlaid CBAL ligands bound structures: CB-AMP (PDB#: 3CW8) and CB-AMP-CoA (PDB#: 3CW9). The aromatic ring of the substrate sits snugly in the pocket and a histidine side chain is observed to block the CoA pantetheine arm. In order for CoA to bind to synthetase, the histidine side chain must move. The figure is made by PyMOL.**

#### *Inhibition Study of saMenE with OSB-AMP Intermediate Analogues*

A series of OSB-AMP intermediate analogs were provided by our collaborator Dr Tan's lab. To test the hypothesis that OSB-AMP intermediate analogs might be potent inhibitors for saMenE, the ability of the enzymes to inhibit saMenE in the kinetic assay was evaluated and the IC<sub>50</sub> values are summarized in **Table 2-3**. Inhibition studies showed that OSB-AMS (#9 in

table 2-3) was an uncompetitive inhibitor for OSB with  $K_i$  value of  $12.2 \pm 1.5$  nM. This result was consistent with an ordered Bi uni uni Bi Ping-Pong mechanism and supported the hypothesis of the formation of OSB-AMP intermediate in the kinetic mechanism.

Table 2- 3: Inhibition constant of OSB-AMP intermediate analogs	
analog	IC50 ( $\mu\text{M}$ )
 <p>1</p>	24.6 $\pm$ 3.5
 <p>2</p>	>200
 <p>3</p>	45.7 $\pm$ 2.8
 <p>4</p>	>200
 <p>5</p>	>200
 <p>6</p>	>200

 <p style="text-align: right;">7</p>	0.21±0.2
 <p style="text-align: right;">8</p>	0.63±0.11
 <p style="text-align: right;">9</p>	0.57±0.03
 <p style="text-align: right;">10</p>	32±5.5

## **2.4 Discussion**

### *Bi uni uni Bi Ping-Pong Kinetic Mechanism*

The kinetic mechanism of saMenE was determined using steady-state kinetic analysis. The parallel lines observed in double-reciprocal plots of the ATP&CoA pair and OSB&CoA pair suggested a Ping-Pong kinetic mechanism, which indicated that either ATP or OSB binds before CoA. The intersecting lines observed in double-reciprocal plots of the ATP and OSB pair was indicative of the formation of a ternary E-ATP-OSB complex, which indicated that ATP and OSB may bind with free enzyme sequentially or randomly.

Based on the above initial velocity studies, there are two possible Ping-Pong mechanisms for the three-substrate, three-product reaction as illustrated in **Figure 2-10**. In order to differentiate between a Bi uni uni Bi Ping-Pong mechanism and Bi Bi uni uni Ping-Pong mechanism, the product inhibition patterns of the three-substrate, three-product reaction were investigated by using AMP as the inhibitor. The intersecting lines observed in double-reciprocal plots indicated that AMP was a competitive inhibitor with respect to ATP, which meant that substrate ATP and product AMP interacted with the same species of enzyme. The parallel lines observed in double-reciprocal plots indicated that AMP was a uncompetitive inhibitor with respect to CoA, which meant that substrate CoA and product AMP interacted with different species of enzyme but these species were connected by a

reversible pathway even when the product AMP was absent. In another word, the product inhibition patterns indicated that CoA bond with the enzyme species before the releasing of AMP as a product. In addition, the OSB-AMP intermediate was proposed to be formed in between of the releasing of the PPI and binding of the CoA.

In order to determine the binding order of ATP and OSB in the kinetic mechanism, direct binding affinity of ATP with free enzyme in the presence of  $Mg^{2+}$  was investigated using florescence titration assay. It supported that ATP may bind with the free enzyme first with OSB following. The bisubstrate inhibitor, as the analogue of OSB-AMP intermediate, observed as a competitive inhibitor against ATP and an uncompetitive inhibitor against OSB, further support the binding order of ATP and OSB.



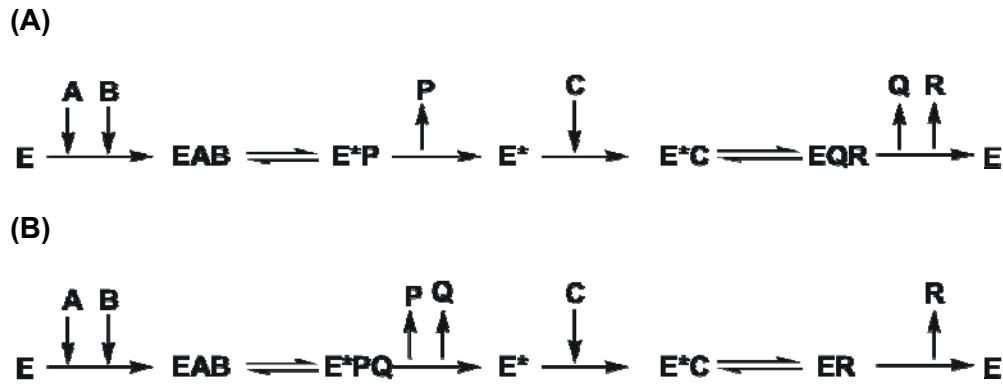


Figure 2- 10: Two types of Ping-Pong mechanisms for the three-substrate, three-product reaction. (A) Bi uni uni Bi Ping-Pong mechanism. (B) Bi Bi uni uni Ping-Pong mechanism. A and B represent ATP and OSB (not necessarily in that order); Q and R represent AMP and OSB-CoA (not necessarily in that order); P represents pyrophosphate; C represents CoA.

#### Sequence alignment

In order to identify residues that might be important for catalysis, a sequence alignment was performed for seven enzymes belonging to the adenylate-forming superfamily. This included firefly luciferase (LUCF), long chain fatty acyl CoA synthetase (LC-FACS), OSB-CoA synthetase (saMenE), NRPS A-domains (DhbE), 4-chlorobenzoate CoA synthetase (CBAL), Acetyl-CoA synthetase (ACS-Se) and gramicidin synthetase A (PheA). The homology among members of the family was assumed to mean that conclusion drawn from one member of the family were able to apply on the others sharing the similar function.

saMenE is 22% identical and 43% similar to the CBAL subunit of *Serratia*

*marcescens*, whose crystal structure was previously determined with bound products (PDB ID#: 3CW8). The sequence alignment was performed by using ClustalW (<http://www.ebi.ac.uk/clustalw/>) shown in **Figure 2-11**. The result of sequence alignment of saMenE and other members will be described respectively in the following paragraph.

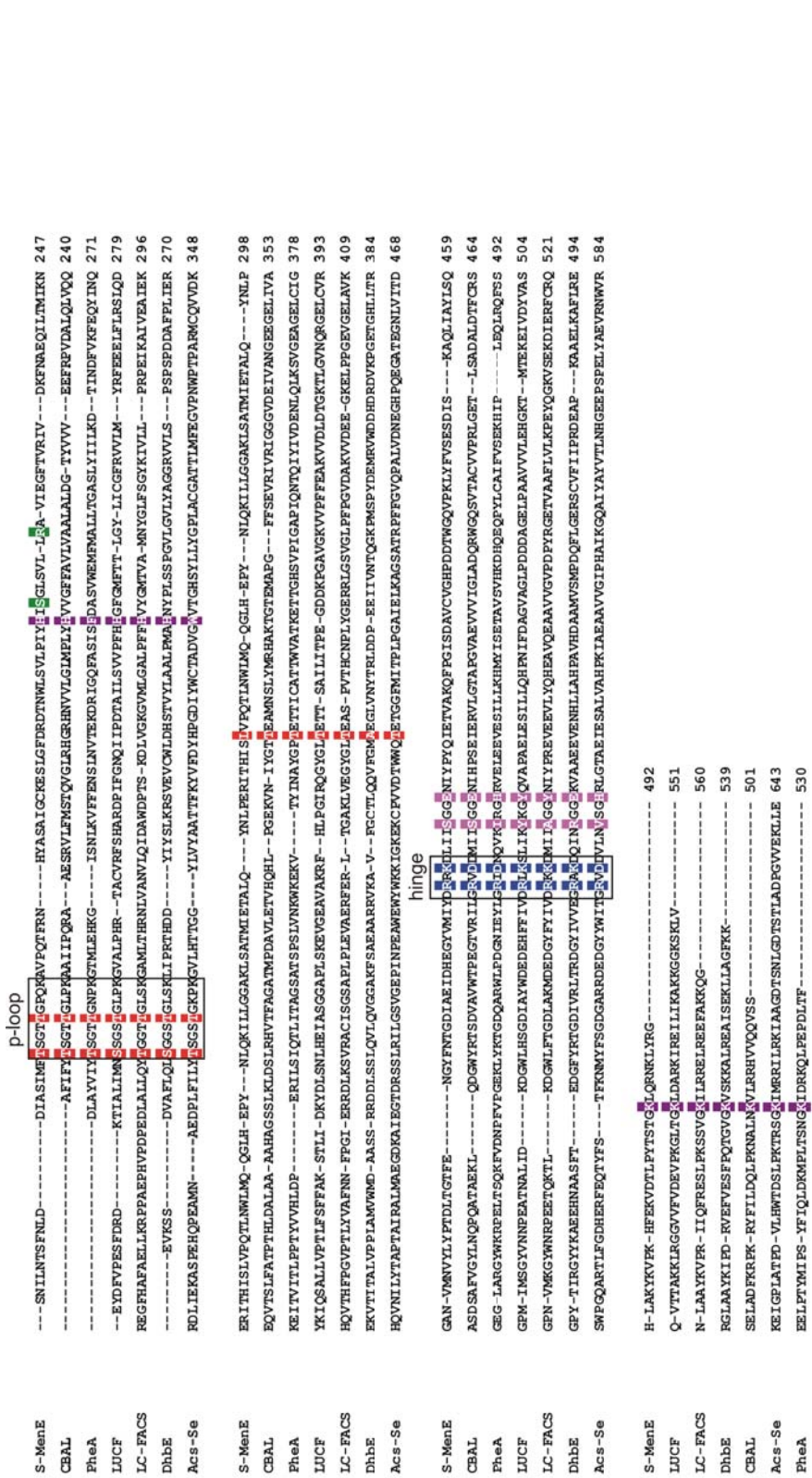


Figure 2- 11: Sequence alignment of enzymes from adenylylate-forming superfamily: firefly luciferase (LUCF), long chain fatty acyl CoA synthetase (LC-FACS), OSB-CoA synthetase (saMenE), NRPS A-domains (DhbE), 4-chlorobenzoate CoA synthetase (CBAL), Acetyl-CoA synthetase (ACS-Se) and gramicidin synthetase A (PheA). Green: substrate binding (COOH group); Light-purple: CoA binding pocket; Red: P-loop; Blue: hinge motif; Purple: substrate binding pocket.

Analysis of the Substrate Binding Pocket

Based on the ClustalW alignment, the residues of the OSB binding pocket (Ala190, His213, Ile214, Ser215, Ser254, Ala282, Ser302, Gly304, Cys309, Ser310, Thr306, Lys483) are mostly conserved with a few exceptions (**Table 2-4**). Substrate specificity study results showed that benzoic acid and o-(3-carboxypropyl)-benzoic acid (OCPB) are very poor substrates, as we might expect based on comparing with the structure of OSB. Since benzoic acid is missing the whole succinyl chain, it has a poor binding affinity with saMenE. Comparing with OSB, OCPB is missing the carboxyl group at C2 position, which is proposed to be important for binding. Based on the previous studies done by Dr. Zhang in our group, it is suggested that the aromatic carboxyl group at C1 position in the OSB is important for binding. The space for fitting the aromatic carboxyl group into the active site is crucial.

**Table 2- 4: Sequence comparison of CBAL and saMenE. The residues belonging to substrate binding pocket are listed**

<b>CBAL</b>	F184	H207	V208	V209	F249	A280	I303	G305	M310	N311	T307	K492
<b>MenE</b>	A190	H213	I214	S215	S254	A282	S302	G304	C309	S310	T306	K483

The analysis of sequence alignment identified the residues that line the hydrophobic binding pocket for OSB. Comparison of the active site residues of saMenE and acetyl-CoA synthetase suggests that the Trp414 residue of ACS constrains the active site in this enzyme so that it operates most efficiently with

smaller substrates. Sequence alignment also demonstrated that a tryptophan is in ACS and a glycine is in saMenE, CBAL, PheA, DhbE and nearly all other enzyme superfamily members. The appearance of the tryptophan at this position distinguishes the enzymes that utilize small acyl substrates from other family members. The residues that form the OSB binding pocket are similar to those residues that form the LC-FACS and CBAL binding sites with some notable differences.

It had been proposed that the homologue of CBAL Val208 is an important specificity determining residue. In PheA, it is an aspartic acid, which interacts with the amino group of the phenylalanine substrate. In DhbE, Asn235 interacts with the hydroxyl groups of the 2,3-dihydroxy-benzoate substrate. However in ACS and CBAL, the homologous residue is a valine, while in the plant 4-coumarate CoA ligase, the residue is an isoleucine which is the same as in saMenE. In all these enzymes, this residue makes van der Waals contacts with the substrate.

The substrate binding pockets of aryl-CoA ligases had been studied using mutagenesis and the construction of hybrid enzymes. From these studies, mutating alanine residues to glycines increased the size of the binding pocket allowing the enzymes to use substituted aromatic substrates more effectively of (26). In saMenE, this residue is an alanine (Ala282). A four residue loop is observed in the CBAL structure that includes Ile303, Gly305, Met310 and Asn311. In another study of plant 4-coumarate CoA ligase demonstrated that

the mutation of the four-residue loop sequences could cause a loss in activity for a number of substrates (27). This suggests that the four-residue loop, which is composed of Ser302, Gly304, Cys309 and Ser310 in saMenE, is important for proper formation of the aryl substrate binding pocket. Rong this is a hypothesis based on homology.

#### *Domain Alternation and the Adenylate-forming Family of Enzymes*

As previously mentioned, enzymes with limited sequence homology often use a common structural and mechanistic architecture to catalyze chemically similar reactions. If this theory can be applied to the adenylate-forming enzymes, it implies that the three subfamilies share the same domain alternation mechanism in which the rotation of the C-terminal domain reconfigures a single active site to catalyze the two distinct half-reactions.

Guilick and coworkers have proposed that the adenylate-forming superfamily of enzymes use a domain alternation strategy in which the enzyme adopts two different conformations to carry out individual steps of a two-step reaction (28). The structural analysis of CBAL, unliganded or bound to compounds that mimic the adenylate intermediate strongly support this hypothesis. For the first adenylation reaction, all crystallographic models demonstrate that the enzymes adopt the A conformation in the unliganded state or when bound to the aromatic substrates or with other nucleotides. In the study of acetyl-CoA synthetase, the B conformation is observed in the

structure of the the enzyme bound to an inhibito or to CoA, which indicates that the binding of CoA might be an apparent trigger for the conformational change. While no single enzyme has been structurally characterized in multiple conformations, the ACS from *S. enterica* and *yeast* provide models for the two proposed conformations, respectively (28-29). Many additional biochemical evidences also support the domain rotation hypothesis (23).

The lysine residue in the active site from the C-terminal domain, which is universally conserved through the enzymes in superfamily, had been shown to be involved in the catalysis of the adenylation reaction but not the thioesterification reaction. This was shown by the site-directed mutagenesis of the Lys483 in saMenE and in propionyl-CoA synthetase (24). The studies of acetylation of this lysine residue in ACS also reached the same conclusion. Similarly, mutation of the C-terminal domain lysine of luciferase results in an enzyme that is unable to carry out the adenylation reaction. No mutations that specifically affected the thioesterification reaction while unaffected the adenylation reaction have been reported for any members of this enzyme superfamily.

The use of the large domain rearrangement by the NRPS enzymes is particularly considered in many studies. The proposed C-terminal domain rotation hypothesis by the NRPS adenylation domains is supported by the conservation of amino acid sequences on both sides of the C-terminal domain.

However, only A conformation has been crystallized and identified for NRPS adenylation domain (17, 30).

The linker between the N-terminal domain and C-terminal domain in saMenE is composed of residues Arg394, Arg395, Lys396, Cys397, Leu398 and Ile399. In addition, the C-terminal CoA binding pocket is composed of residues Ser401, Gly402, Gly403, Glu404, Trp434, Tyr464, Val466 and Lys468 in saMenE. These residues are conserved in CBAL with the exception of Tyr464 and Val466, which in the CBAL are Phe473 and Arg475. The comparison is summarized in **Table 2-5**.

**Table 2- 5: Sequence comparison of CBAL and saMenE. (A) The residues**



belonging to phosphate-binding loop are listed. (B) The residues belonging to linker region are listed. (C) The residues belonging to CoA binding pocket are listed

**A phosphate-binding loop**

<b>CBAL</b>	T161	S162	G163	T164	T165	G166	L167	P168	K169
<b>MenE</b>	T169	S170	G171	T172	T173	G174	P175	Q176	K177

**B linkage region**

<b>CBAL</b>	R400	V401	D402	D403	M404	I405
<b>MenE</b>	R394	R395	K396	D397	L398	I399

**C CoA binding pocket**

<b>CBAL</b>	S407	G408	G409	E410	W440	F473	R475	K477
<b>MenE</b>	S401	G402	G403	E404	W434	Y464	V466	K468

Other examples of enzymes that use the domain alternation mechanism are pyruvate phosphate dikinase, thioredoxin reductase, methionine synthase and some biotin-dependent decarboxylases. However the mechanism of domain alternation by the adenylate-forming enzymes is unique when compared to these other examples. A distinguishing feature from transporting the substrate or cofactor from one active site to another in the other examples, the adenylate-forming enzymes only had one single active site and appeared to use the conformational change to catalyze two half reactions in one active site. This strategy is therefore a way to utilize most efficiently the common

features of a single active site, which are shared for both the andenylation reaction and thioesterification reaction. The different sides of the C-terminal domain are presented sequentially to the active site in the individual half-reactions. (**Fig 2-12**)

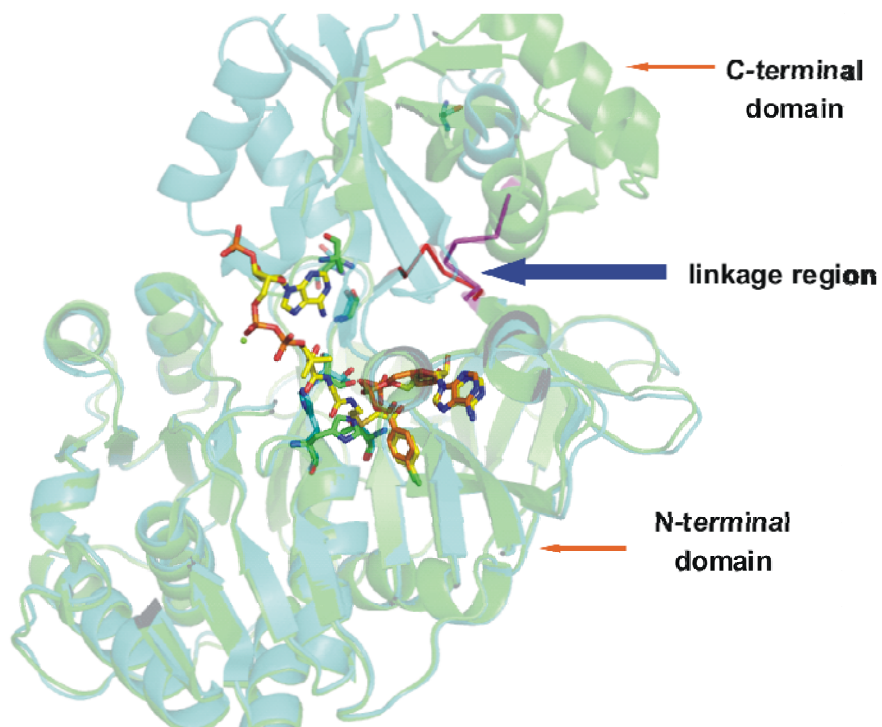


**Figure 2- 12: CBAL is composed of two structural domains, a larger N-terminal domain and a smaller C-terminal domain. After the initial adenylation step, the C-terminal domain rotates by about 140 degree via hinge movement to adopt the second conformation for thioester formation**

*Essential Residues as Functional Anchors in Active Site Architecture*

Based on the available data, we can propose the catalytic mechanism for saMenE, which is separated into two half reactions. This consists of an adenylation step followed by a thioesterification step. The OSB aryl substrate occupies a binding pocket that is similar to the corresponding pocket that accommodates the 4-chlorobenzoate ring of CBAL. The comparison of the active sites of saMenE and CBAL are shown in **Figure 2-13**.

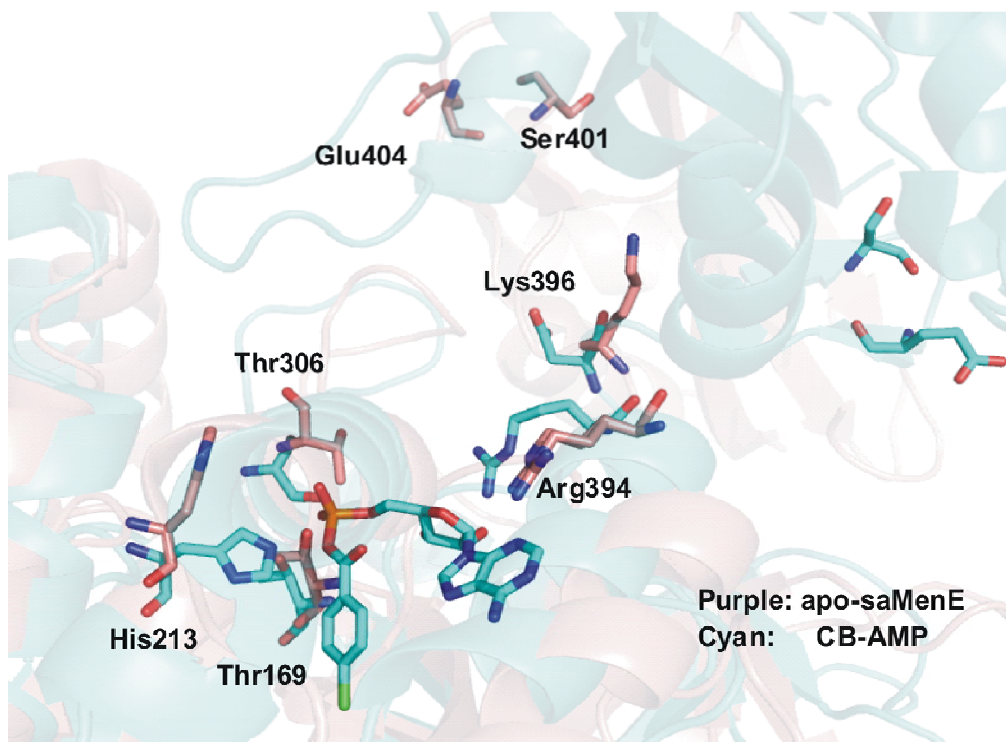


**Figure 2- 13: A comparison of the active sites of bacterial MenE and CBAL. Atoms shown in purple are from the saMenE structure (PDB# 3IPL); atoms shown in cyan are from CBAL structure (PDB #3CW8).**

In the first partial step, an essential histidine, His213, activates the OSB carboxylate group for nucleophilic attack at the phosphorus atom of a negatively charged ATP reactant. Although the C1 carboxylate group is not directly involved in catalysis, the poor binding of OSB analogues indicates that this position is essential for optimal binding. We propose that Arg222 and Ser215 interact with the C1 carboxylate group to stabilize the o-succinylbenzoic acid. In addition to

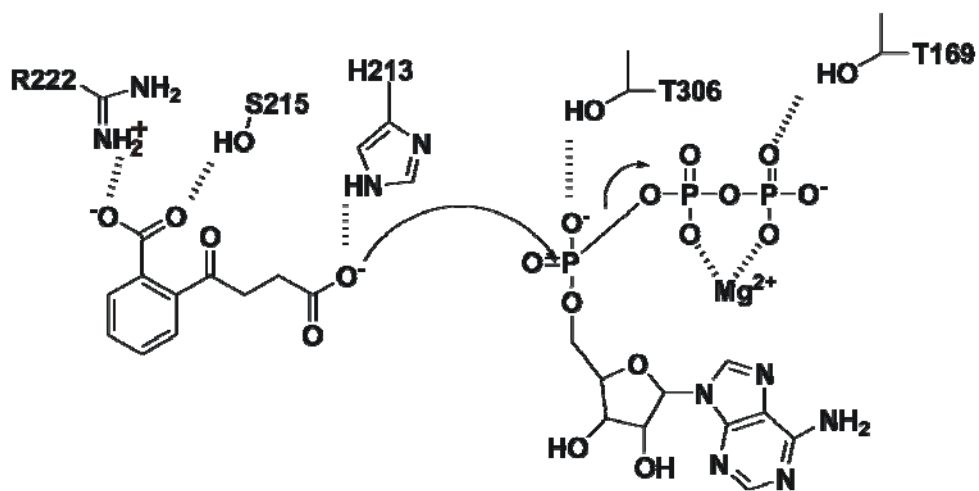
His213, another electropositive group that is also thought to orient the phosphoryl group to shield unfavorable charge-charge interaction with o-succinylbenzoic acid is Thr306. The side chain of Thr306 forms a hydrogen bond with negatively charged phosphoryl group. Thr169 enrolled in the P-loop region is proposed to assist in orienting the PPi unit for displacement. The  $Mg^{2+}$  may also participate in positioning the PPi unit for displacement. (**Figure 2-14A**)

In the second partial step, the CoA thiol functions as a nucleophile attacking the OSB-AMP carbonyl group to displace AMP. Thr306 is proposed to activate the AMP for displacement via forming hydrogen bonds with phosphoryl group oxygen atoms. Meanwhile His213 orients the OSB in an appropriate conformation for the thiol nucleophilic reaction. Corresponding residues that surround the CoA ligand are proposed to be Ser401 and Arg349, which form hydrogen bonds between the main chain carbonyl and the amide NH of the CoA pantetheine group. Interestingly, in the CBAL structure, Glu410, which is found in the vicinity of CoA, does not directly interact with the CoA group but instead forms a hydrogen bond with the His207 side chain. Thus, we propose that Glu404 may have a significant contribution to saMenE catalytic efficiency. (**Figure 2-14B**)

As we mentioned before, domain alternation is widely observed in the adenylate-forming superfamily based on numerous structural studies. Here we propose that many active site residues play multiple roles in catalysis. For

instance, Thr169 stabilizes the ATP phosphoryl group for the adenylation reaction while at the same time activating the AMP group for the thioesterification reaction. Induced by the domain alternation via rotation of peptide linker, some activate site residues adopt different positions in the adenylation and thioesterification reactions.

A



B

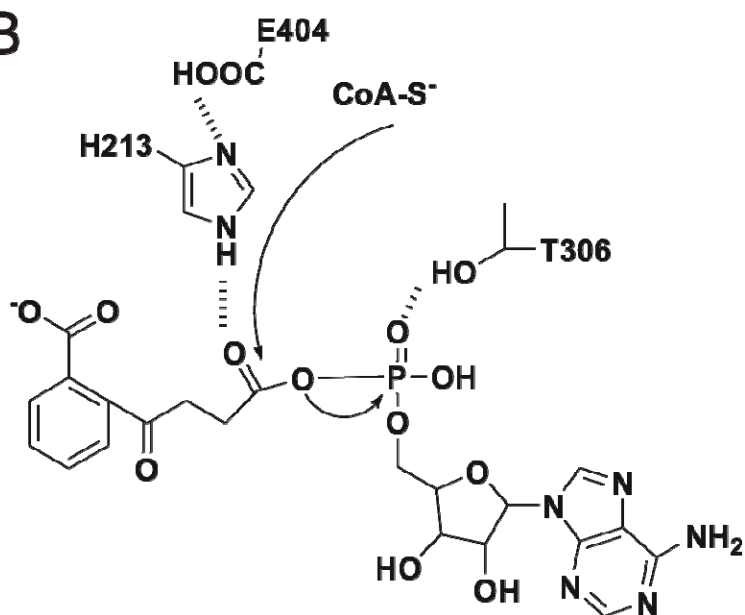


Figure 2- 14: Proposed saMenE mechanism. A. adenylation partial reaction; B. thioesterification partial reaction.

## 2.5 Conclusion

In summary, *S. aureus* MenE was cloned, overexpressed, purified and characterized. The Bi uni uni Bi ping-pong mechanism for saMenE was determined by steady-state kinetic analysis, using OSB, CoA and ATP as substrates. A profile of active site residues as functional anchors of the saMenE substrates has been proposed based on the steady-state kinetic analysis of the mutants. We have identified key residues within OSB binding pocket, phosphate binding loop, CoA binding pocket and hinge motif. Furthermore, we have proposed a catalytic mechanism that includes a series of essential residues in the active site and that are involved in domain alternation.

The essentiality of menaquinone biosynthesis for the survival of bacteria and the lack of this pathway in humans suggests that enzymes in this pathway may be potential targets for the discovery of antibiotics. The kinetic mechanism of OSB-CoA synthetase, a key enzyme in menaquinone biosynthetic pathway, has been determined. The formation of OSB-AMP intermediate was suggested by the kinetic mechanism. The proposed Bi uni uni Bi ping pong mechanism for the OSB-CoA synthetase reaction is a potentially a more universal kinetic scheme for enzymes belonging to adenylate-forming enzyme superfamily. We are currently attempting to obtain the crystal structure of saMenE to reveal the structural mechanism and domain alternation for the two-half reaction mechanism.

## **Reference**



1. Babbitt, P. C., Kenyon, G. L., Martin, B. M., Charest, H., Slyvestre, M., Scholten, J. D., Chang, K. H., Liang, P. H., and Dunaway-Mariano, D. (1992) Ancestry of the 4-chlorobenzoate dehalogenase: analysis of amino acid sequence identities among families of acyl:adenyl ligases, enoyl-CoA hydratases/isomerases, and acyl-CoA thioesterases, *Biochemistry* 31, 5594-5604.
2. Bentley, R., and Meganathan, R. (1982) Biosynthesis of vitamin K (menaquinone) in bacteria, *Microbiol Rev* 46, 241-280.
3. Hiratsuka, T., Furihata, K., Ishikawa, J., Yamashita, H., Itoh, N., Seto, H., and Dairi, T. (2008) An alternative menaquinone biosynthetic pathway operating in microorganisms, *Science* 321, 1670-1673.
4. Reger, A. S., Wu, R., Dunaway-Mariano, D., and Gulick, A. M. (2008) Structural characterization of a 140 degrees domain movement in the two-step reaction catalyzed by 4-chlorobenzoate:CoA ligase, *Biochemistry* 47, 8016-8025.
5. Cole, S. T., Brosch, R., Parkhill, J., Garnier, T., Churcher, C., Harris, D., Gordon, S. V., Eiglmeier, K., Gas, S., Barry, C. E., 3rd, Tekaiia, F., Badcock, K., Basham, D., Brown, D., Chillingworth, T., Connor, R., Davies, R., Devlin, K., Feltwell, T., Gentles, S., Hamlin, N., Holroyd, S., Hornsby, T., Jagels, K., Krogh, A., McLean, J., Moule, S., Murphy, L., Oliver, K., Osborne, J., Quail, M. A., Rajandream, M. A., Rogers, J., Rutter, S., Seeger, K., Skelton, J., Squares, R., Squares, S., Sulston, J.

- E., Taylor, K., Whitehead, S., and Barrell, B. G. (1998) Deciphering the biology of *Mycobacterium tuberculosis* from the complete genome sequence, *Nature* 393, 537-544.
6. Meganathan, R., and Bentley, R. (1979) Menaquinone (vitamin K2) biosynthesis: conversion of o-succinylbenzoic acid to 1,4-dihydroxy-2-naphthoic acid by *Mycobacterium phlei* enzymes, *J Bacteriol* 140, 92-98.
  7. Kwon, O., Bhattacharyya, D. K., and Meganathan, R. (1996) Menaquinone (vitamin K2) biosynthesis: overexpression, purification, and properties of o-succinylbenzoyl-coenzyme A synthetase from *Escherichia coli*, *J Bacteriol* 178, 6778-6781.
  8. Curran, J. P., and Al-Salihi, F. L. (1980) Neonatal staphylococcal scalded skin syndrome: massive outbreak due to an unusual phage type, *Pediatrics* 66, 285-290.
  9. Lodise, T. P., Jr., McKinnon, P. S., and Rybak, M. (2003) Prediction model to identify patients with *Staphylococcus aureus* bacteremia at risk for methicillin resistance, *Infect Control Hosp Epidemiol* 24, 655-661.
  10. Lodise, T. P., McKinnon, P. S., Swiderski, L., and Rybak, M. J. (2003) Outcomes analysis of delayed antibiotic treatment for hospital-acquired *Staphylococcus aureus* bacteremia, *Clin Infect Dis* 36, 1418-1423.
  11. Hiramatsu, K., Hanaki, H., Ino, T., Yabuta, K., Oguri, T., and Tenover, F.

- C. (1997) Methicillin-resistant *Staphylococcus aureus* clinical strain with reduced vancomycin susceptibility, *J Antimicrob Chemother* 40, 135-136.
12. Menichetti, F. (2005) Current and emerging serious Gram-positive infections, *Clin Microbiol Infect* 11 Suppl 3, 22-28.
  13. Moran, G. J., Krishnadasan, A., Gorwitz, R. J., Fosheim, G. E., McDougal, L. K., Carey, R. B., and Talan, D. A. (2006) Methicillin-resistant *S. aureus* infections among patients in the emergency department, *N Engl J Med* 355, 666-674.
  14. Klevens, R. M., Edwards, J. R., Tenover, F. C., McDonald, L. C., Horan, T., and Gaynes, R. (2006) Changes in the epidemiology of methicillin-resistant *Staphylococcus aureus* in intensive care units in US hospitals, 1992-2003, *Clin Infect Dis* 42, 389-391.
  15. Luo, L., Taylor, K. L., Xiang, H., Wei, Y., Zhang, W., and Dunaway-Mariano, D. (2001) Role of active site binding interactions in 4-chlorobenzoyl-coenzyme A dehalogenase catalysis, *Biochemistry* 40, 15684-15692.
  16. Martinez-Blanco, H., Reglero, A., Fernandez-Valverde, M., Ferrero, M. A., Moreno, M. A., Penalva, M. A., and Luengo, J. M. (1992) Isolation and characterization of the acetyl-CoA synthetase from *Penicillium chrysogenum*. Involvement of this enzyme in the biosynthesis of penicillins, *J Biol Chem* 267, 5474-5481.

17. May, J. J., Kessler, N., Marahiel, M. A., and Stubbs, M. T. (2002) Crystal structure of DhbE, an archetype for aryl acid activating domains of modular nonribosomal peptide synthetases, *Proc Natl Acad Sci U S A* 99, 12120-12125.
18. Lu, X., Zhang, H., Tonge, P. J., and Tan, D. S. (2008) Mechanism-based inhibitors of MenE, an acyl-CoA synthetase involved in bacterial menaquinone biosynthesis, *Bioorg Med Chem Lett* 18, 5963-5966.
19. Zheng, R., and Blanchard, J. S. (2001) Steady-state and pre-steady-state kinetic analysis of Mycobacterium tuberculosis pantothenate synthetase, *Biochemistry* 40, 12904-12912.
20. Wu, R., Cao, J., Lu, X., Reger, A. S., Gulick, A. M., and Dunaway-Mariano, D. (2008) Mechanism of 4-chlorobenzoate:coenzyme a ligase catalysis, *Biochemistry* 47, 8026-8039.
21. Branchini, B. R., Magyar, R. A., Murtiashaw, M. H., Anderson, S. M., Helgerson, L. C., and Zimmer, M. (1999) Site-directed mutagenesis of firefly luciferase active site amino acids: a proposed model for bioluminescence color, *Biochemistry* 38, 13223-13230.
22. Wisplinghoff, H., Bischoff, T., Tallent, S. M., Seifert, H., Wenzel, R. P., and Edmond, M. B. (2004) Nosocomial bloodstream infections in US hospitals: analysis of 24,179 cases from a prospective nationwide

- surveillance study, *Clin Infect Dis* 39, 309-317.
23. Reger, A. S., Carney, J. M., and Gulick, A. M. (2007) Biochemical and crystallographic analysis of substrate binding and conformational changes in acetyl-CoA synthetase, *Biochemistry* 46, 6536-6546.
  24. Hisanaga, Y., Ago, H., Nakagawa, N., Hamada, K., Ida, K., Yamamoto, M., Hori, T., Aii, Y., Sugahara, M., Kuramitsu, S., Yokoyama, S., and Miyano, M. (2004) Structural basis of the substrate-specific two-step catalysis of long chain fatty acyl-CoA synthetase dimer, *J Biol Chem* 279, 31717-31726.
  25. Horswill, A. R., and Escalante-Semerena, J. C. (2002) Characterization of the propionyl-CoA synthetase (PrpE) enzyme of *Salmonella enterica*: residue Lys592 is required for propionyl-AMP synthesis, *Biochemistry* 41, 2379-2387.
  26. Kaneko, M., Ohnishi, Y., and Horinouchi, S. (2003) Cinnamate:coenzyme A ligase from the filamentous bacterium *Streptomyces coelicolor* A3(2), *J Bacteriol* 185, 20-27.
  27. Lindermayr, C., Fliegmann, J., and Ebel, J. (2003) Deletion of a single amino acid residue from different 4-coumarate:CoA ligases from soybean results in the generation of new substrate specificities, *J Biol Chem* 278, 2781-2786.
  28. Gulick, A. M., Starai, V. J., Horswill, A. R., Homick, K. M., and Escalante-Semerena, J. C. (2003) The 1.75 Å crystal structure of

acetyl-CoA synthetase bound to adenosine-5'-propylphosphate and coenzyme A, *Biochemistry* 42, 2866-2873.

29. Jogl, G., and Tong, L. (2004) Crystal structure of yeast acetyl-coenzyme A synthetase in complex with AMP, *Biochemistry* 43, 1425-1431.
30. Yonus, H., Neumann, P., Zimmermann, S., May, J. J., Marahiel, M. A., and Stubbs, M. T. (2008) Crystal structure of DltA. Implications for the reaction mechanism of non-ribosomal peptide synthetase adenylation domains, *J Biol Chem* 283, 32484-32491.

## **Chapter III: Inhibition Studies of MenE, an o-Succinylbenzoyl-Coenzyme A Synthetase from *Mycobacterium tuberculosis***

### **3.1 Introduction**

Enzymes that catalyze the adenylation of the carboxylic acid reactant by ATP, followed by displacement of the adenylate by the thiol coreactant, belong to the adenylate-forming superfamily (PFAM00501). This large adenylate-forming enzyme superfamily is composed of three subfamilies: acyl-CoA synthetases, firefly luciferase and the adenylation domains of nonribosomal peptide synthetases (NRPSs) (1-3). Despite the low sequence identity, members of the superfamily exhibit very similar structural elements, folding into a large N-terminal domain and a small C-terminal domain with the active site at the interface between the two domains. X-ray structural data are currently available for members of the adenylate-forming superfamily. Five different conformations have been identified that are associated with different stages of the reaction according to the mechanistic diversity of the superfamily. The movement of small C-terminal domain, induced by the rotation of a solvent peptide linker, is reported to play an essential role in the catalytic mechanism of acyl-CoA synthetases (4).

The adenylate-forming enzyme family catalyze the activation of carboxylic acids through the formation of an AMP anhydride intermediate. A successful

strategy that has previously been used to develop inhibitors of these enzymes has involved the synthesis of 5'-O-(N-arylsulfamoyl) adenosines (aryl-AMS) in which the labile anhydride linker is replaced by a sulfamate group. These compounds are high affinity inhibitors of their target enzymes and mirror the cognate, tightly bound aryl-AMP intermediate (5). The core structures of representative inhibitors are shown in **Fig 3-1**. These molecules were inspired by a class of sulfamoyladenine natural products.

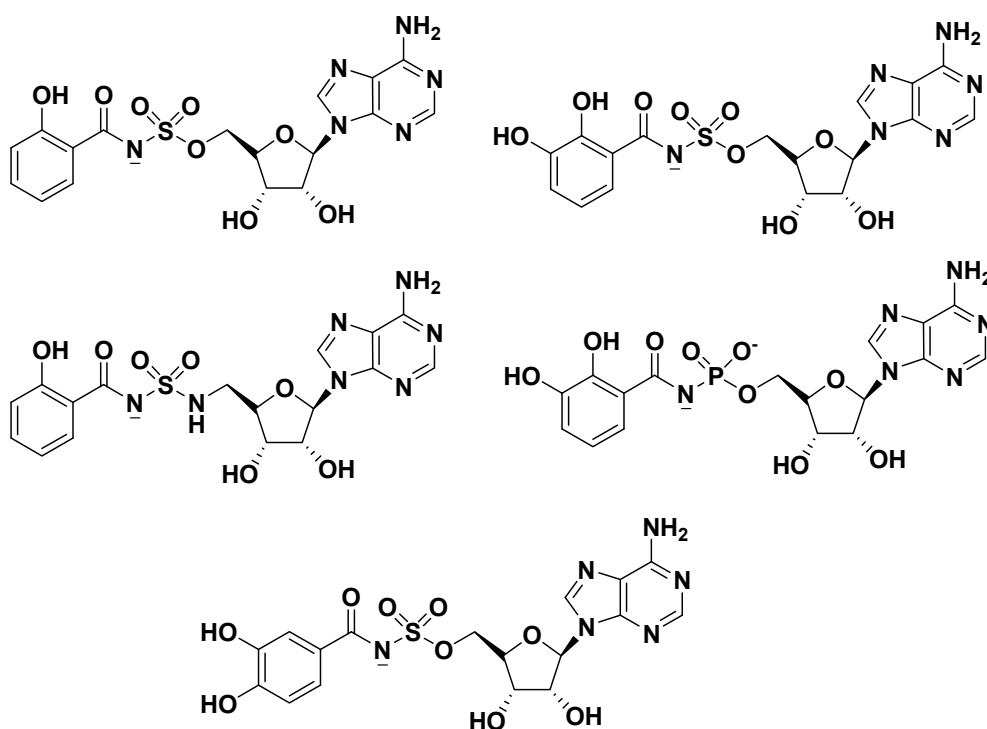


**Figure 3- 1: Inhibitors of aryl acid adenylation enzymes.**

In our efforts to develop inhibitors of menaquinone biosynthesis we have followed a similar strategy to that described above and evaluated the ability of OSB-AMP analogues to inhibit the saMenE as well as the MenE enzymes from *M. tuberculosis* (tbMenE) and *E. coli* (ecMenE). These inhibitors were



provided by our collaborator Dr. Tan. Due to problems expressing mtMenE obtained by direct PCR from genomic *M. tuberculosis* DNA, the mtMenE protein has been obtained using a synthetic codon optimized gene. Several inhibitors have low nanomolar IC<sub>50</sub> values for tbMenE, ecMenE and saMenE.

Based on the inhibition kinetics, some of the bisubstrate analogues bind to the MenE enzymes with extremely high affinity and specificity, which accomplishes the two critical aspects of any effective therapeutic agent. The tight-binding of OSB-AMS to tbMenE suggests that this series of compounds has great promise for use as novel antibacterial agents that target the menaquinone biosynthetic pathway.

## **3.2 Materials and methods**

### *Materials and Substrates*

O-succinylbenzoic acid, the starting reagent of the reactions, was synthesized as described in chapter II. ATP, Coenzyme A and isopropyl- $\beta$ -D-thiogalactopyranoside (IPTG) were purchased from Sigma. Restriction enzymes, DNA ligase, pfu DNA polymerase and DpnI were from stratagene (LA Jolla, CA). Primers were ordered from IDT. Ni-NTA metal affinity chromatography and His-bind metal affinity chromatography were from Novagen. Sephadex<sup>TM</sup> G-25 resin was purchased from Amersham Biosciences. Millipore centriplus YM-30 was from Fisher. All other chemical reagents were purchased from Sigma.

### *Cloning, Expression and Purification of *tbMenE**

The *menE* gene from *M. tuberculosis* was synthesized by changing rare codons to major codons and cloned into pET 15b vector (Novagen) containing a His<sub>6</sub>-tag at the N-terminus. This construct was a gift from Dr. Kisker. The plasmid, pET15bTbMenE, was transformed into XL1Blue cells (Stratagene) and then isolated from a culture of the cells using a DNA purification and gel extraction kit from Qiagen Inc. The correct sequence of the construct was verified by ABI DNA sequencing.

Protein expression was performed by transforming the pET15bTbMenE

plasmid into *E. coli* BL21(DE3)pLysS cells which were grown in 10 mL of Luria Broth (LB) media containing 0.1 mM ampicillin in a 50 mL falcon tube at 37°C overnight. The overnight culture was used to inoculate 500 mL of LB media containing 1 mM ampicillin which was then incubated at 37°C at 250 rpm until the optical density at 600 nm (OD<sub>600</sub>) reached 0.8-1.0. Induction of protein expression was initiated by adding 0.5 mM IPTG and the culture was then incubated with shaking for an additional 20h at 16°C. Cells were harvested by centrifugation at 5,000 rpm for 20 min at 4°C. The cell pellet was resuspended in 30 mL of His-binding buffer (5 mM imidazole, 0.5 M NaCl, 20 mM Tris-HCl, pH 7.9) and the bacteria were disrupted by three passages through a French Press cell (1000 psi). Cell debris was removed by centrifugation at 33,000 rpm for 90 min at 4°C. The clear supernatant was loaded onto a His-bind column (1.5 cm x 15 cm) containing 4 mL His-bind resin (Novagen) that had been charged with 10mL of charge buffer (Ni<sup>2+</sup>). The protein was eluted from the column using the standard His-bind purification procedure using a gradient of 30 mL elute buffer and 30 mL binding buffer mixture. The eluted fractions, which contained the protein, were loaded onto a Sephadex G-25 column (1.5 cm x 55 cm) and eluted using 50 mM Tris-HCl, 0.15M NaCl at pH 7.5 in order to remove imidazole. The protein that eluted from the G-25 column was concentrated at 5,000 rpm for 2h. The purity of tbMenE was determined by 15% SDS-PAGE gel which gave an apparent molecular weight for the protein consistent with the known MW of the protein which is 37kDa. The final

concentration of protein was determined by measuring the absorption at 280 nm and using a calculated extinction coefficient of  $18,575 \text{ M}^{-1}\text{cm}^{-1}$ . The protein was stored at  $-80^{\circ}\text{C}$ .

#### *Reaction of OSB-CoA Synthetase with O-succinylbenzoic Acid*

tbMenE OSB-CoA synthetase activity was monitored according to a previously reported assay coupled to DHNA-CoA synthetase tbMenB in chapter II. tbMenB was cloned, overexpressed and purified, which is stored in 20mM Tris-HCl solution with pH 7.5 at  $-80^{\circ}\text{C}$ . In order to determine the *in vitro* activity, tbMenE and tbMenB were incubated with OSB, baselined from 220-400 nm and scans incrementally taken over this wavelength range wavelengths. Reactions of tbMenE (at concentration 50nm) coupled with tbMenB (at concentration  $4\mu\text{M}$ ) were performed at  $25^{\circ}\text{C}$  in 20mM Tris-HCl buffer, 150mM NaCl,  $1\text{mM Mg}^{2+}$  at pH 7.5 by varying the concentrations of OSB. Formation of DHNA-CoA was monitored by following the increase in the absorbance at 392 nm using an extinction coefficient of  $4000 \text{ M}^{-1}\text{cm}^{-1}$ . A Varian 300-Cary UV-Vis spectrophotometer was used for all kinetic studies.

#### *Steady-state Kinetic Assay*

In order to determine the kinetic mechanism, three sets of kinetic data were obtained in which OSB, ATP and CoA were each varied at fixed concentrations of the other substrates. The first sets of kinetic data were measured by varying the concentration of OSB (20-850 $\mu\text{M}$ ) at different fixed

ATP (240 $\mu$ M) and CoA (360 $\mu$ M) concentrations. The second sets of kinetic data were measured by varying the ATP (60-480 $\mu$ M) concentration at different fixed OSB (240 $\mu$ M) and CoA (360 $\mu$ M) concentrations. The third sets of kinetic data were measured by varying the CoA (60-480 $\mu$ M) concentration at different fixed OSB (120mM) and ATP (240 $\mu$ M) concentrations. Individual data sets were then fit to the Michaelis-Menten equation (**Eq. 3-1**) using Grafit 4.0.

$$v = V_{max} [S] / (K_m + [S]) \qquad \text{Equation 3-1}$$

#### *Inhibition Study and Data Analysis*

The assumption for the steady-state inhibition kinetics is that the inhibitor concentration in solution should be much greater than the enzyme concentration in the assay. However this assumption could fail in two conditions. One is that the inhibitor binds to the target enzyme with very high affinity, which means that the apparent  $K_i$  value is within 10 fold of the total enzyme concentration. In this case, the population of the free inhibitor in solution is significantly decreased due to the formation of the enzyme-inhibitor complex. To measure the  $K_i$  value, it has to decrease the inhibitor concentration so that the inhibitor concentration becoming comparable with enzyme concentration. Another possibility is that the poor solubility of inhibitor could increase the inaccuracy of the free inhibitor concentration. In both cases, the molecules are called tight-binding inhibitors.

In general,  $IC_{50}$  values are measured at least inhibitor concentration

being 5 times of concentration of enzyme. If the  $IC_{50}$  changes significantly as a function of the enzyme concentration, the inhibitor is characterized as tight-binding inhibitor and original steady-state assumption is not appropriate for this case. To characterize the properties of tight-binding inhibitor, Morrison equation is applied for analyzing the inhibition data, where apparent  $K_i$  values can be calculated at various inhibitor concentrations (**Equation. 3-2**). Furthermore,  $IC_{50}$  values can be calculated from the equation  $IC_{50} = 1/2[E] + K_i^{app}$

$$\frac{vi}{vc} = 1 - \frac{([E]_T + [I]_T + K_i^{app}) - \sqrt{([E]_T + [I]_T + K_i^{app})^2 - 4[E]_T[I]_T}}{2[E]_T}$$

**Equation 3-2: Morrison equation for kinetic analysis of tight-binding inhibitors**

Initial velocities of the MenE reaction were determined using the coupled assay described in chapter II. Assays were performed at saturating OSB (240 $\mu$ M), saturating ATP (480 $\mu$ M) and saturating CoA (240 $\mu$ M) at varied concentrations of bisubstrate inhibitors. In each case the concentration of MenE was 50nM and reactions were performed at 25°C.

To determine the inhibition modalities of inhibitors for different substrates, the inhibition data was fitted using equations (**Eq 3-3**) for competitive, noncompetitive and uncompetitive patterns, respectively.  $K_i$  and  $K_{ij}$  values are the inhibition constants for the slope and intercept term, respectively.

$$K_i^{\text{app}} = K_i (1 + [S] / K_m) \quad (\text{A})$$

$$K_i^{\text{app}} = ([S] + K_m) / [ (K_m / K_i) + ([S] / K_{ii}) ] \quad (\text{B})$$

$$K_i^{\text{app}} = K_{ii} (1 + K_m / [S]) \quad (\text{C})$$

**Equation 3-3 (A) Competitive inhibition. (B) Noncompetitive inhibition. (C)**

**Uncompetitive inhibition**

### **3.3 Experimental Results**

#### *Overexpression and Purification of tbMenE*

Overexpression strain pLysS was grown and tbMenE was induced and purified as described before. The purity of tbMenE during various stages of purification was determined by 15% SDS-PAGE gel, which is shown in **Figure 3-2**.

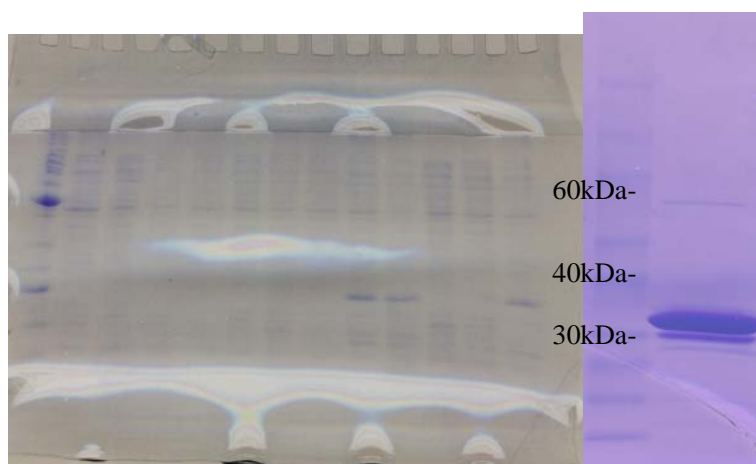


**Figure 3- 2: 15% SDS-PAGE analysis of the fractions from purification of wild-type tbMenE before (left) and after (right) AKTA purification.**

After the purification of tbMenE from Ni-NTA metal affinity chromatography, the concentrated fractions were reloaded onto AKTA purification system and further purified to remove impurities observed on SDS-PAGE gel.



Since tbMenE rapidly lost catalytic activity at 4°C, it was concentrated to 10mg/mL and stored at -80°C right away. The concentration of tbMenE was determined by UV absorbance at 280nm ( $\epsilon = 18575 \text{ M}^{-1} \text{ cm}^{-1}$ ).

The overexpressed and purified tbMenE was shown to catalyze the adenylation and thioesterification of o-succinylbenzoic acid with CoA and ATP as cofactors. No activity was observed in the absence of  $\text{Mg}^{2+}$  ion.

#### *pH Optimum*

The pH optimum was determined by using the range of pH 6.5 to 8.5 manipulated on tbMenE. For tbMenE, the enzyme exhibited optimum OSB-CoA synthetase activity between pH 7.0 and pH 8.5, while at pH=6.5 the enzyme activity decreased significantly. There were no differences in the activity whether Tris-HCl or phosphate buffer was used in the assay.

#### *Kinetics Constants of Enzymes*

tbMenE's activities were analyzed by using previously described assays in Materials and method session. *In vitro*, tbMenE exhibited OSB-CoA synthetase activity. The activity was  $\text{Mg}^{2+}$  dependent. The OSB-CoA synthetase activity of tbMenE increased with increasing the substrate concentration under a fixed  $\text{Mg}^{2+}$  concentration and proper pH range. The data were plotted by using the Michaelis-Menten equation in order to determine the kinetics constant. It was obtained apparent  $K_{m, \text{OSB}}$  value of  $77.3 \pm 9.9 \mu\text{M}$ ,  $K_m$ ,

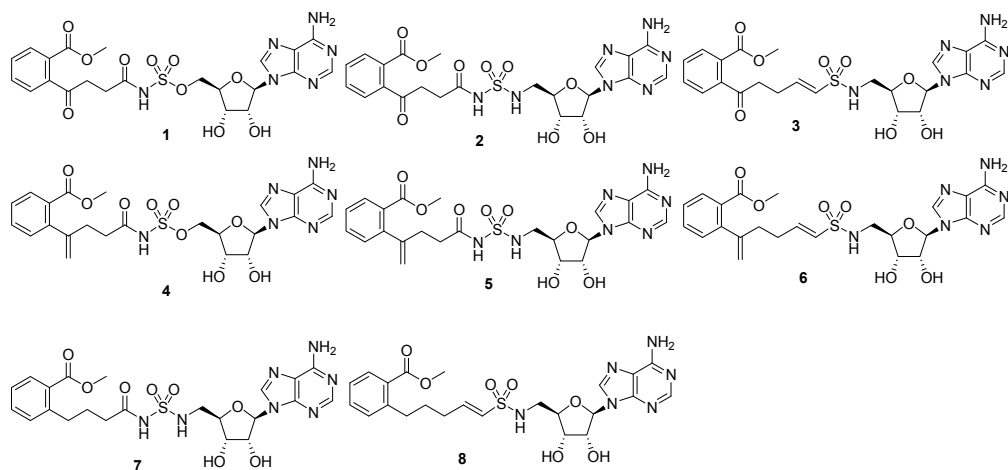
$K_{m, \text{ATP}}$  value of  $120.5 \pm 7.8 \mu\text{M}$  and  $K_{m, \text{CoA}}$  value of  $104.9 \pm 10.2 \mu\text{M}$ ;  $k_{\text{cat}}$  value of  $17.8 \pm 0.3 \text{ min}^{-1}$ . Since the kinetic constants were determined using coupled reaction with *tbMenB*, which converted OSB-CoA to DHNA-CoA. The preincubation control experiment was applied to insure the rate limited reaction was carried out by *tbMenE* in the assay. The data were plotted by using the Michaelis-Menten equation in order to determine the kinetics constant. The two sets of kinetic constant were comparable with each other.

#### *IC<sub>50</sub> values of tbMenE with OSB-AMP intermediate analogs*

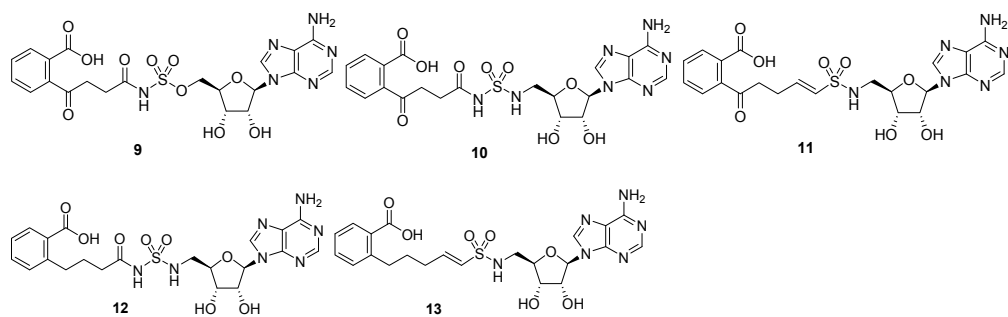
A series of OSB-AMP intermediate analogs were provided by our collaborator Dr Tan. These bisubstrate inhibitors, which closely mimic the OSB-AMP intermediate, can be arranged into two groups (**Fig 3-3**). In group I, to avoid the potential pharmacological liabilities of the OSB fragment, the  $\alpha$ carboxylate is methylated. In group II, the  $\alpha$  carboxylate is not protected and the exo-methylene analogues are not presented. To test the hypothesis that OSB-AMP intermediate analogues might be potent inhibitors for *tbMenE*, the inhibition assays were used to determine  $\text{IC}_{50}$  values which are summarized in **Table 3-1**. The  $\text{IC}_{50}$  values with *saMenE* and *ecMenE* were also determined and are also given in **Table 3-1**. From the data, it demonstrates that the sulfamate MeOSB-AMS, sulfamide MeOSB-AMSN, sulfamate OSB-AMS and sulfamide OSB-AMSN are effective inhibitors against *tbMenE*. The non-protected sulfamate OSB-AMS is proved to be the

most potent inhibitor, with an  $IC_{50}$  value of  $0.049 \pm 0.007 \mu\text{M}$

### Group I

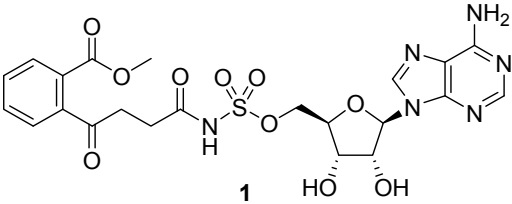
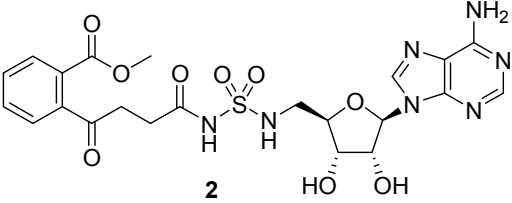
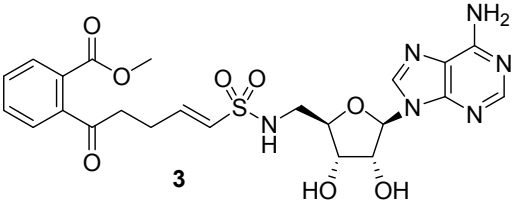
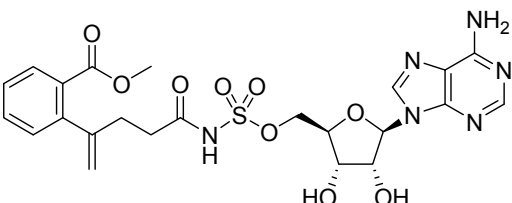


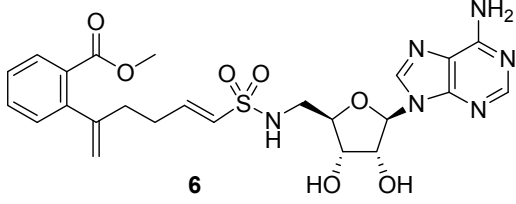
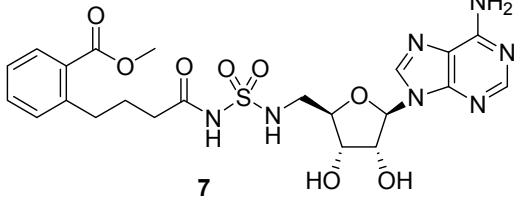
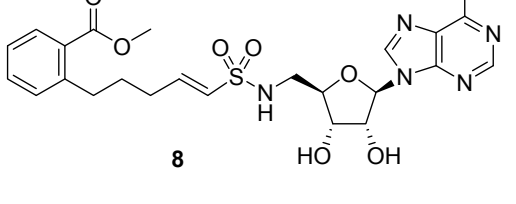
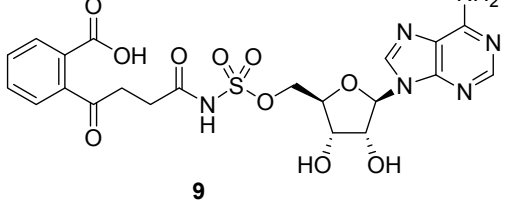
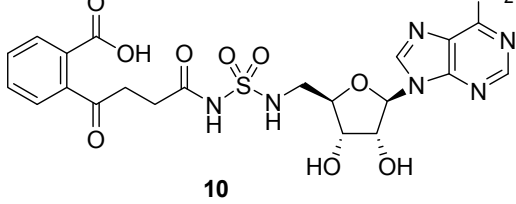
### Group II

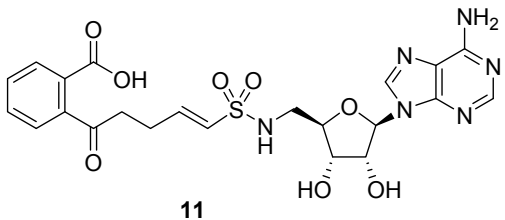
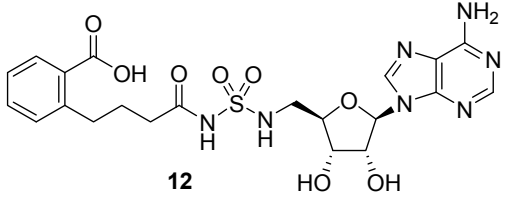
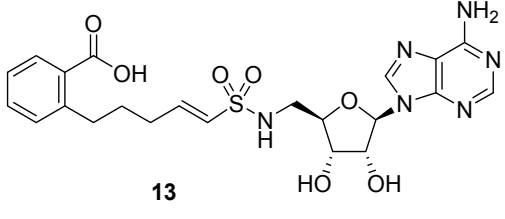


**Figure 3- 3: The bisubstrate inhibitors, which closely mimic the OSB-AMP intermediate can be divided into two groups.**

**Talbe 3- 1: IC<sub>50</sub> values of tbMenE, saMenE and ecMenE against designed bisubstrate inhibitors**

Inhibitors	tbMenE IC <sub>50</sub> (μM)	saMenE IC <sub>50</sub> (μM)	ecMenE IC <sub>50</sub> (μM)
 <p><b>1</b></p>	14.2±0.22	24.6±3.5	38.0±3.0
 <p><b>2</b></p>	23.5±1.0	>200	74.1±2.8
 <p><b>3</b></p>	117±3.9	45.7±2.8	5.7±0.7
 <p><b>4</b></p>	>200	>200	>200

 <p style="text-align: center;"><b>6</b></p>	>200	>200	>200
 <p style="text-align: center;"><b>7</b></p>	>200	>200	>200
 <p style="text-align: center;"><b>8</b></p>	>200	>200	>200
 <p style="text-align: center;"><b>9</b></p>	0.049±0.00 7	0.24±0.01 2	0.21±0.2
 <p style="text-align: center;"><b>10</b></p>	0.20±0.015	0.59±0.04 8	0.63±0.1 1

 <p style="text-align: center;"><b>11</b></p>	0.16±0.052	0.33±0.06 4	0.57±0.0 3
 <p style="text-align: center;"><b>12</b></p>	101±1.4	85±9.8	N/A
 <p style="text-align: center;"><b>13</b></p>	106±4.2	54.4±2.3	32±5.5

#### *Inhibition Kinetics of Sulfamate OSB-AMS*

In chapter II, a Bi uni uni Bi Ping-Pong reaction mechanism has been proposed for saMenE is supported by steady-state kinetic study and the formation of an OSB-AMP reaction intermediate is proposed based on the reaction mechanism. Therefore, we hypothesize that the bisubstrate inhibitors, which closely mimic the native OSB-AMP intermediate, could exhibit potent inhibitory effects on the enzyme reaction.

Initial estimates of the inhibitory potencies of sulfamate OSB-AMS and derivatives with tbMenE using steady-state Michaelis-Menten kinetics indicated these bisubstrate inhibitors that mimic the OSB-AMP intermediate were tight-binding inhibitor with a  $K_i^{app}$  in the nanomolar range. Under the conditions that are used to generate initial velocity data that the amount of enzyme-bound inhibitor could be a significant fraction of the total inhibitor concentration. Therefore, the Michaelis-Menten equation is not appropriate to use for the analysis of kinetic data. Instead, the Morrison equation (**Eq 3-2**) was used to analyze the kinetic data. As an example, the  $K_i^{app}$  value of tbMenE with OSB-AMS is  $16.7 \pm 0.5$  nM by fitting the data to the Morrison equation. (**Fig 3-4**)

$$\frac{v_i}{v_c} = 1 - \frac{([E] + [I] + K_i^{app}) - \sqrt{([E] + [I] + K_i^{app})^2 - 4[E][I]}}{2[E]}$$

**Equation 3-2 Morrison equation for kinetic analysis of tight-binding inhibitors**

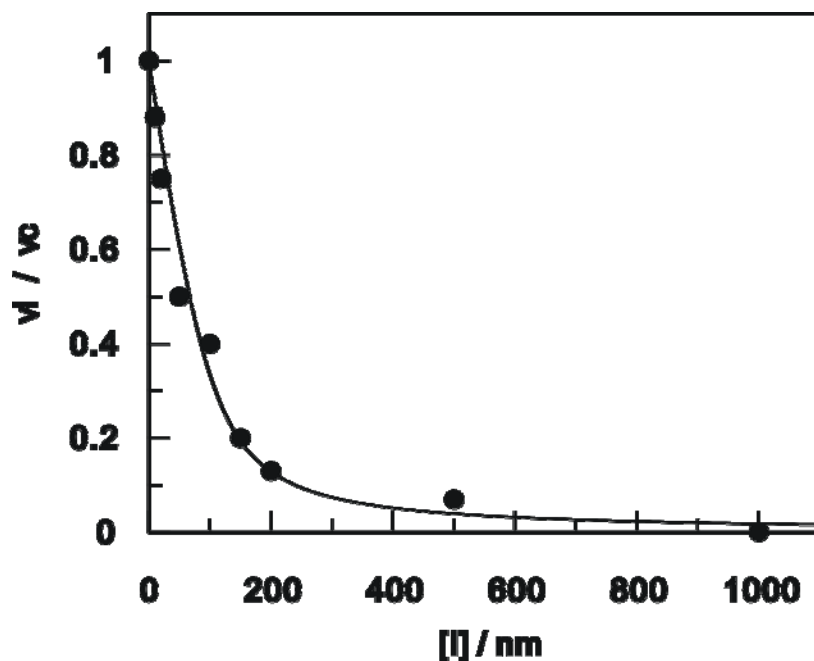


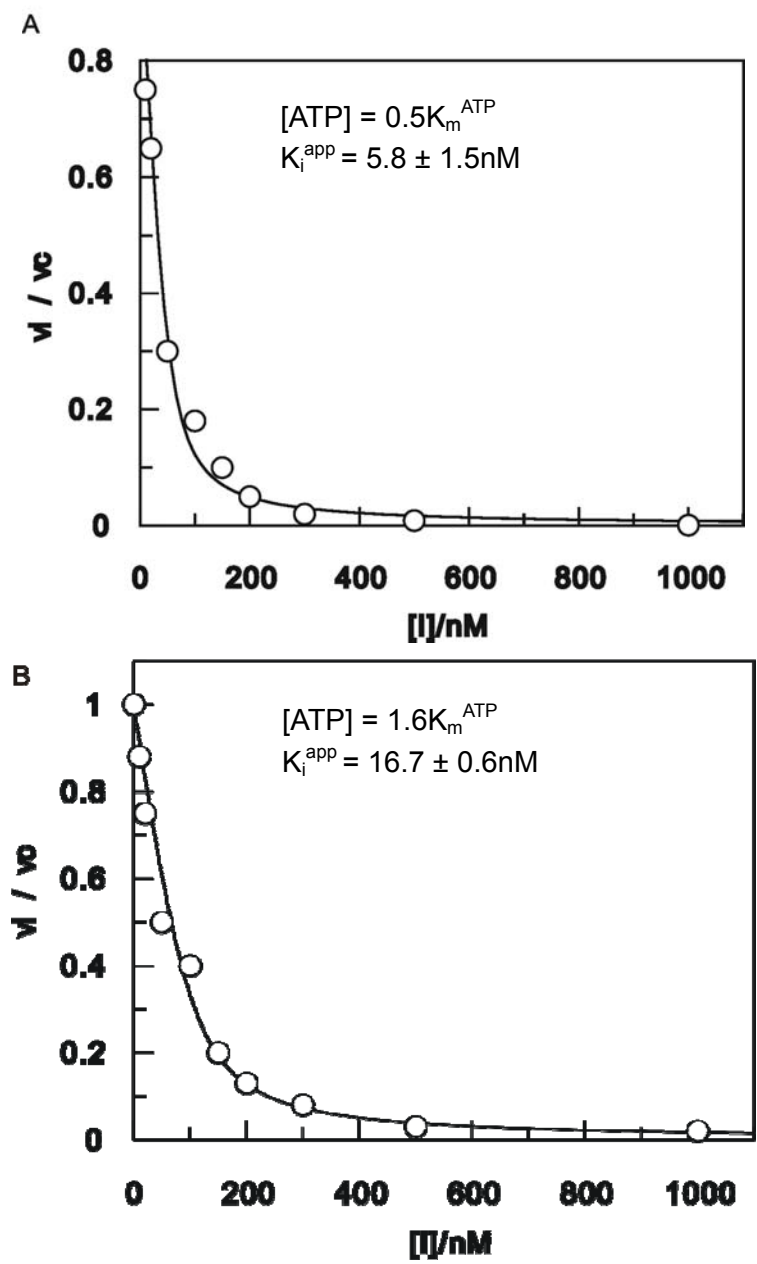
**Figure 3- 4: Morrison analysis of tight-binding inhibition of tbMenE by sulfamate OSB-AMS inhibitor. The  $K_i^{app}$  value of  $16.7 \pm 0.6\text{nM}$  is determined by nonlinear fitting data collected at different inhibitor concentrations (0-1 $\mu\text{M}$ ) to the Morrison equation.**

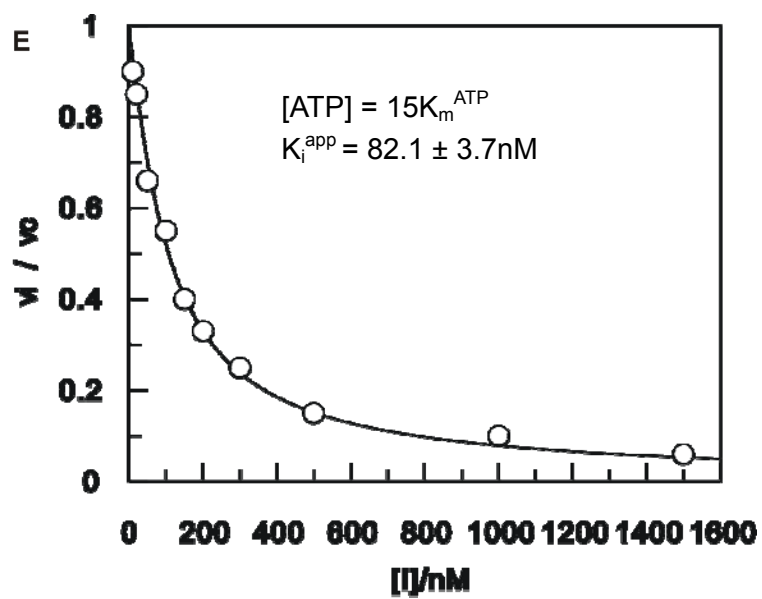
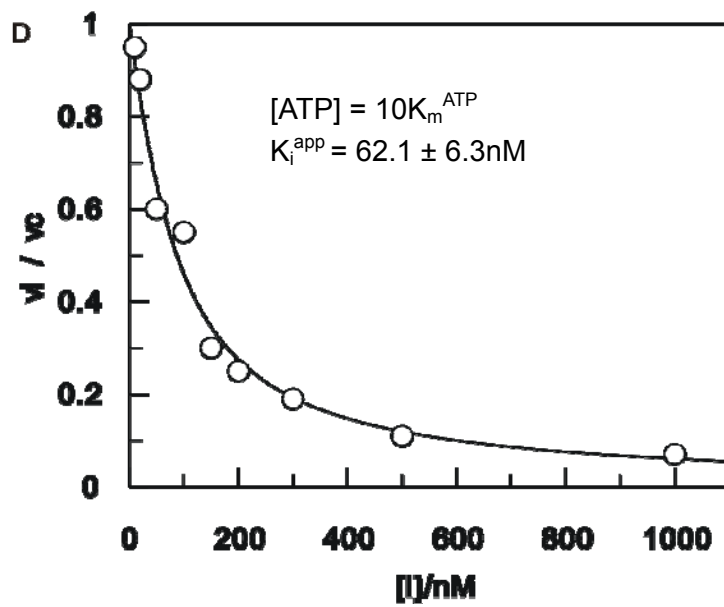
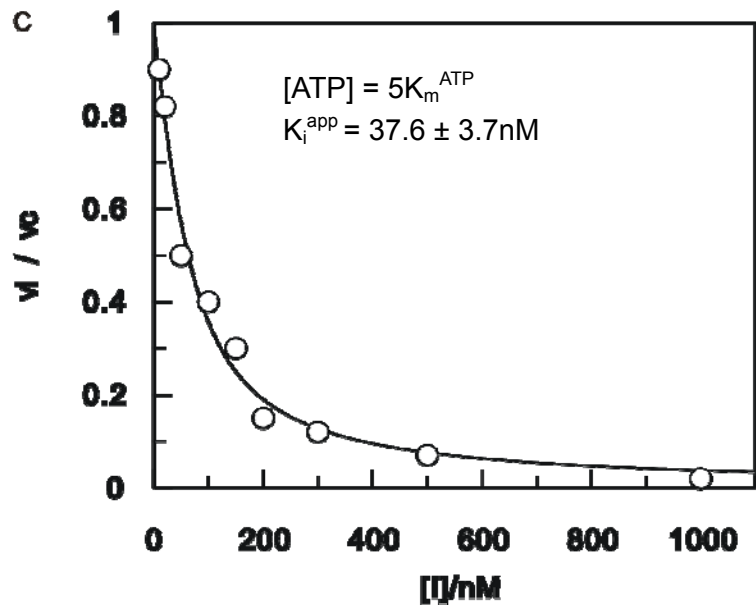
The inhibition of tbMenE by sulfamate OSB-AMS against each of the two substrates OSB and ATP can be used to determine the inhibition mechanism. In the methods section, three equations, which correspond to competitive, uncompetitive and noncompetitive inhibition, were used to analyze the data.

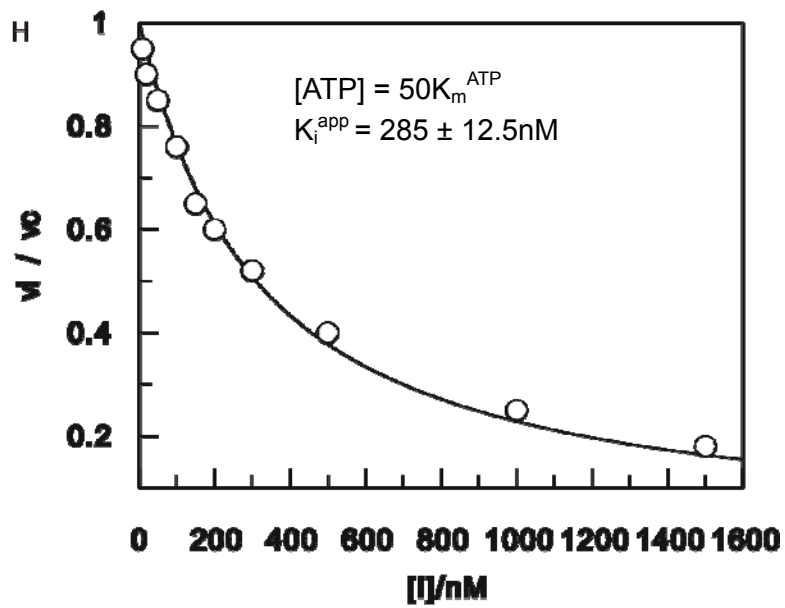
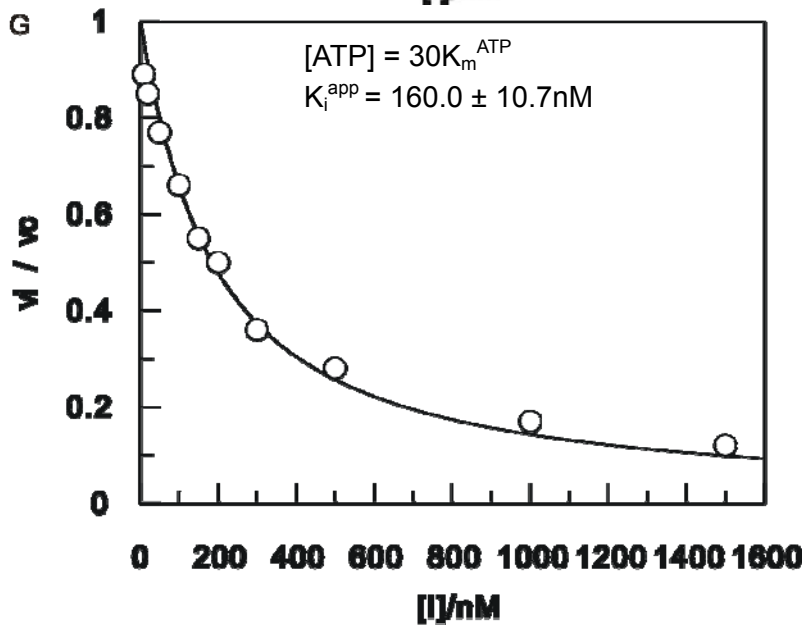
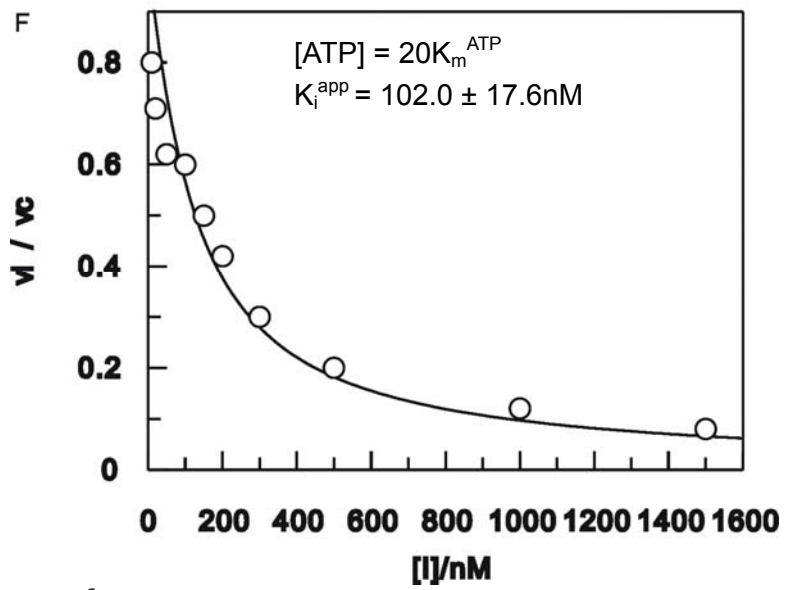
When the concentrations of ATP (0.06-6mM) and inhibitor (0-1 $\mu\text{M}$ ) are varied at fixed saturating concentrations of OSB (120 $\mu\text{M}$ ) and CoA (240 $\mu\text{M}$ ), data analysis using the Morrison equation gave a series of  $K_i^{app}$  values. The  $K_i^{app}$  values changed on the choice of a range of ATP concentrations that span the  $K_m$ . Similarly, another series of  $K_i^{app}$  values are estimated by using the



Morrison equation, when OSB and inhibitor concentrations are varied at fixed concentration of ATP and CoA. However, the  $K_i^{app}$  value is not very sensitive to changes in the concentration of these substrates. The analysis of steady-state kinetics is shown in **Figure 3-5**.







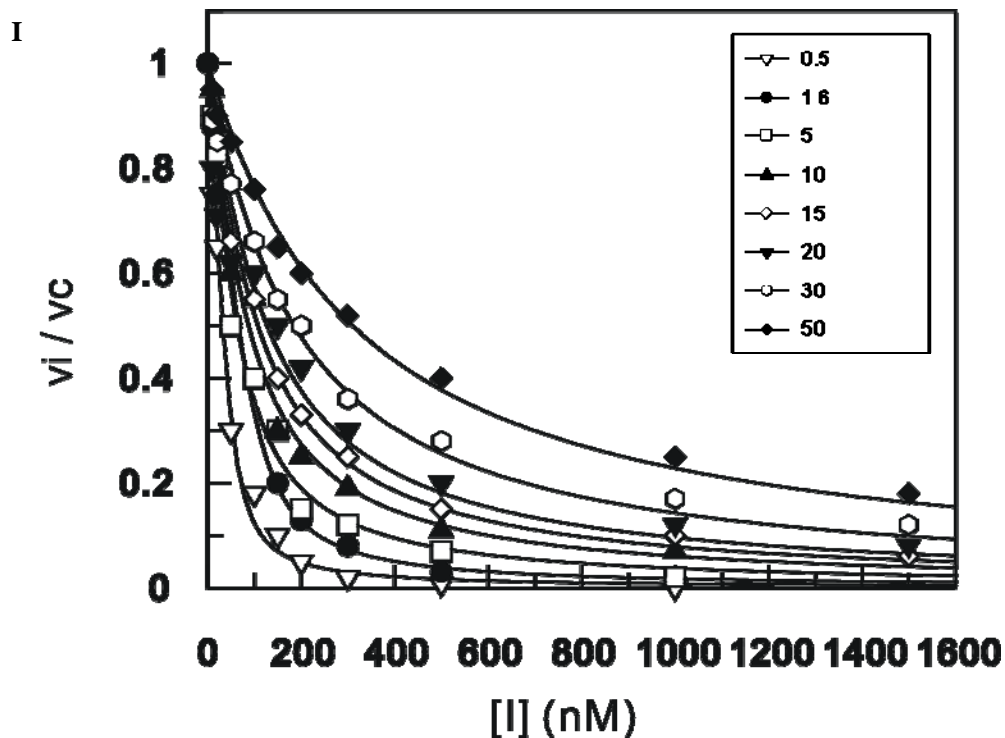
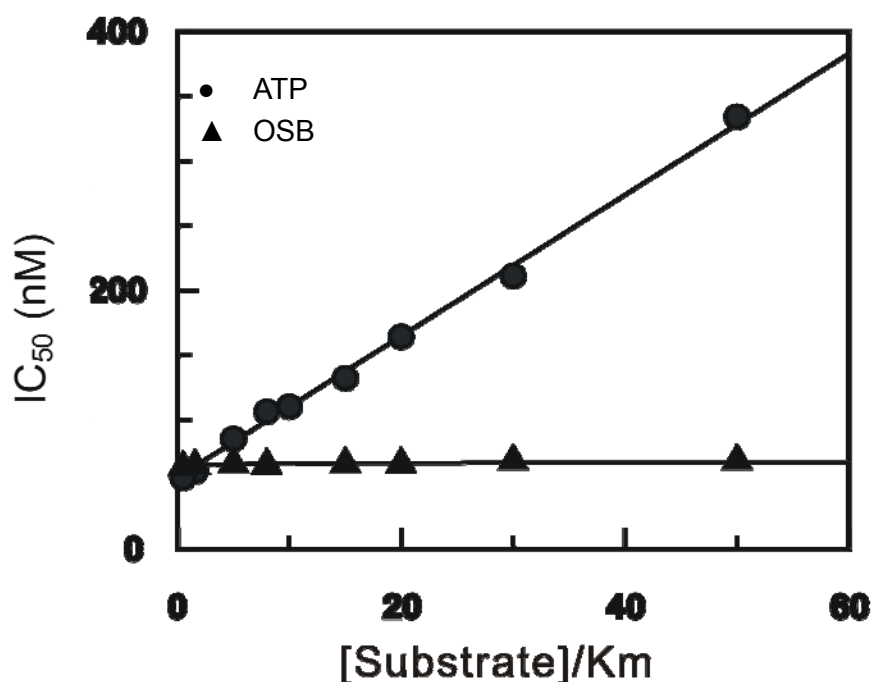


Figure 3- 5: Morrison analysis of tight-binding inhibitor sulfamate OSB-AMS against tbMenE under various inhibitor and ATP concentrations.  $K_i^{app}$  values are obtained having OSB concentration fixed at  $120\mu\text{M}$  and CoA concentration fixed at  $240\mu\text{M}$ . The  $K_i^{app}$  values varied as a function of ATP concentration at 0.06mM, 0.2mM, 0.6mM, 1.8mM, 2.4mM, 3.6mM, 6.0mM (A-H).

As illustrated in **Figure 3-6**, the change in  $K_i^{app}$  versus substrate concentrations is described by the equations discussed in experiment and method section previously in this chapter. It can be used to calculate the real binding potency,  $K_i$  and  $K_{ii}$ , which reflects the type of inhibition. Thus, replotting of  $K_i^{app}$  versus substrate concentration reveals the binding modality for the tight-binding inhibitor. The quality of the assessment is predicted on the choice

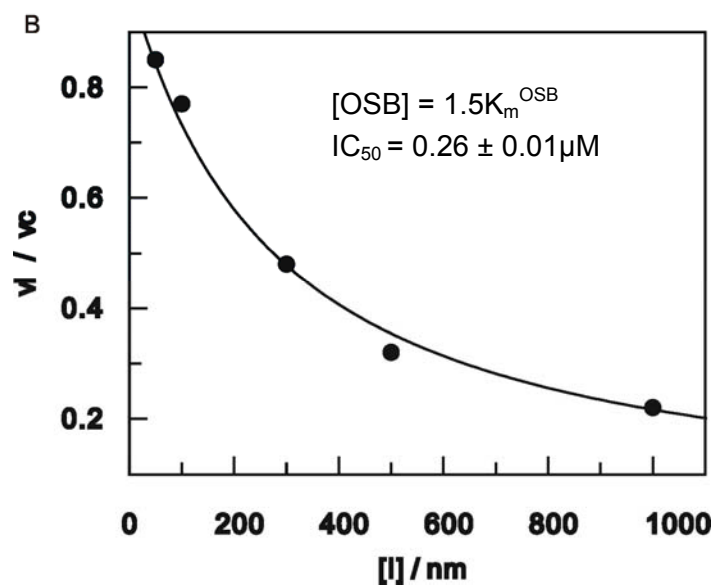
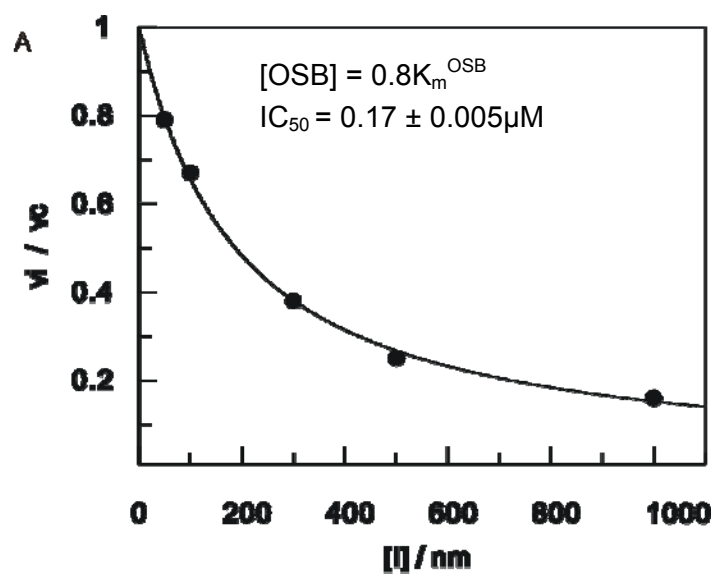
of a range of ATP concentrations that span the  $K_m$ , which indicated that sulfamate OSB-AMS is a competitive inhibitor for ATP with  $K_i$  value of  $5.4 \pm 0.07$  nM and an uncompetitive inhibitor for OSB with  $K_i$  value of  $11.2 \pm 0.9$  nM.

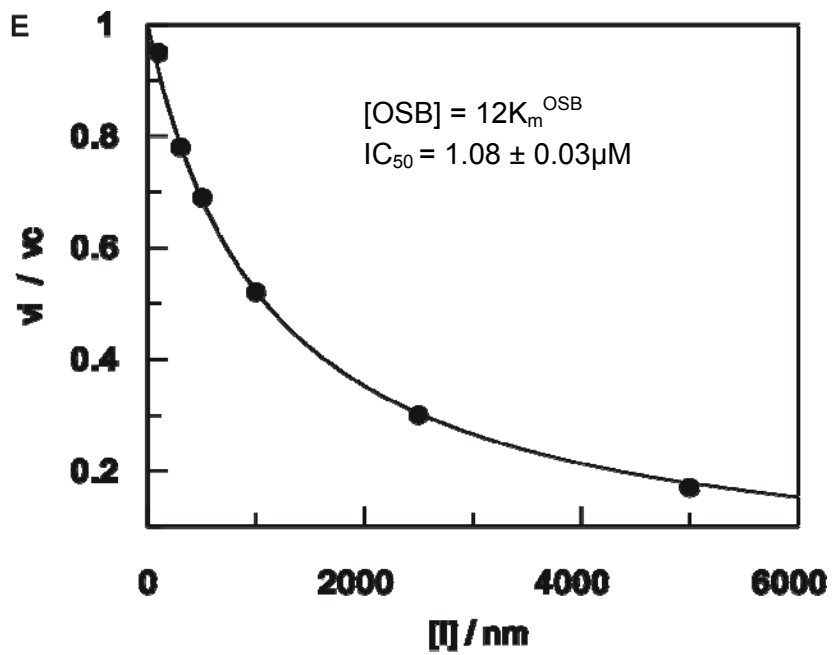
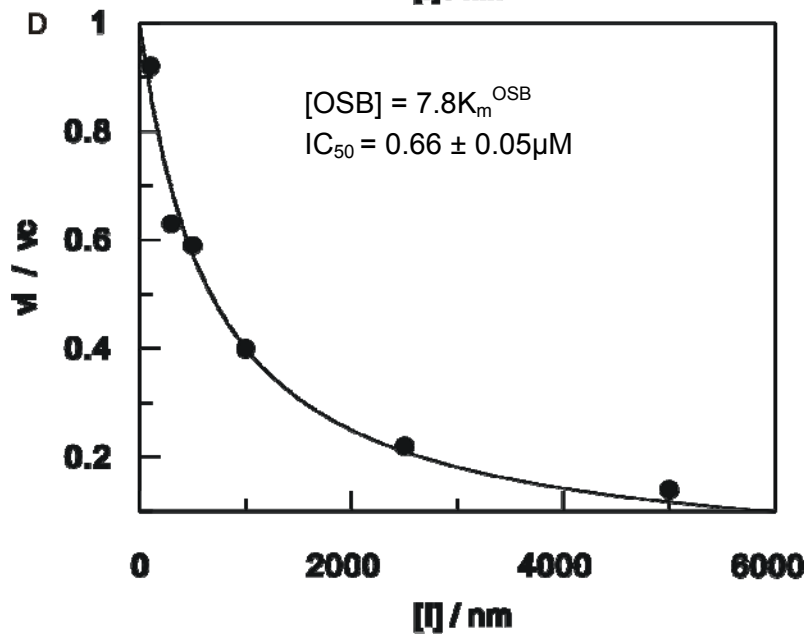
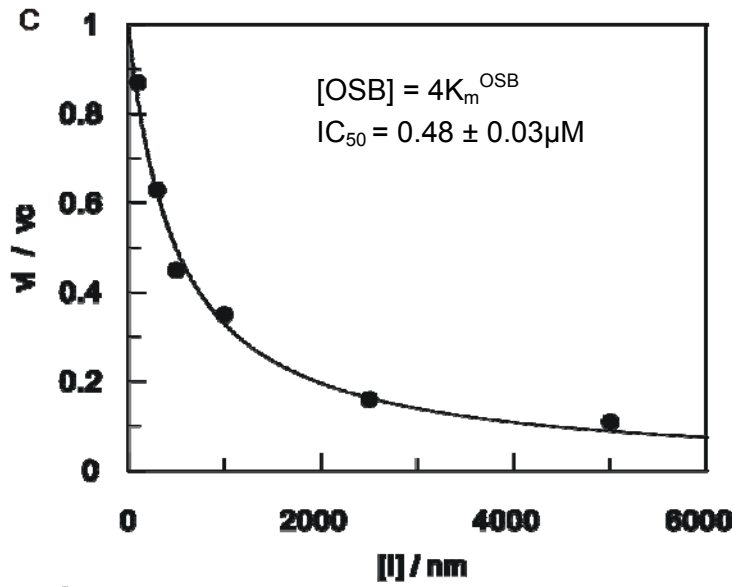


**Figure 3- 6: A plot of  $K_i^{app}$  vs substrate concentration can reveal the binding modality for the tight-binding inhibitor. The real  $K_i$  and  $K_{ii}$  values can be obtained from a fit using the appropriate inhibition mechanism model. Sulfamate OSB-AMS is a competitive inhibitor for ATP and an uncompetitive inhibitor for OSB. Mention tbMenE. Give the  $K_i$  values obtained**

The inhibition of ecMenE with sulfamate OSB-AMS was also detected and kinetic data was analyzed as described before. Herein we varied the OSB concentration at fixed concentration of ATP (1.2 mM). A series of  $K_i^{app}$  values are obtained via fitting curves using the Morrison equation. Then the inhibition modality is determined by replotting the  $IC_{50}$  values versus different substrate

concentrations, which indicates that sulfamate OSB-AMS is a competitive inhibitor for OSB with a  $K_i$  value of  $128 \pm 5$  nM. (Figure 3-7)





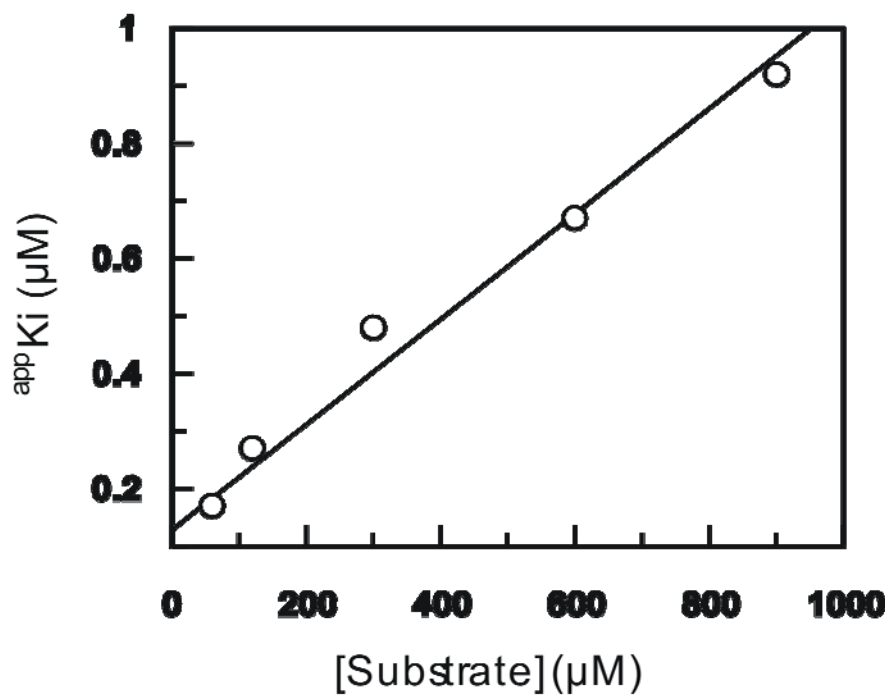


Figure 3- 7:  $K_i^{app}$  values of inhibitor sulfamate OSB-AMS against ecMenE under various OSB concentrations at 0.062mM, 0.116mM, 0.308mM, 0.600mM and 0.924mM (A-E).  $K_i^{app}$  values are obtained having ATP concentration fixed at 1.2mM and CoA concentration fixed at 1.0mM. The  $K_i^{app}$  values then are replotted versus substrate concentration, which indicates that sulfamate OSB-AMS is competitive inhibitor against OSB with ecMenE.



### **3.4 Discussion**

#### *Expression of tbMenE*

Previously, we have encountered difficulty while expressing tbMenE in *E. coli* expression system via pET15b, pET23b and pET43b expression vectors, in which the His-tag is incorporated at either the N- or C- terminus. The expression of tbMenE also failed in *M. smegmatis* expression system using pVVP, pVV16 and pJAM2 vectors.

The frequencies, with which the different codons appear in genes in *E. coli*, are different from those in genes derived from other organisms. The amount of specific tRNAs is also reflected by the frequency of the codons, which means that a tRNA which recognizes a rarely used codon is present in low amounts. Consequently, various genes that contain codons which are rare in *E. coli* may be inefficiently expressed by this organism. Rare codons can cause poor expression of the synthesized protein or disincorporation of amino acids (6). Clusters of rare codons may have a higher chance to create translation errors and reduce the expression level. This problem can be solved in two ways. One choice is to exchange codons in the target gene for codons which are more frequently used in *E. coli*. Alternatively, it can be solved by co-production of the rare tRNAs. In the host strain Rosetta(DE3)pLysS (Novagen), the rare codons AGG, AGA, AUA, CUA, CCC, and GGA are supplemented.

Unfortunately, tbMenE has 35 rare codon sites, which may be the reason why we failed to obtain expression in *E. coli*. Consequently, our collaborator Dr

Kisker designed and synthesized the *tbmenE* gene, in which rare codons are replaced with codons commonly used by *E. coli*. Subsequently, the synthetic *tbmenE* gene was expressed in *E. coli* using standard strategies. Although the expression level of tbMenE was significantly improved, most of expressed tbMenE was insoluble. To solve this problem, we tried to lower the IPTG induction temperature to 16°C, decrease the IPTG concentration as low as 0.5mM for induction and add 10% glycerol during overexpression. Also we varied the length of induction from 12h to 24h in order to find the best condition 0.5mM IPTG for induction followed by overexpression at 16°C for about 20h obtaining higher overexpression level and better solubility. Under this condition, the yield of enzyme purification is about 0.5mg per 1L LB broth media and the protein didn't precipitate out during the concentration anymore.

#### *Design of Mechanism-based Bisubstrate Inhibitors*

5'-O-(N-acylsulfamoyl) adenosines (acyl-AMS) and derivatives are bisubstrate inhibitors (7). These compounds are expected to occupy both the OSB and nucleoside binding sites. Compared to the the individual binding affinity of the two substrates, bisubstrate inhibitors generally can enhance the binding energy due to a smaller entropy barrier as reported by Jencks and coworkers (8). However in some cases simply linking of each fragment may cause the loss of some interaction energy and can result in failure of bisubstrate inhibitor binding. In this chapter, we have used kinetic

mechanism study results and steady-state initial velocity study results of MenE mutants discussed in chapter II to guide modifications to the OSB-AMS **9**. The scaffold of OSB-AMP analogues are shown in **Figure 3-8**.

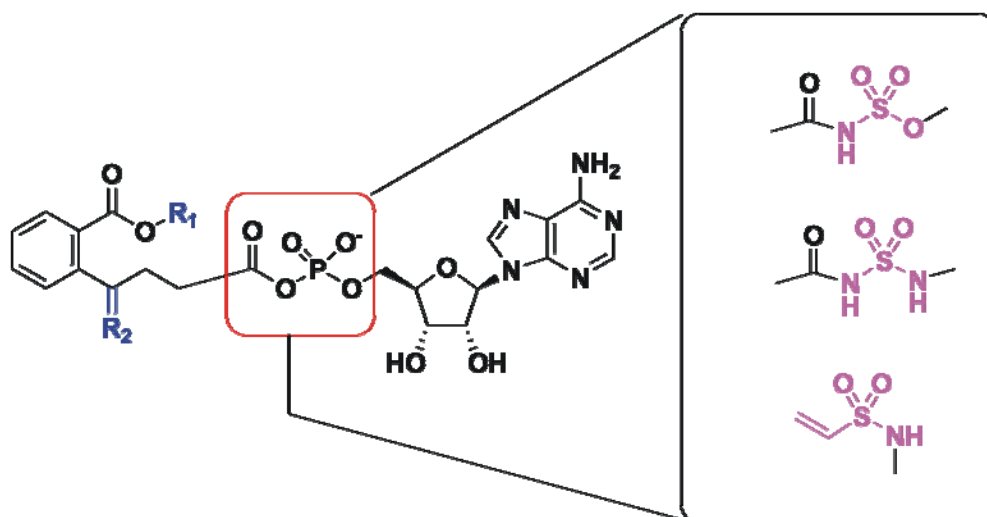


**Figure 3- 8: Scaffold of OSB-AMP intermediate analogues. R1 and R2 represent two alternative functional groups**

Three different types of linkers inspired from natural intermediate OSB-AMP were designed to mimic the phosphate moiety (9). Adrich and coworkers reported that the acylsulfamate linkage of inhibitor **1**, **4**, **7**, **9** and **12** is extremely acidic (10). Inhibitors **2**, **5** and **10** had substitution of the sulfamate oxygen with a nitrogen to raise the pK<sub>a</sub> of the central NH, which expected to improve stability relative to the acylsulfamate linkages (10). Replacement of the carbonyl function with vinyl group in inhibitors **3**, **6**, **8**, **11** and **13** also expected to raise the pK<sub>a</sub> of the sulfamate NH even higher than sulfonamide linkage with an attendant decrease in overall polarity (10). The inhibitors **1**, **4**, **7**, **9** and **12** with most acidic sulfamate linkage illustrated smaller IC<sub>50</sub> values comparing with inhibitors containing the other two linkages with the exception

of inhibitor **3** and **13** having vinyl sulfonamide demonstrating better IC<sub>50</sub> values in ecMenE. It indicated that ecMenE may have a more hydrophobic active site binding pocket than tbMenE and saMenE. Another possibility could be that the inhibitors containing a vinylsulfonamide linkage might react with the CoA thiol nucleophile, and mimic the tetrahedral intermediate which may form during the thioesterification reaction (7, 11-12). However, no tetrahedral intermediate was observed by incubating inhibitor **3** with same molarity of CoA in 20mM Tris-HCl buffer at pH 7.5.

In previous study done by Dr. Zhang (in doctoral thesis), it has been reported that OSB-CoA is not a stable compound, and can decompose spontaneously in solution into a spirodilactone. Since this reaction must involve the aromatic OSB carboxyl group, one group of inhibitors **1-8** were synthesized in which this carboxyl group was converted into a methyl ester (MeOSB-AMS). Another group of inhibitors **9-13** retained the C1 carboxyl group, which were observed a nanomolar IC<sub>50</sub> values in all three enzymes whereas inhibitors **1-8** having micromolar IC<sub>50</sub> values. This indicated that although C1 carboxyl group didn't directly participate in the catalysis, it is crucially important for the intermediate binding through all three enzymes from different organisms.

To probe the importance of the aromatic ketone functionally for binding, the *exo*-methylene inhibitors **4**, **5** and **6** were designed, while the removal of ketone groups in inhibitor **7**, **8**, **12** and **13** designed in same purpose. The

significant decrease of IC<sub>50</sub> values among all three enzymes proved that the aromatic ketone was important for retention of intermediate activity.

Overall, inhibitor **9** demonstrated the lowest nanomolar IC<sub>50</sub> against three MenEs from different organisms. Furthermore, the real Ki values generated from tight-binding inhibitory analysis were 11.2±0.9nM for tbMenE, 12.2±1.5nM for saMenE and 128±4.6nM for ecMenE, respectively. It has been reported that unlike the stand-alone aryl adenylating enzymes, most NRPS adenylateion domains were embedded with carrier domains in multifunctional proteins favored, which meant that the tight-binding of the intermediate was not necessary in these cases (13). If it is true, it may be proposed that catalytically ecMenE may be closely regulated with downstream ecMenB, which required the less binding affinity of OSB-AMS inhibitor to enzyme species comparing with tbMenE and saMenE. In another word, ecMenE may have a different catalytic mechanism comparing with tbMenE and saMenE.

#### *Steady-State Kinetic Mechanism*

The kinetic mechanisms of adenylate enzymes have been significantly studied and widely reported from fatty acyl-CoA synthetase from *E. coli*, Cysteine Ligase from *Mycobacterium smegmatis*, OSB-CoA synthetase from *Bacillus anthracis* and different types of tRNA synthetases (14-16). The inhibition studies of bisubstrate inhibitors, which closely mimic the OSB-AMP intermediate, supported the Bi uni uni Bi Ping-Pong kinetic mechanism

discussed in chapter II. The bisubstrate analogues are predicted to be able to occupy the ATP binding site via the AMS portion and the OSB active binding site via MeOSB or OSB portion. Since the enzyme follows an ordered mechanism for ATP and OSB binding, it is expected that inhibitors can bind to free enzyme either as a competitive inhibitor of ATP or a competitive inhibitor of OSB (11).

The Bi uni uni Bi Ping-Pong mechanism is utilized by several members of acyl-CoA synthetase subfamily of enzymes belonging to adenylate-forming enzyme superfamily. Interestingly, significant differences of binding order of the first two substrates are observed among these enzymes (17-19). However, the reaction mechanisms of enzymes mostly proceed with an ordered addition of first two substrates, while yeast acetyl-CoA synthetase follows random addition of the first two substrates (17). The binding order of OSB and ATP with tbMenE is illustrated from the inhibition modalities of bisubstrate inhibitors versus each substrate respectively. The data indicates that inhibitor acts as a competitive inhibitor against ATP and a noncompetitive inhibitor against OSB. It demonstrates that ATP binds to the free tbMenE first followed by the binding of OSB, forming a ternary complex. Subsequently, the enzyme releases PPI and OSB-AMP remains bound to the enzyme's active site. Then CoA reacts with the adenylate anhydride. Two products AMP and OSB-CoA are subsequently released however with unknown order. However, the binding order of ATP and OSB may be different, in which OSB-AMS inhibitor **9** is a

competitive inhibitor against OSB. It indicated that OSB may bind first with free enzyme followed by the binding of ATP in ecMenE case. The inhibitory parameters were summarized in **Table 3-2**.

<b>Table 3- 2: Inhibitory parameters against OSB for tbMenE and ecMenE</b>			
	$K_i$ (nM)	$K_{ii}$ (nM)	Inhibition pattern
tbMenE	11.2±0.9	16.9±0.5	noncompetitive
ecMenE	128±4.6	-	competitive

### **3.5 Conclusion**

In summary, *M. tuberculosis* MenE (tbMenE) was cloned, overexpressed, purified and characterized in this study. We identify 1 (or more) OSB-AMS analogues with low nanomolar inhibition and dissociation constants for with tbMenE. These small molecules are rationally designed bisubstrate analogues that are hydrolytically stable structural isosteres of the adenylyate intermediate and designed to simultaneously occupy both substrate binding sites at the enzyme active site (13, 20). Based on the kinetic data, the bisubstrates analogues have the potential to bind to the enzyme with extremely high affinity and specificity, which accomplished the two critical aspects of any effective therapeutic agent. The tight-binding of OSB-AMS to tbMenE suggests that these series of compounds have great promise to be used as novel

antibacterial agents targeted to menaquinone biosynthesis pathway. Moreover, because this pathway is absent in mammals, it is likely that this class of inhibitors will be specific and selective to bacteria, thus causing little or no effect to the human host.

Furthermore, many other adenylate analogues based on the prototypical Sal-AMS, which has the similar structure of OSB-AMS we used here, have been shown to inhibit EntE from *Escherichia coli*, DhbE from *B subtilis*, MbtA from *M. tuberculosis* and YbtE from *Y. petis* (11, 20-22). These adenylate analogue inhibitors have been shown *in vitro* to abolish mycobactin synthesis in *M. tuberculosis*. Furthermore, none of these latter inhibitors displayed toxicity when evaluated against a murine leukemia cell line at inhibitor concentrations up to 400 times higher than the MIC<sub>99</sub> values (10). The use of these bisubstrate inhibitors of adenylate-forming enzymes is proving to be a promising approach for the development of novel antibacterial therapeutics.



## Reference

1. Lodise, T. P., McKinnon, P. S., Swiderski, L., and Rybak, M. J. (2003) Outcomes analysis of delayed antibiotic treatment for hospital-acquired *Staphylococcus aureus* bacteremia, *Clin Infect Dis* 36, 1418-1423.
2. Luo, L., Taylor, K. L., Xiang, H., Wei, Y., Zhang, W., and Dunaway-Mariano, D. (2001) Role of active site binding interactions in 4-chlorobenzoyl-coenzyme A dehalogenase catalysis, *Biochemistry* 40, 15684-15692.
3. Martinez-Blanco, H., Reglero, A., Fernandez-Valverde, M., Ferrero, M. A., Moreno, M. A., Penalva, M. A., and Luengo, J. M. (1992) Isolation and characterization of the acetyl-CoA synthetase from *Penicillium chrysogenum*. Involvement of this enzyme in the biosynthesis of penicillins, *J Biol Chem* 267, 5474-5481.
4. May, J. J., Kessler, N., Marahiel, M. A., and Stubbs, M. T. (2002) Crystal structure of DhbE, an archetype for aryl acid activating domains of modular nonribosomal peptide synthetases, *Proc Natl Acad Sci U S A* 99, 12120-12125.
5. Qiao, C., Gupte, A., Boshoff, H. I., Wilson, D. J., Bennett, E. M., Somu, R. V., Barry, C. E., 3rd, and Aldrich, C. C. (2007) 5'-O-[(N-acyl)sulfamoyl]adenosines as antitubercular agents that inhibit MbtA: an adenylation enzyme required for siderophore biosynthesis of the mycobactins, *J Med Chem* 50, 6080-6094.

6. Kane, J. F. (1995) Effects of rare codon clusters on high-level expression of heterologous proteins in *Escherichia coli*, *Curr Opin Biotechnol* 6, 494-500.
7. Lu, X., Zhang, H., Tonge, P. J., and Tan, D. S. (2008) Mechanism-based inhibitors of MenE, an acyl-CoA synthetase involved in bacterial menaquinone biosynthesis, *Bioorg Med Chem Lett* 18, 5963-5966.
8. Page, M. I., and Jencks, W. P. (1971) Entropic contributions to rate accelerations in enzymic and intramolecular reactions and the chelate effect, *Proc Natl Acad Sci U S A* 68, 1678-1683.
9. Isono, K., Uramoto, M., Kusakabe, H., Miyata, N., Koyama, T., Ubukata, M., Sethi, S. K., and McCloskey, J. A. (1984) Ascamycin and dealanylascamycin, nucleoside antibiotics from *Streptomyces* sp, *J Antibiot (Tokyo)* 37, 670-672.
10. Somu, R. V., Boshoff, H., Qiao, C., Bennett, E. M., Barry, C. E., 3rd, and Aldrich, C. C. (2006) Rationally designed nucleoside antibiotics that inhibit siderophore biosynthesis of *Mycobacterium tuberculosis*, *J Med Chem* 49, 31-34.
11. Ferreras, J. A., Ryu, J. S., Di Lello, F., Tan, D. S., and Quadri, L. E. (2005) Small-molecule inhibition of siderophore biosynthesis in *Mycobacterium tuberculosis* and *Yersinia pestis*, *Nat Chem Biol* 1, 29-32.

12. Arora, P., Goyal, A., Natarajan, V. T., Rajakumara, E., Verma, P., Gupta, R., Yousuf, M., Trivedi, O. A., Mohanty, D., Tyagi, A., Sankaranarayanan, R., and Gokhale, R. S. (2009) Mechanistic and functional insights into fatty acid activation in *Mycobacterium tuberculosis*, *Nat Chem Biol* 5, 166-173.
13. Neres, J., Labello, N. P., Somu, R. V., Boshoff, H. I., Wilson, D. J., Vannada, J., Chen, L., Barry, C. E., 3rd, Bennett, E. M., and Aldrich, C. C. (2008) Inhibition of siderophore biosynthesis in *Mycobacterium tuberculosis* with nucleoside bisubstrate analogues: structure-activity relationships of the nucleobase domain of 5'-O-[N-(salicyl)sulfamoyl]adenosine, *J Med Chem* 51, 5349-5370.
14. Faergeman, N. J., and Knudsen, J. (1997) Role of long-chain fatty acyl-CoA esters in the regulation of metabolism and in cell signalling, *Biochem J* 323 ( Pt 1), 1-12.
15. Fan, F., Luxenburger, A., Painter, G. F., and Blanchard, J. S. (2007) Steady-state and pre-steady-state kinetic analysis of *Mycobacterium smegmatis* cysteine ligase (MshC), *Biochemistry* 46, 11421-11429.
16. Tian, Y., Suk, D. H., Cai, F., Crich, D., and Mesecar, A. D. (2008) *Bacillus anthracis* o-succinylbenzoyl-CoA synthetase: reaction kinetics and a novel inhibitor mimicking its reaction intermediate, *Biochemistry* 47, 12434-12447.
17. Farrar, W. W., and Plowman, K. M. (1979) Kinetics of acetyl-CoA

- synthetase-II. Products inhibition studies, *Int J Biochem* 10, 583-588.
18. Kim, Y. S., and Kang, S. W. (1994) Steady-state kinetics of malonyl-CoA synthetase from *Bradyrhizobium japonicum* and evidence for malonyl-AMP formation in the reaction, *Biochem J* 297 ( Pt 2), 327-333.
  19. Vessey, D. A., and Kelley, M. (2001) Characterization of the reaction mechanism for the XL-I form of bovine liver xenobiotic/medium-chain fatty acid:CoA ligase, *Biochem J* 357, 283-288.
  20. Gupte, A., Boshoff, H. I., Wilson, D. J., Neres, J., Labello, N. P., Somu, R. V., Xing, C., Barry, C. E., and Aldrich, C. C. (2008) Inhibition of siderophore biosynthesis by 2-triazole substituted analogues of 5'-O-[N-(salicyl)sulfamoyl]adenosine: antibacterial nucleosides effective against *Mycobacterium tuberculosis*, *J Med Chem* 51, 7495-7507.
  21. Miethke, M., Bisseret, P., Beckering, C. L., Vignard, D., Eustache, J., and Marahiel, M. A. (2006) Inhibition of aryl acid adenylation domains involved in bacterial siderophore synthesis, *FEBS J* 273, 409-419.
  22. Sikora, A. L., Cahill, S. M., and Blanchard, J. S. (2009) Enterobactin synthetase-catalyzed formation of P(1),P(3)-diadenosine-5'-tetrphosphate, *Biochemistry* 48, 10827-10829.

## **Chapter IV: MbtI Catalyze Chorismate Isomerization and Isochorismate**

### **Elimination**

The work in this chapter is published in:

*Biochemistry*, **2007**, 46 (4), pp 946–953 and *Biochemistry*, **2007**, 46 (4), pp 954–964

### **4.1 Background**

#### *Mycobactin Biosynthetic Pathway*

Iron, an essential element for growth of pathogenic bacteria, is scavenged from human hosts by iron chelators, especially in iron-limited extracellular spaces. In order to take up ferric iron through bacteria cell wall, *M. tuberculosis* produces mycobactin as iron chelators, distinguished as mycobactin T and carboxymycobactins based on structural analysis. The proposed mechanism for uptake of iron is reviewed by C. Ratledge in 2004 (1). The core structures of these two siderophores are highly related and vary mainly in their fatty acid substituent. Comparing with the water-soluble carboxymycobactins, which have a short unsaturated side chain, the lipid-soluble mycobactins have longer saturated side chain. Mycobactin is now generally identified among large number of mycobacteria (2-4).

According to the structure, salicylic acid is synthesized by salicylate synthase annotated MbtI, which is the first enzyme involved in the mycobactin

biosynthetic pathway. Revealed from the genome of the H37Rv strain (5), there is a cluster of 10 genes (*mbtA-J*) starting with *mbtI*, which is proposed to encode enzymes in mycobactin pathway. Particularly, the six genes *mbtA* to *mbtF* consists of a genomic sequence for producing of a 20-domain assembly line, which could manufacture the portions needed for mycobactin shown in Fig. 4-1 (6). The mycobactin pathway is reviewed in details by C.T. Walsh in 2002 (7)

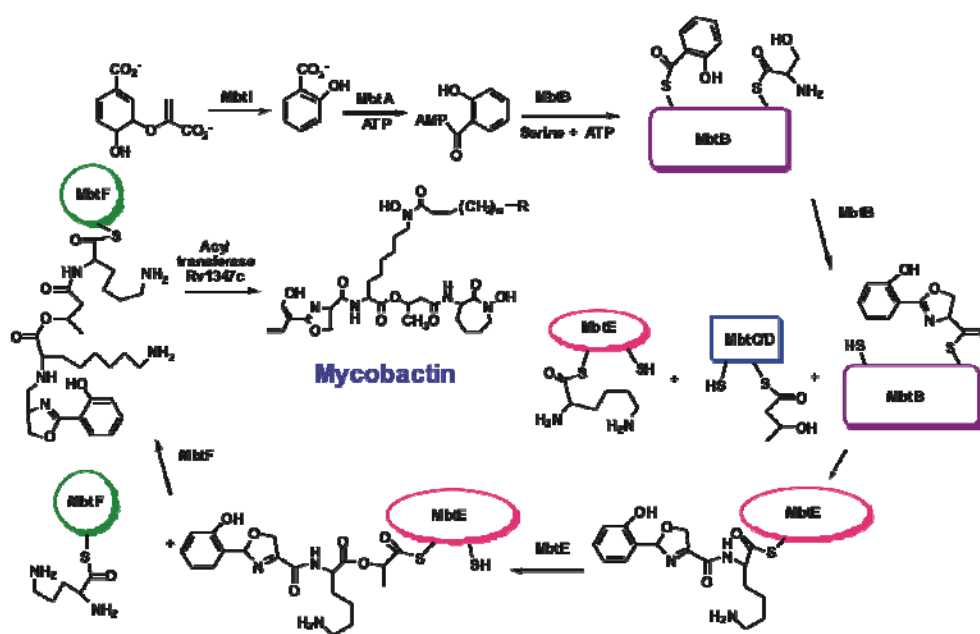


Figure 4- 1: Summarization of mycobactin biosynthetic pathway

#### Family of Chorismate-utilizing Enzymes

Bacterial chorismate binding enzymes (CBE's) are a large family of enzymes, which have highly similarity in structures and mechanism due to their evolutionarily relationship. The enzymes, belonging to this family, are involved in various microbial metabolic pathways including menaquinone,

mycobactin, tryptophan, enterobactin and etc. Since the enzymes that utilize chorismate as substrate lack human homologues, they become attractive drug target for treatment of pathogens with serious impact on global public health, such as *M. tuberculosis*. Common reactions catalyzed by some member of the family is shown in **figure 4-2**, in which MbtI assigned as salicylate synthase (SS) converts chorismate to salicylate via isochorismate as intermediate, MenF and EntC are isochorismate synthase (ICS), TrpE, anthranilate synthase (AS), induces the formation of anthranilate and PabB known as 4-amino-4 deoxychorismate synthase (ADCS) replaces the 4-OH by 4-NH<sub>2</sub> in folate biosynthesis pathway (8-10). These enzymes maintain a common fold and active site architecture. In the family, there are other non related enzymes which are known as chorismate mutase AroH and AroQ turning chorismate to prephenate through coup rearrangement (11). Despite the sequence and structural dissimilarities, there exist certain commonalities in substrate recognition relevant to the enzymes shown in **Fig. 4-2**.

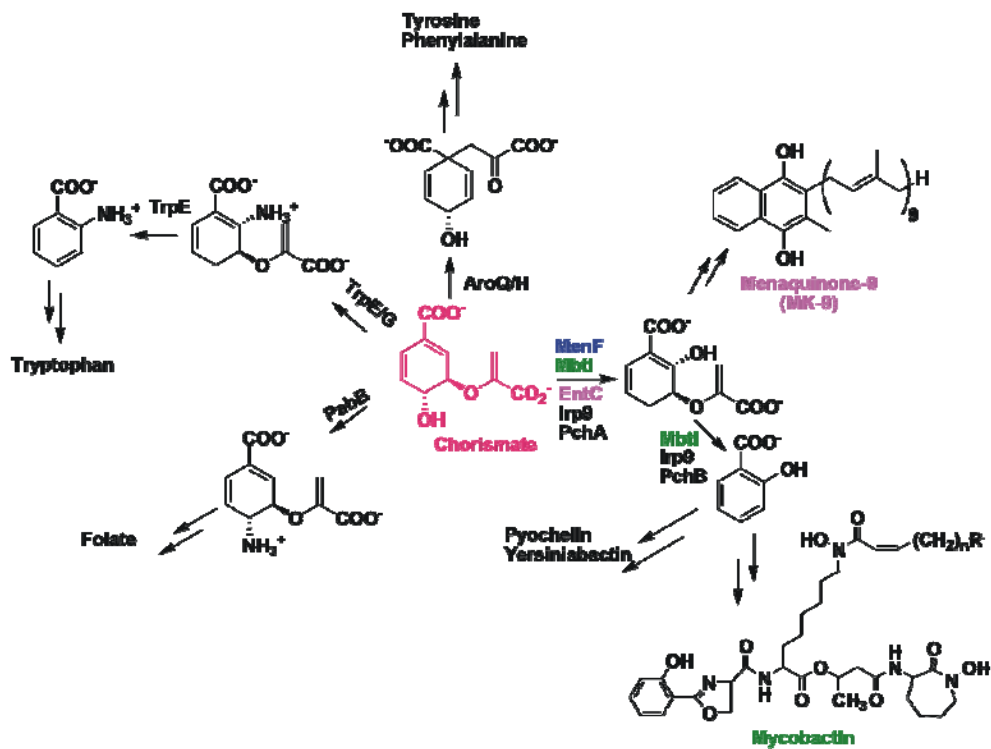


Figure 4- 2: Chorismate is an important starting material in numerous biosynthetic pathways to form metabolites, including aromatic amino acids, quinones, siderophores, folate and phenazines



## **4.2 Materials and Methods**

### *Materials and Substrates*

Chorismate, the starting reagent of the reactions, was purchased from Sigma-Adrich. Lactate dehydrogenase (LDH), DTT, BME and isopropyl-b-D-thiogalactopyranosid (IPTG) were purchased from Sigma. Restriction enzymes, DNA ligase, pfu DNA polymerase and DpnI were from stratagene (LA Jolla, CA). Primers were ordered from IDT. 15% SDS-PAGE pre-made gels were obtained from Bio-Bad. Ni-NTA metal affinity chromatography and His-bind metal affinity chromatography were from Novagen. Sephadex<sup>TM</sup> G-25 resin was purchased from Amersham Biosciences. Millipore centriplus YM-30 was from Fisher.

### *Cloning of menF and mbtI*

*E. coli* MenF is cloned from *E. coli* BL21 whole cell lysate. The MenF gene was amplified from a whole cell template using the primers 5'-gga att cca tat gca atc act tac tac ggc gct-3' (forward) and 5'-ccc aag ctt gat atg aat cgg taa tga tgc gac-3' (reverse). The amplified gene was purified by DNA gel and then was cloned into Novegen's pET28b vector including NdeI and HindIII restriction enzymes sites. *M. tuberculosis* mbtI was cloned from HV37Rv genomic DNA using the primers 5'-gga att cca tat gtc cga gct cag cgt cgc-3' (forward) and 5'-ccg ctc gag tta ctg gcg tgc aac cag ata agg cg-3' (reverse).

Using the underlined NdeI and XhoI restriction enzymes sites, *mbtI* was cloned into Novagen's pET15b vector for expression.

#### *Overexpression and Purification of MenF (Isochorismate Synthase)*

For expression, the plasmid carrying *menF* gene was transformed to BL21pLysS and 2x10mL overnight LB culture were inoculated into 2 x 500mL LB. Kanamycin and glucose were added to 30µg/ mL and 2mg/ mL respectively and the cells were grown at 37°C (250rpm) to an O.D.600 of 1.0-1.2. IPTG was added to 0.5mM and expression continued for 16 hours at 25°C. The cells were harvested by centrifugation at 5,000 x g for 15min and the pellet was stored frozen -20°C. The pellet was resuspended in 20mM Tris-HCl buffer (pH=7.9) and lysed by 5 passages through sonication for 2min. Cell debris was removed by centrifugation at 33,000 rpm for 90min at 4°C. MenF was purified using Novagen Ni-NTA metal affinity chromatography according to the manufacturer's instruction. 10mM β-mercaptoethanol (BME) was included in all the purification steps for MenF. After Ni-NTA column, collected fractions were loaded onto 50mM Tris-HCl, 1mM EGTA, 5mM BME pH=7.5 using Sephadex G-25 chromatography and concentrated to 25mg/mL using a Millipore YM-30 centriplus. MenF was frozen in liquid N<sub>2</sub> 60µL per microcentrifuge tube.

#### *Overexpression and Purification of MbtI (Salicylic Synthase)*

For expression, the plasmid carrying *mbtI* gene was transformed to

BL21pLysS and 2×10mL overnight LB culture was inoculated into 2 x 500mL LB. Ampicillin and glucose were added to 200µg/mL and 2mg/mL respectively and the cells were grown at 37° (250rpm) to an O.D.600 of 1.0-1.2. IPTG was added to 0.5mM and expression continued for 4 hours at 37°C. The cells were harvested by centrifugation at 5,000 x g for 15min and the pellet was stored frozen -20°C. The pellet was resuspended in 20mM Tris-HCl buffer (pH=7.9) and lysed by 5 passages through sonication for 2min. Cell debris was removed by centrifugation at 33,000 rpm for 90min at 4 °C. MbtI was purified using Novagen his-bind metal affinity chromatography. The column was washed 3 column volumes of buffer B (20mM Tris-HCl, 200mM NaCl, 60mM imidazole pH=7.9). MbtI was eluted with a linear gradient (20mL) of 0.005-1M imidazole in buffer A (20mM Tris-HCl, 200mM NaCl, 5mM imidazole pH=7.9) and buffer C (20mM Tris-HCl, 200mM NaCl, 1M imidazole pH=7.9). After his-bind column, collected fractions were loaded onto 50mM Tris-HCl, 0.1mM EDTA pH=7.5 using Sephadex G-25 chromatography and concentrated to 25mg/mL using a Millipore YM-30 centriplus. MbtI was frozen in liquid N<sub>2</sub> 60µL per microcentrifuge tube.

### *Mutagenesis*

MenF mutant Lys190Ala, Glu240Gln, Leu255Ala, Ala244Thr, Arg387Ala and MbtI mutant Lys205Ala, Leu258Ala, His398Met, Arg405Ala, Leu274Ala were constructed using Stratagene's site directed mutagenesis kit according to

the manufacturers instructions. The amplified PCR products were evaluated by agarose gel electrophoresis. The PCR products were purified by QIAquick™ PCR purification kit. The methylated, nonmutated parental DNA template was digested with DpnI by incubating at 37°C for 1h. An aliquot of 1 µL above product was transformed into XL1-Blue cells and plated on agar plates containing the appropriate antibiotic for the plasmid vector. For MenF mutants, the antibiotic was 200 µg/mL ampicillin and kanamycin was treated as 30µg/mL for MbtI mutants. A total of 5 colonies were selected and their plasmids were isolated by mini-prep. The mutated site was confirmed with ABI sequencing.

### *Enzyme Assays*

Enzyme activity assays were operated as follows:

Isochorismate synthase activity was assayed in a coupled reaction using EntB. Isochorismate pyruvate lyase and salicylate synthase activity were monitored by coupling the elimination of pyruvate to lactate dehydrogenase. Chorismate mutase activity was assayed both by monitoring the disappearance of chorismate by UV absorbance spectroscopy (200-400 nm) as well as the formation of phenylpyruvate upon acid hydrolysis to prephenate. All reactions were performed at 37°C in 50-100 mM Tris-HCl at pH 7.5 (EntB) or pH 8 (lactate dehydrogenase). Chorismate and Mg<sup>2+</sup> concentrations were varied accordingly. A Varian CARY 300 spectrophotometer was used for all

reactions. Reactions and ligands were routinely analyzed by HPLC on a Waters X-terra C-18 semi prep column using isochorismate synthesized by MenF and commercially available salicylate as standards. Chromatography was performed using 5% acetic acid in H<sub>2</sub>O for 16 minutes at a flow rate of 1.0mL/min after which the concentration of acetonitrile was linearly increased to 100% at 23 min. Isochorismate and chorismate had retention times of 9 and 11 min, respectively, and salicylate eluted at 23 min. For the HPLC analysis, reaction mixtures containing 50 mM Tris-HCl pH 7-8, chorismate, and 1mM Mg<sup>2+</sup> were monitored using absorption spectroscopy and 100  $\mu$ L aliquots were combined with 400  $\mu$ L 5% acetic acid prior to injection.

MenF isochorismate synthase activity was monitored according to a previously reported assay coupled to isochorismatase EntB. EntB was cloned, overexpressed and purified, which is stored in 20mM Tris-HCl, 5mM DTT solution with 50% glycerol added at -20°C.

Mbtl isochorismate synthase activity was monitored by the same assay as MenF. Isochorismate pyruvate lyase and overall activity were monitored by coupling the elimination of pyruvate to lactate dehydrogenase (LDH).

Chorismate mutase activity of MenF and Mbtl was assayed both by monitoring the disappearance of chorismate and the formation of benzoylpyruvate upon acid hydrolysis of prephenate.

In order to determine the certain activity, MenF and Mbtl were also incubated with chorismate, baselined from 220-400 nm and scans

incrementally taken at the same wavelengths. These assays are summarized in **Fig 4-3**.

Reactions of and MenF and MbtI were respectively carried out at 37°C in either 200 mM phosphate or Tris-HCl buffer, 1mM EGTA and 1mM DTT; 100mM phosphate or Tris-HCl buffer, 1mM EGTA at various pH, chorismate, and Mg<sup>2+</sup> concentrations. A varian 300-Cary UV-Vis spectrophotometer was used for all reactions.

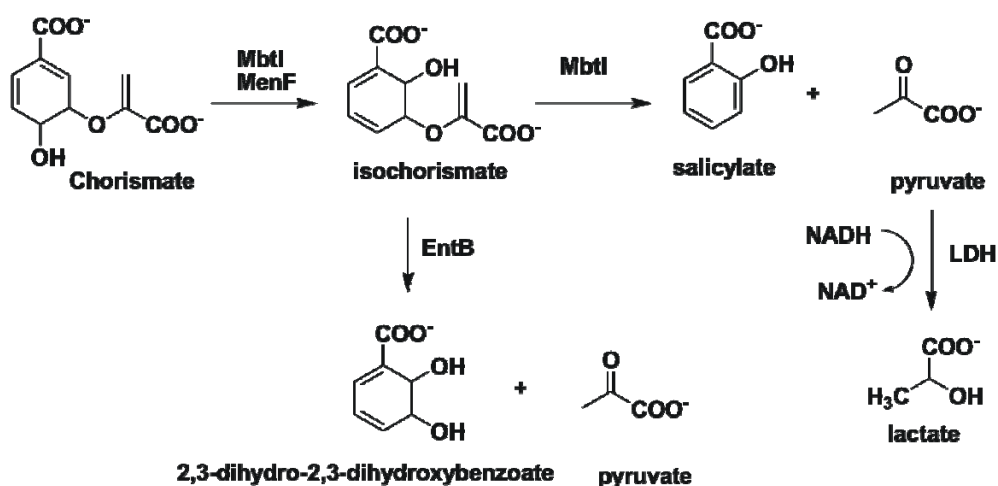


**Figure 4- 3: Summarization of enzyme assays**

#### *Kinetic Analysis*

K<sub>m</sub> values for chorismate and Mg<sup>2+</sup> were measured under the standard assay conditions described above by varying the concentration of one substrate and fixing the concentration of the other. Initial velocities were obtained by measuring the linear rates over the first 30-60 sec and analyzed by non-linear methods using the software program GraFit 4.0. The

experiments were repeated two times and the mean values were presented.

In order to estimate the enzyme kinetic mechanism, a matrix of kinetic data was collected where chorismate concentration was varied at several fixed  $Mg^{2+}$ . Correspondingly, another matrix of kinetic data was obtained by varying the  $Mg^{2+}$  at several fixed chorismate concentration. Individual data sets were analyzed using the Michaelis-Menten equation (**Eq. 4-1**) and presented by Hanes plot.

$$v = V_{max} [S] / (K_m + [S]) \quad \text{Equation 4-1}$$

Enzyme was assayed in a coupled reaction using the isochorismatase EntB which converts isochorismate to 2,3-dihydro-2,3-dihydroxybenzoate. All coupled reactions were performed in 20 mM Tris pH 7.5, 1 mM EGTA, 1 mM DTT. After ensuring that the EntB reaction was not limiting, kinetic parameters were obtained by varying the concentrations of both  $MgCl_2$  and chorismate. Activity was monitored on a Varian CARY 300 spectrophotometer at 37°C by following the increase in absorbance at 275 nm using an extinction coefficient of  $5520 \text{ cm}^{-1} \text{ M}^{-1}$ . The method described by Albell and coworkers was used to obtain the kinetic parameters, which is based on the general rate equation (**Eq. 4-2**) for a ternary complex random order mechanism (14).

$$v = (V_{max}[Mg^{2+}][S]) / (\beta K_a^{Mg^{2+}} K_S^{chor} + \beta K_a^{Mg^{2+}} [S] + \beta K_S^{chor} [Mg^{2+}] + [Mg^{2+}][S])$$

**Equation 4-2 Rate equation for the ternary complex random order mechanism**

To determine the affinity of the enzyme for  $Mg^{2+}$  in the absence ( $K_a^{Mg^{2+}}$ ) and presence ( $K_m^{Mg^{2+}}$ ) of chorismate, initial velocities were measured while varying the [chorismate] at several fixed  $[Mg^{2+}]$ . A double reciprocal plot ( $1/v$  against  $1/[chorismate]$ ) of these data gave a family of curves with slopes and intercepts as a function of  $[Mg^{2+}]$ . Subsequent plots of the slopes against  $1/[Mg^{2+}]$  and intercepts against  $1/[Mg^{2+}]$  yielded  $K_a^{Mg^{2+}}$  and  $K_m^{Mg^{2+}}$ , respectively, while the latter plot also furnished  $k_{cat}$ . An analogous procedure was used to determine the affinity of the enzyme for chorismate in the absence ( $K_S^{chor}$ ) and presence ( $K_m^{chor}$ ) of  $Mg^{2+}$ . Note that in **equation 4-2**,  $\beta K_S^{chor} = K_m^{chor}$  while  $\beta K_a^{Mg^{2+}} = K_m^{Mg^{2+}}$ .

A ternary kinetic mechanism was proposed for the enzymes. Equation 4-2 mathematically described the mechanism, which defined four steady state constants. Chemically, the mechanism was simplified in **Fig 4-4**, which indicated the chemical conception of four parameters.

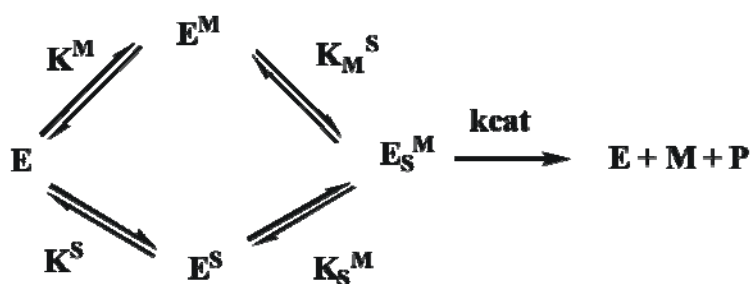


**Figure 4- 4: Ternary random mechanism**

$V_{max}$  is the maximum rate,  $[S]$  is the concentration of substrate and  $[M]$  is the concentration of metal.  $K^M$  is the Michaelis constant for M in the absence of



substrate and  $K^S$  is the Michaelis constant for S in the absence of metal.  $K_M^S$  is the Km for M in the presence of substrate and  $K_S^M$  is the Km for S in the presence of metal.  $\beta$  is a proportionality constant used to describe the following relationships for the thermodynamic scheme in **Fig 4-4**.

$$K_M^S = \beta K^S$$

$$K_S^M = \beta K^M$$

To further investigate the mechanism and determine the certain steady state constants, one the kinetic data set, obtained from varying one substrate at several fixed other substrate concentration, were transformed and presented by a double reciprocal plots. Then another two double reciprocal plots were obtained by manipulating the reciprocal of slope and reciprocal of Y-intercept versus reciprocal of the other substrate respectively. Consequently, two parameters  $K^S$  and  $K^M$  from the four were calculated from the plots.

#### *Crystallization of MenF and MbtI*

wtMenF (25 mg/mL) was crystallized by vapor diffusion. 1 $\mu$ L of MbtI was mixed with 1 $\mu$ L of a reservoir solution containing 0.1 M Hepes pH 7.5, and 0.8 M potassium sodium tartrate tetrahydrate and equilibrated against the same reservoir solution. MenF, which was cocrystallized with benzoate and pyruvate, was obtained by using the above described conditions including 5mM each of MgCl<sub>2</sub>, salicylate and pyruvate.

wtMbtI (25 mg/mL) was crystallized by vapor diffusion. 1 $\mu$ L of MbtI was

mixed with 1 $\mu$ L of a reservoir solution containing 0.1 M sodium acetate trihydrate pH 4.6 and 2.0 M sodium formate and equilibrated against the same reservoir solution. MbtI that cocrytallized with ligand was screened by Hampton Research Crystal Screen I & II; Emerald Biosystems Wizard Crystal Screen I & II; Clear Strategy Screen I & II.

### *<sup>1</sup>H NMR study*

<sup>1</sup>H NMR experiments were carried out on a Varian INOVA 500 MHz spectrometer at 30°C. Solvent suppression was accomplished by use of the PRESAT gradient spin echo sequence. The sample for analysis contained 25 $\mu$ M His6-MbtI and 2mM chorismate in 20mM phosphate buffer and 5mM MgCl<sub>2</sub> (pD= 7.5 or 8.0) in D<sub>2</sub>O in a total volume of 0.7 ml. pD is defined as the apparent pH value reading in D<sub>2</sub>O. A series of NMR spectra were collected every 5 min over 240 min at 30°C in order to monitor the reaction carried out by MbtI.

The 5.8 to 8.8 ppm region was displayed to show the formation of intermediate isochorismate, one product salicylate.

### *Liquid Chromatography-mass Spectrometry Analysis (LC/MS)*

Spectra were acquired on a Shimadzu Semi-Preparative LC-6AD HPLC with a Agilent 1100 LS-MSD electrospray ionization single quadrupole mass spectrometer. Chromatography was performed on a 2.1 mm diameter by 150

mm Luna RP column (Phenomenex, Torrance, CA) eluted with a mobile phase consisting of water (A) and acetonitrile (B). A gradient elution at 300  $\mu$ L/min starting from 70% A to 5% A in 10 min, with a 10 min hold at 5% A was used to separate the compounds of interest prior to mass spectral analysis. DAD/UV spectra were collected at 2 nm resolution. The electrospray ionization single quadrupole mass spectrometer was operated in negative ion electrospray mode with 3.0 kV applied to the inlet capillary. The LM and HM resolutions on the quadrupole filter were set to 5, resulting in a bandwidth of 1.5 Da. and the inlet cone was set at 50 V. Prior to the analysis, the TOF analyzer was calibrated with NaI/RbI to 10 ppm accuracy.

### **4.3 Results**

#### *Overexpression and Purification of MenF from E. coli*

Overexpression strain pLysS was grown and MenF was induced and purified as described in the method section. The purity of MenF during various stages of purification was determined by 15% SDS-PAGE gel, which is shown in **Figure 4-5**

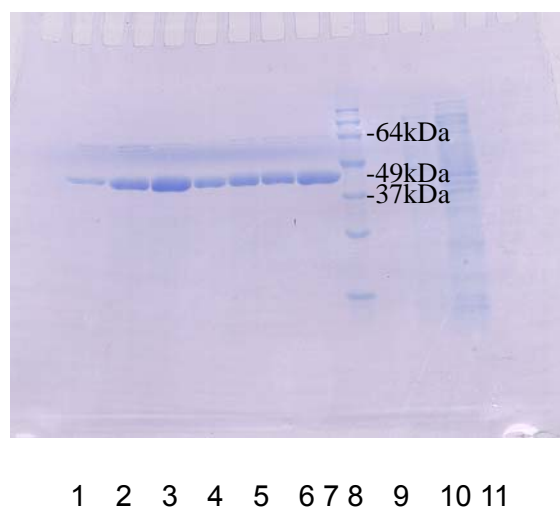


**Figure 4- 5: 15% SDS-PAGE analysis of the fractions from purification of wild-type MenF. Lane 1-4, G-25 purified fractions; Lane 5-7, Ni-NTA metal affinity chromatography purified fractions; Lane 8, protein ladder; Lane 9, wash solution; Lane 10, flow through solution; Lane 11, supernate after ultrasonication**

Since MenF rapidly lost most of kinetically activity at 4°C, it was concentrated to 25mg/mL and stored at -80°C right away. At the same time, MenF would lose ability to crystallize, if it was stored at 4°C overnight. The

concentration of MenF was determined by UV absorbance at 280nm (  $\epsilon = 71910 \text{ M}^{-1} \text{ cm}^{-1}$  ).

#### *Overexpression and Purification of MbtI from M. tuberculosis*

Overexpression strain pLysS was grown and MbtI was induced and purified as described in the method section. The purity of MbtI during various stages of purification was determined by 15% SDS-PAGE gel, which is shown in **Figure 4-6**.

Since MbtI rapidly lost most of kinetically activity at 4°C, it was concentrated to 25mg/mL and stored at -80°C right away. At the same time, MbtI would lose ability to crystallize, if it was stored at 4°C overnight. The concentration of MbtI was determined by UV absorbance at 280nm (  $\epsilon = 35254 \text{ M}^{-1} \text{ cm}^{-1}$  ).

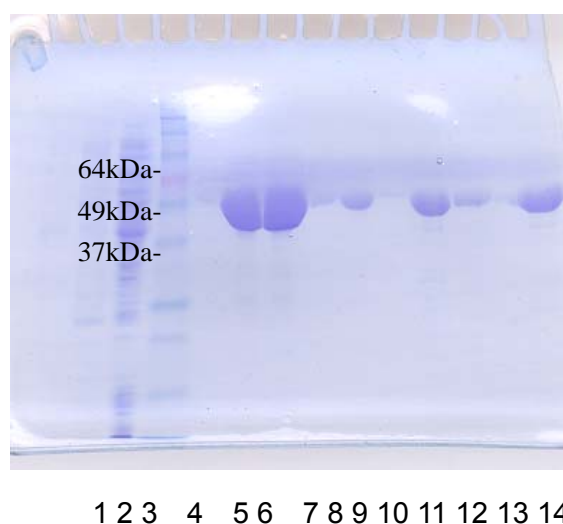


**Figure 4- 6: 15% SDS-PAGE analysis of the fractions from purification of wild-type MenF. Lane 1, wash solution; Lane 2, flow through solution;**

**Lane 3, supernate after ultrasonication; Lane 4, protein ladder; Lane 5-8, his-bind metal affinity chromatography purified fractions; Lane 9-14, G-25 purified fractions**

#### *pH Optimum*

The pH optimum was determined by studying MenF and MbtI over the range of pH 6.5 to 8.5. For MenF, the enzyme exhibited optimum isochorismate synthase activity between pH 7.0 and 8.5, while at pH=6.5 the enzyme activity decreased significantly. There were no differences in the activity whether Tris-HCl or phosphate buffer was used in the assay. For MbtI, the isochorismate synthase activity was pH dependent in the range of pH 7.0 to pH 7.9. As soon as the pH was raised to 8.0, the enzyme exhibited salicylate synthase activity, which was consisted at even higher pH. Similarly with MenF, enzyme activities of MbtI were no difference in Tris-HCl or phosphate buffer.

#### *Kinetics Constants of Enzymes and Mutants*

MenF's activities were analyzed by using previously described assays in Materials and method session. *In vitro*, MenF exhibited isochorismate synthase and chorismate mutase activity. The former one was  $Mg^{2+}$  dependent and the latter one was exhibited in the absence of  $Mg^{2+}$ . The isochorismate synthase activity of MenF increased with increasing the substrate concentration under a fixed Mg concentration and proper pH range.

The data were plotted by using the Michaelis-Menten equation in order to determine the kinetics constant. The corresponding Hanes plot showed an apparent  $K_m$  of  $197 \pm 10 \mu\text{M}$ ;  $k_{\text{cat}}$  value of  $250 \pm 4 \text{ min}^{-1}$  for ICS and  $K_m$  of  $334 \pm 38 \mu\text{M}$ ;  $k_{\text{cat}}$  value of  $1.9 \pm 0.2 \text{ min}^{-1}$  for CM.

Site directed mutants K190A, A344T, R387A, and L255A were constructed using site directed mutagenesis and confirmed with ABI sequencing. All mutants were inactive with  $\text{Mg}^{2+}$  and exhibited chorismate mutase activity in the absence of  $\text{Mg}^{2+}$  with the exception of L255A which was compromised in  $k_{\text{cat}}$  and  $K_m$  in ICS.

*In vitro*, according to the incubation assay described previously in material and method session, MbtI was found to have three activities including isochorismate synthase, salicylate synthase and chorismate mutase. Both ICS and SS activities required the present of  $\text{Mg}^{2+}$  while the CM activity was  $\text{Mg}^{2+}$  independent. The kinetic constants of these three activities were characterized respectively. ICS activity had  $K_m$  of  $92 \pm 28 \mu\text{M}$ ;  $k_{\text{cat}}$  value of  $2.6 \pm 0.5 \text{ min}^{-1}$  (pH = 7.0); SS activity had  $K_m$  of  $18 \pm 3 \mu\text{M}$ ;  $k_{\text{cat}}$  value of  $2.8 \pm 0.08 \text{ min}^{-1}$  (pH=8.0); CM activity had  $K_m$  of  $26 \pm 8 \mu\text{M}$ ;  $k_{\text{cat}}$  value of  $4.5 \pm 0.4 \text{ min}^{-1}$  (pH independent range 6.5-8.5)

Site directed mutants K205A, H398M, R405A and L268A were constructed using site directed mutagenesis and confirmed with ABI

sequencing. All mutants didn't have ICS and SS as wtMbtI with  $Mg^{2+}$  while R405A and L268A exhibited chorismate mutase activity in both the presence and the absence of  $Mg^{2+}$ . The data were shown in **Table 4.1**.

**Table 4- 1: Kinetic evaluation of wtMbtI and mutant MbtI enzymes of chorismate mutase activity**

Enzyme	Km	kcat	Km	kcat
	with $Mg^{2+}$ ( $\mu M$ )	with $Mg^{2+}$ ( $min^{-1}$ )	no $Mg^{2+}$ ( $\mu M$ )	no $Mg^{2+}$ ( $min^{-1}$ )
wt MbtI	n/a	n/a	$26 \pm 8$	$4.5 \pm 0.4$
R405A	$73 \pm 5$	$8.6 \pm 0.2$	$290 \pm 75$	$14 \pm 2$
L268A	$273 \pm 28$	$6.2 \pm 0.2$	$174 \pm 37$	$7.6 \pm 0.5$
K205A	n/a	n/a	$85 \pm 10$	$3.1 \pm 0.1$

#### *Kinetic Mechanism for MenF and MbtI*

Both MenF and MbtI were  $Mg^{2+}$  dependent enzymes. A full matrix of initial rates was determined with both substrates being varied in the absence of added products. A ternary kinetic mechanism of MenF and MbtI was determined by the double reciprocal plot. Initial  $K_m$  values for chorismate and  $Mg^{2+}$  were established under the standard assay conditions by varying the concentration of one substrate at the same time having the other substrate at a fixed, saturating level. GraFit was used as the software to non-linear fit the



data. Analysis of the results was plotted in the form of double reciprocal plots (Fig. 4-7A, B). The four parameters in equation 2 were determined by simultaneously replotting the data slope and Y-intercept versus reciprocal of one varied substrate respectively. The plots of MbtI were shown in Fig. 4-8, which had same definition as in Fig. 4-7. It is obvious to notice that substrate binding lowered the  $K_m$  of free  $Mg^{2+}$ , on the other hand,  $Mg^{2+}$  binding didn't have sharp effect on  $K_m$  of free substrate. It suggested that a ternary mechanism could be well applied to this system. These experiments had well correlations which supported the accuracy of the kinetic constants. The kinetic constants for MenF and MbtI, obtained from these experiments were summarized in Table 4-2.

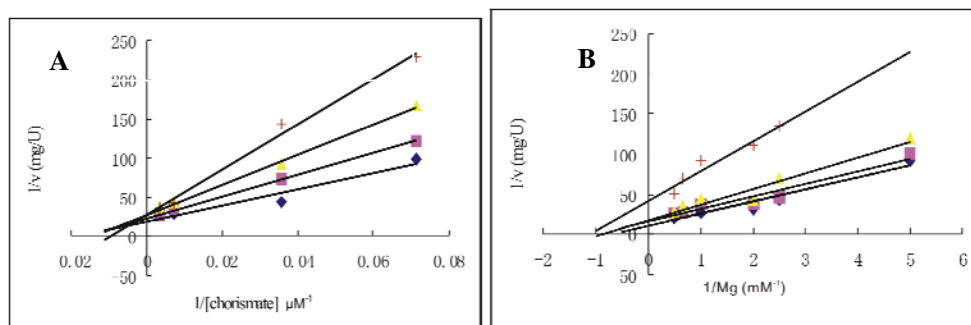


**Figure 4- 7: Kinetics of  $Mg^{2+}$  activation of MenF at 37°C, pH 7.5. A) Double reciprocal plot of initial velocity versus free substrate concentration at the following concentration of  $Mg^{2+}$ : brown 0.8mM, yellow 1.0mM, pink 1.5mM, blue 2.0mM. Other components present were 200mM Tris-HCl, 1mM DTT and 1mM EGTA. B) Double reciprocal plot of initial velocity versus free  $Mg^{2+}$  concentration at the following concentration of chorismate: brown 0.282mM, yellow 0.141mM, pink 0.028mM, blue**

0.014mM. Other components present were 200mM Tris-HCl, 1mM DTT and 1mM EGTA.

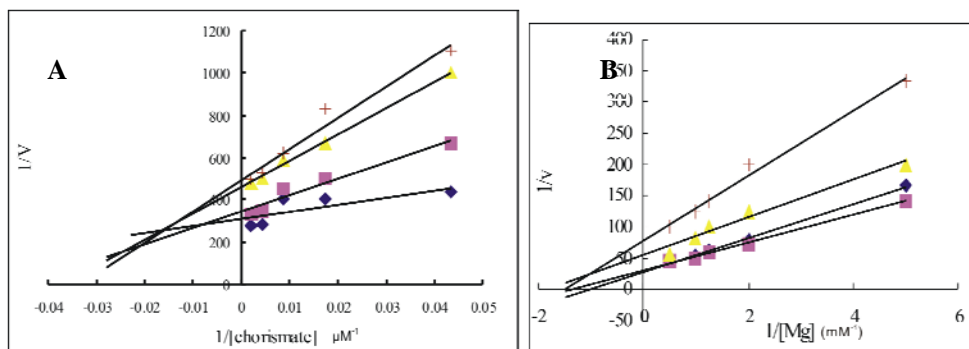


**Figure 4- 8: Kinetics of  $Mg^{2+}$  activation of MbtI at 37°C, pH 7.5. A) Double reciprocal plot of initial velocity versus free substrate concentration at the following concentration of  $Mg^{2+}$ : brown 0.8mM, yellow 1.0mM, pink 1.5mM, blue 2.0mM. Other components present were 200mM Tris-HCl, 1mM DTT and 1mM EGTA. B) Double reciprocal plot of initial velocity versus free  $Mg^{2+}$  concentration at the following concentration of chorismate: brown 0.282mM, yellow 0.141mM, pink 0.028mM, blue 0.014mM. Other components present were 200mM Tris-HCl, 1mM DTT and 1mM EGTA**

**Table 4- 2: Kinetic evaluation of wtMenF, wtMbtI and mutant MbtI enzymes of ternary mechanism**

Enzyme	$K_m^{Mg^{2+}}$ ( $\mu$ M)	$K_m^{chor}$ ( $\mu$ M)	$K_S^{chor}$ ( $\mu$ M)	$K_a^{Mg^{2+}}$ ( $\mu$ M)	$k_{cat}$ ( $min^{-1}$ )
wtMenF	3000 $\pm$ 500	320 $\pm$ 5	192 $\pm$ 7	770 $\pm$ 12	213 $\pm$ 5
wtMbtI	4500 $\pm$ 230	126 $\pm$ 4	91 $\pm$ 10	710 $\pm$ 15	2.8 $\pm$ 0.5
MenFL255A	4700 $\pm$ 550	433 $\pm$ 22	319 $\pm$ 13	2100 $\pm$ 95	19 $\pm$ 0.8

Enzyme Kinetics Four distinct activities can be detected for MbtI *in vitro*. These include isochorismate synthase, isochorismate pyruvate lyase, salicylate synthase and chorismate mutase. The first three activities require the presence of  $Mg^{2+}$  while chorismate mutase activity is observed for wtMbtI in the absence of  $Mg^{2+}$ . For MbtI, the formation of isochorismate can be detected by coupling the reaction to the isochorismatase, EntB. Accumulation of isochorismate at pH values below 7.5 can be observed using UV-vis absorption spectroscopy and HPLC analysis of reaction mixtures (**Fig. 4-9**). At pH 8 the primary product is salicylate. Small amounts of isochorismate can be detected in the HPLC chromatograms of reactions performed at pH 8 (**Fig. 4-10**) and at this pH MbtI converts isochorismate to salicylate with a  $k_{cat}/K_m$

value of  $0.81\text{M}^{-1}\text{min}^{-1}$ . Since the  $k_{\text{cat}}/K_{\text{m}}$  value for salicylate synthesis at pH 8 is  $0.5\text{M}^{-1}\text{min}^{-1}$ , these data suggest that isochorismate is a kinetically competent intermediate in the conversion of chorismate to salicylate catalyzed by MbtI. The  $k_{\text{cat}}$  value of  $2.8\text{min}^{-1}$  for the conversion of chorismate to salicylate is more than 2 orders of magnitude smaller than the anthranilate synthase activity of the MST family member AS-sm ( $558\text{min}^{-1}$ ) but is comparable to the salicylate synthase activity of Irp9 ( $8\text{min}^{-1}$ ) from *Yersinia enterocolitica*. In the absence of  $\text{Mg}^{2+}$ , wtMbtI displays chorismate mutase activity at pH 7 to 8 and converts chorismate to prephenate at a rate comparable to the  $\text{Mg}^{2+}$  dependent activities. Thus, the chorismate mutase activity of wide type MbtI is substantially less efficient compared to other chorismate mutases from *M. tuberculosis*. In contrast to the wide typeT enzyme, only chorismate mutase activity could be detected in the K205A, L268A, T271A, H398M, and R405A MbtI mutants in both the presence and absence of  $\text{Mg}^{2+}$ , while no activity could be detected for the E252Q mutant.

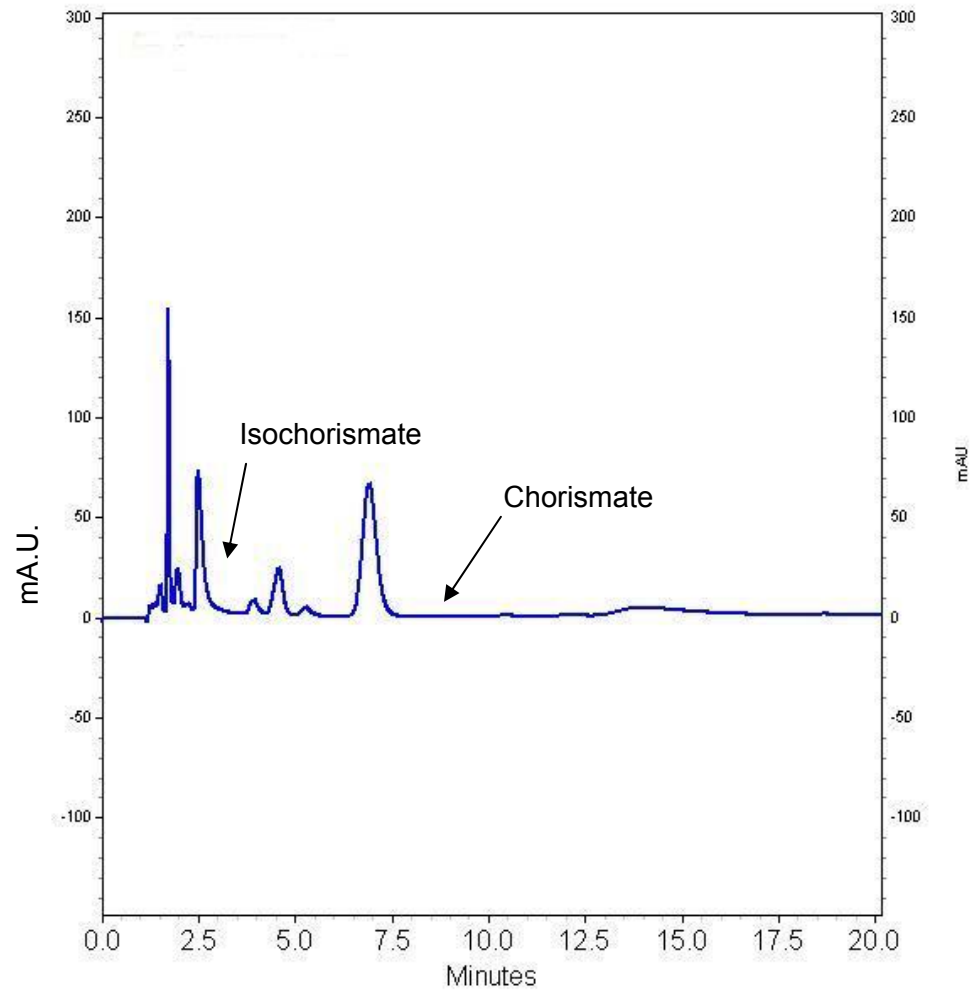
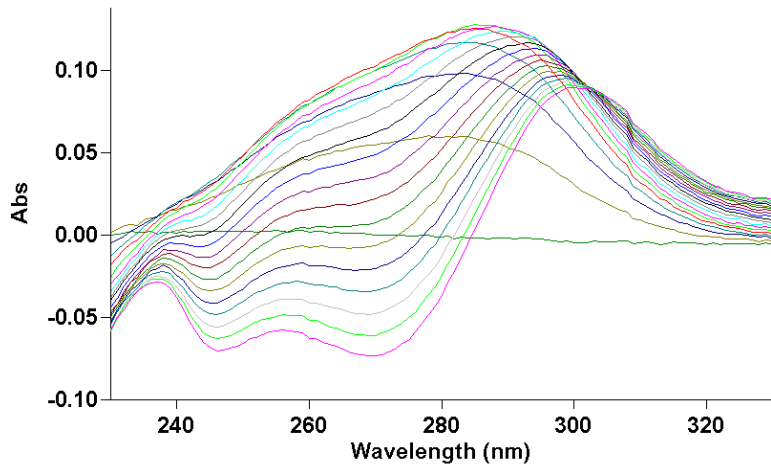


**Figure 4- 9: UV-vis absorption spectroscopy and HPLC analysis of MbtI reaction mixtures at pH 7.5**

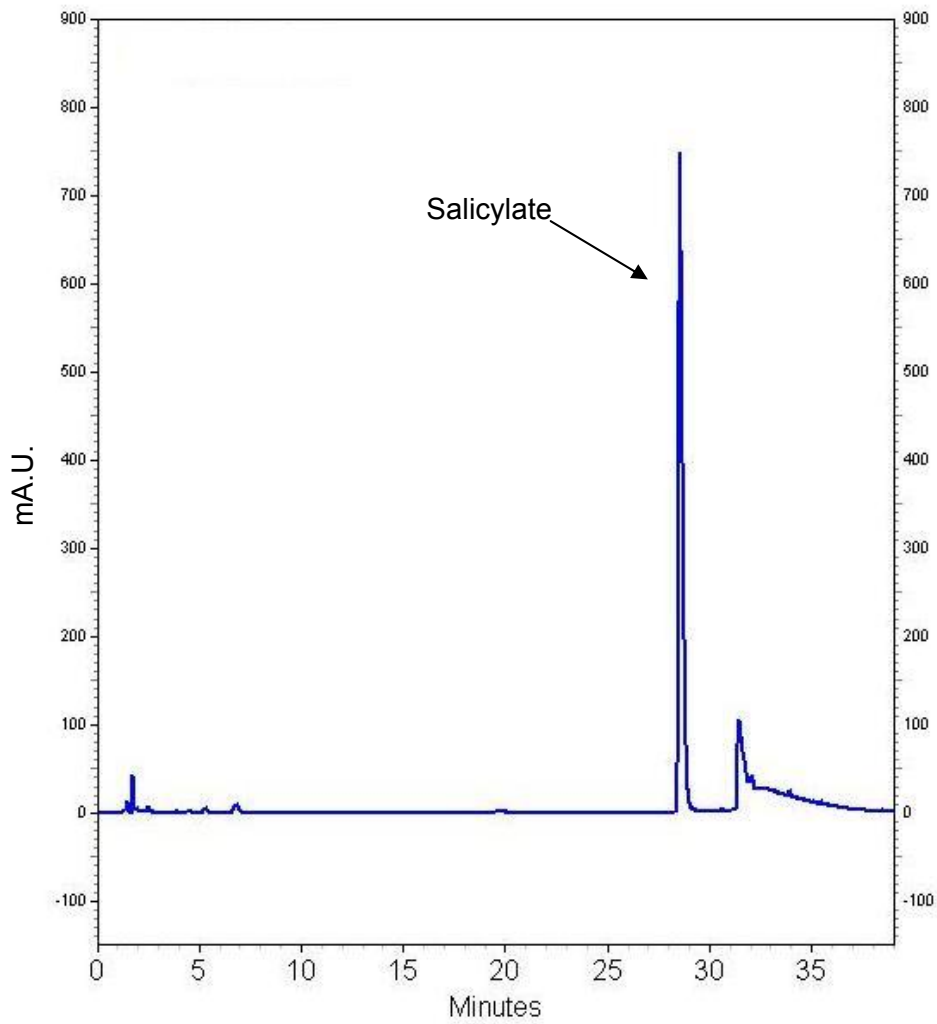
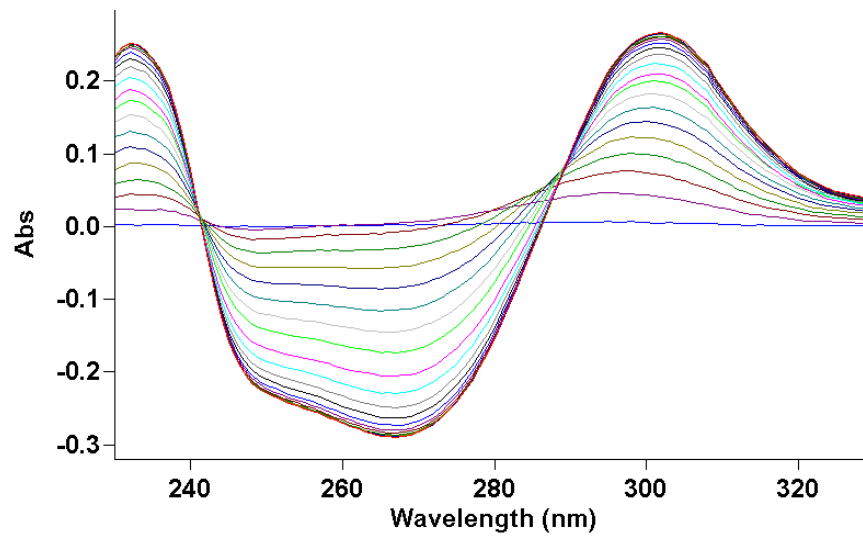


**Figure 4- 10: UV-vis absorption spectroscopy and HPLC analysis of MbtI reaction mixtures at pH 8.0**

*Products Characterization of MbtI Reaction in Response to Changes in pH  
Using LC/MS and NMR*

The intermediate of MbtI reaction, isochorismate, is unstable and nonenzymatically decomposes to 2-hydroxyl benzoic acid or pyruvic benzoic acid in solution as shown in **Figure 4-11**. The degradation was observed immediately by NMR spectra and therefore the equilibrium of chorismate and isochorismate might exist in solution while MbtI behaving as isochorismate synthase activity under proper pH values.

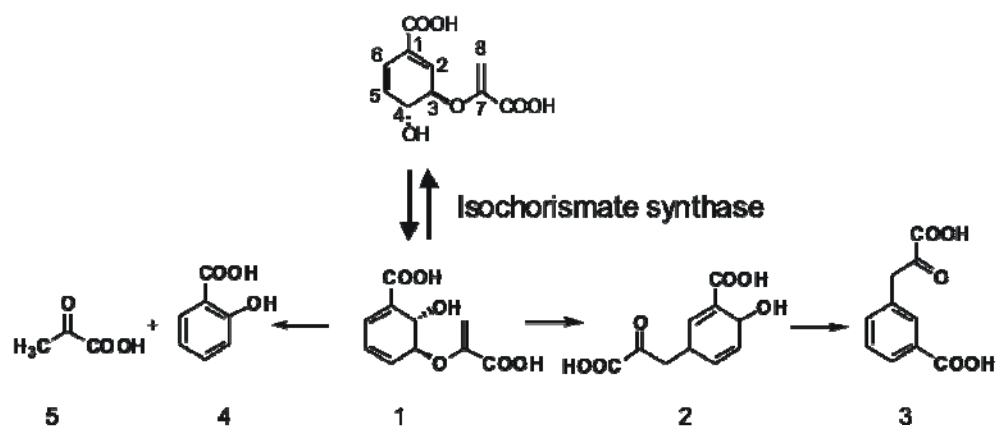


**Figure 4- 11: The nonenzymatic degradation of isochorismate**

When MbtI reaction was operated at pH 7.5 or pH 8.0 in separate reaction buffers, differences in end products were observed. The terminal pH differed from the initial buffer pH by <0.1. As the buffer pH was 7.5 or under, reaction produced more isochorismate than pH above buffers did. Isochorismate was the major accumulated product, according to the formation of salicylate in solution. There is equilibrium between the chorismate and isochorismate,

which made the turn over of substrate not complete. **(Fig. 4-12)** Salicylate concentration was highest under pH 8.0 or above and isochorismate is a kinetically competent intermediate on the reaction pathway. **(Fig. 4-14)** In this study, the formations of different end products were detected and characterized using LC/MS and NMR. The control experiment using MenF was also operated, which only observed isochorismate synthase activity. **(Fig. 4-13)** Isochorismate can be dissimilated the pyruvic side chain to salicylate through pyruvate lyase activity, which is pH dependent. Pyruvate lyase activity was detected in higher pH than in lower pH buffers, but salicylate was produced only when isochorismate synthase activity was present to meet requirements for intermediate accumulation first. Isochorismate synthase activity, which is also pH dependent, was detected only in pH 7.5 or under buffer. Salicylate activities increased about fivefold in pH 8.0 buffers.



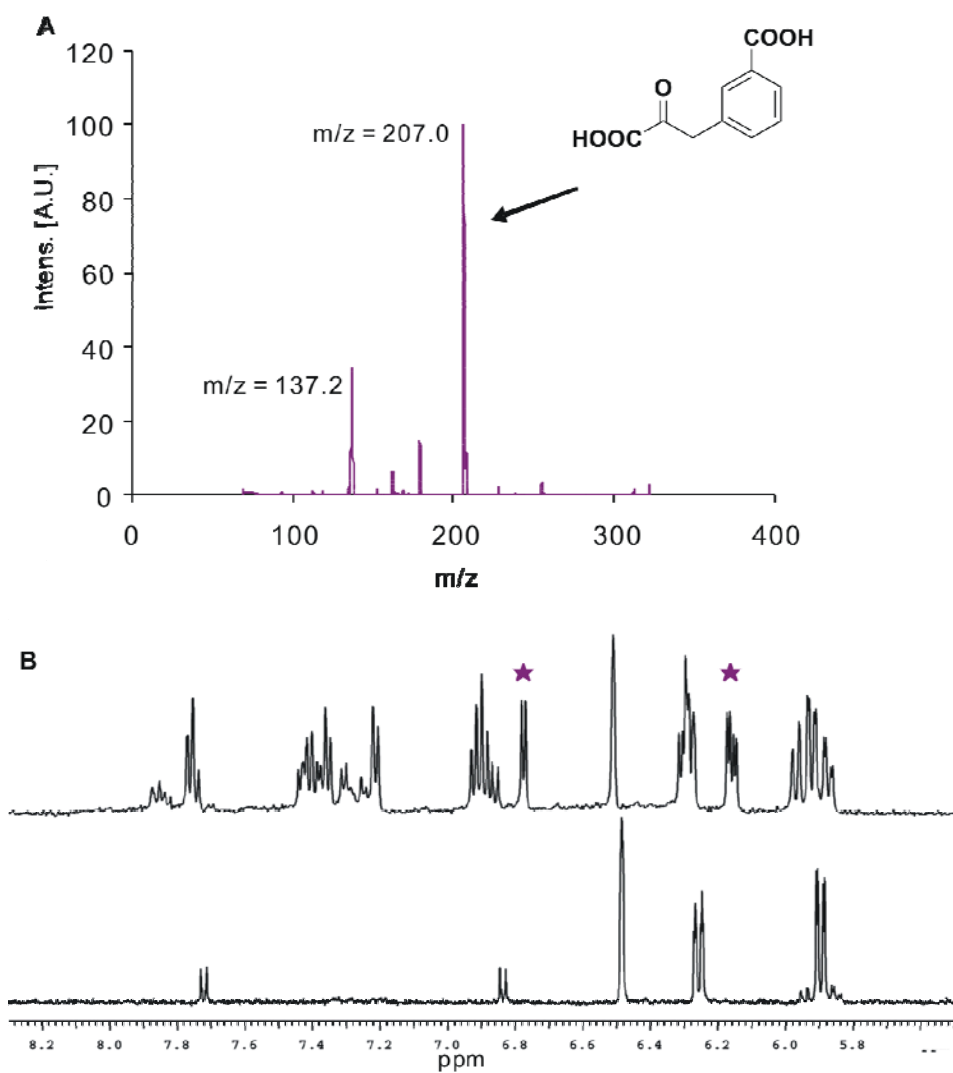


**Figure 4- 12: The characterization of MbtI reaction products in pD 7.5 buffer.**

**A) Mass spectra; B) NMR spectra in D<sub>2</sub>O buffer (pD 7.5) with 4 hours incubation. Asterisk key signed for isochorismate peaks.**

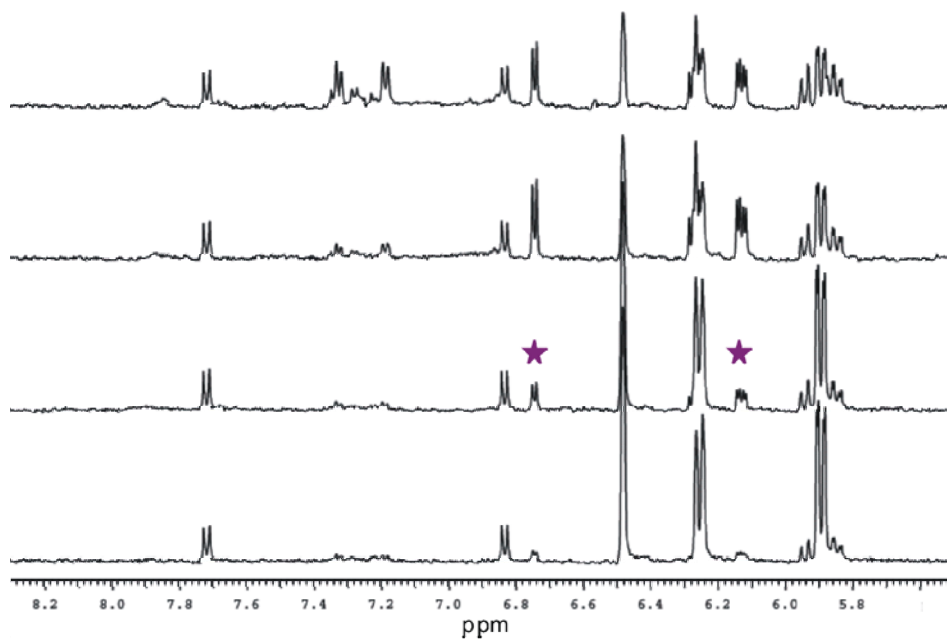


**Figure 4- 13: The characterization of MenF reaction products in pD 8.0**

**buffer**

**NMR spectra in D<sub>2</sub>O buffer (pD 8.0) with 4 hours incubation. Asterisk key**

**signed for isochorismate peaks**

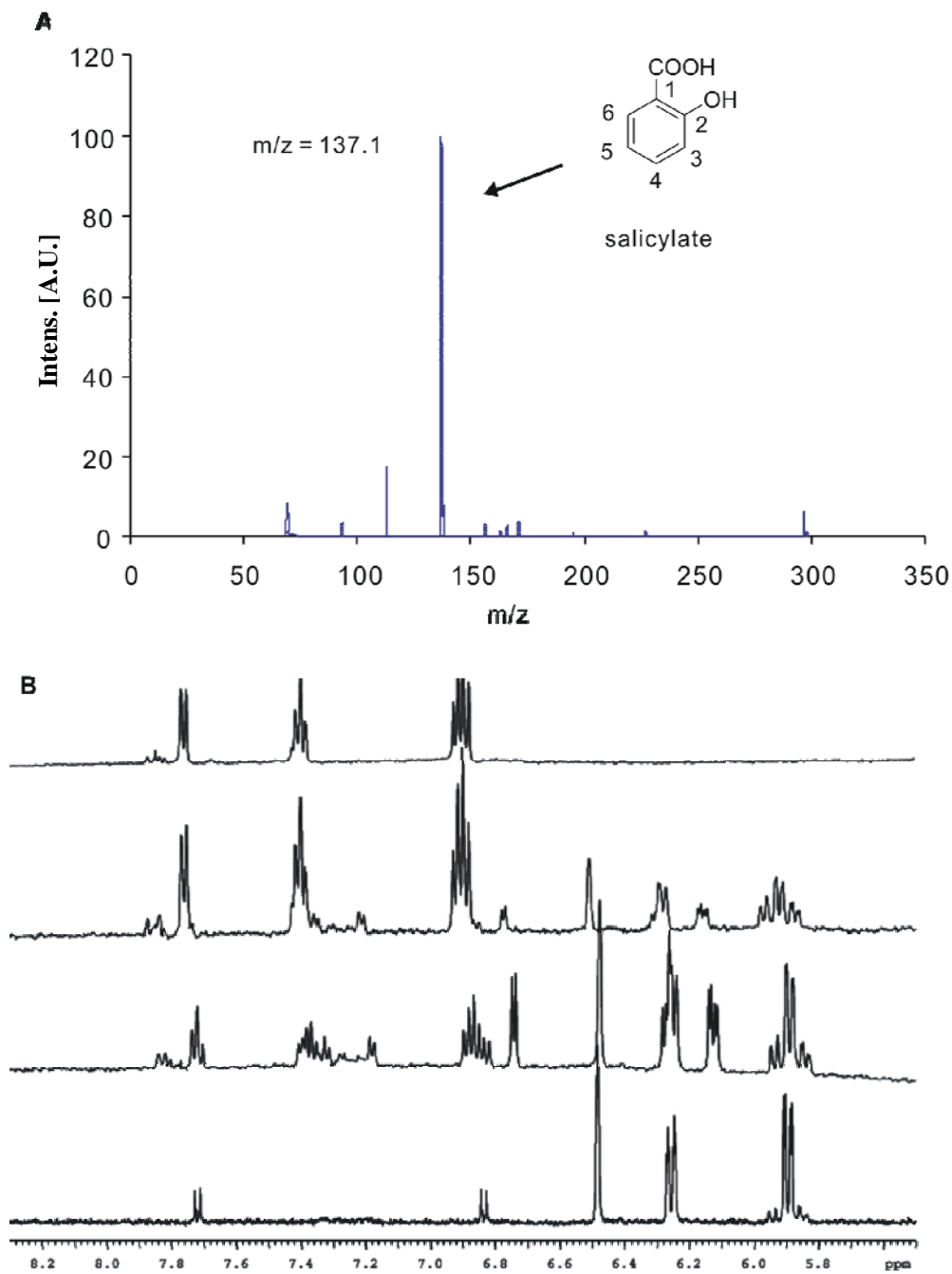


**Figure 4- 14: The characterization of MbtI reaction products in pD 8.0 buffer A) Mass spectra; B) NMR spectra in D<sub>2</sub>O buffer (pD 8.0) with 4 hours incubation**

#### **4.4 Discussion**

##### *Sequence Comparison*

Based on the idea that enzyme's sequence reveals function, sequence

alignment was done for the four enzymes that belong to the chorismate binding enzyme family; including isochorismate synthase (ICS) MenF, salicylate synthase (SS) MbtI, antranilate synthase (AS) TrpE and 4-amino-4-deoxychorismate synthase (ADCS) PabB (12-13). The sequence result indicated that although the enzymes have functional diversity they maintain a common fold and active site architecture. The homology among members of the family was assumed to mean that conclusion drawn from one member of the family were able to apply on the others sharing the similar function.

MenF is 28% identical and 43% similar over the C-terminal 254 residues to the TrpE subunit of *Serratia marcescens*, whose crystal structure was previously determined with bound products (PDB ID#: 1I7Q). On the other hand, compared with protein sequence of TrpE, MbtI is 31% identical and 45% similar (C-terminal 251 residues). At a distance of up to 6Å from the bound product 18 of out of 26 amino acids are conserved in MenF and 20 of them are conserved in MbtI. The sequence alignment result was demonstrated by online tool ClustalW (<http://www.ebi.ac.uk/clustalw/>) shown in **Figure 4-15**. The result of sequence alignment of MenF and MbtI will be described respectively in the following paragraph.

Based on the ClustalW alignment, MenF K190 (MbtI K205) is conserved in all enzymes which are hydroxylate chorismates, but is a Glu or Asp in all animating enzymes as TrpE and PabB. MenF L255 (MbtI L258) is conserved

in most of hydroxylation enzymes while it is conserved as an Ile in animating enzymes. MenF R387 (MbtI R405) is absolutely maintained in all the enzymes of this family, which is proposed to be essential in pyruvic side chain binding. MenF E240, corresponding to MbtI E252, is universally remained in the same position in all the enzymes. Since MenF and PabB retain pyruvate while MbtI and TrpE eliminate pyruvate during the reactions, it also reflects from the sequence alignment. MenF A344 is conserved in all isochorismate synthases but conserved as a threonine in salicylate synthase (MbtI) and anthranilate synthase (TrpE). However in 4-amino-4-deoxychorismate synthase (PabB) it is a serine. MbtI R417 (MenF Y399) corresponds to TrpE *Serratia marcescens* Q481 and directly precedes a conserved AGAG sequence that recognizes both 1' carbonyl group and the displacement of pyruvate in the AS *Serratia marcescens* structure. While in PabB it changes to S422. This XAGAG motif is likely initiate ligand binding, which will be discussed later.

The C-terminal 251 residues of MbtI are 31% identical and 45% similar to the TrpE subunit of AS-sm. MbtI superimposes on the AS-sm ligand structure with a deviation of 2.5 Å, and, at a distance of up to 6 Å from the bound ligands, 20 out of 26 amino acids are conserved in MbtI. When compared with other MST sequences, none of these amino acids are unique to pyruvate eliminating enzymes that could assume a role in the originally proposed pyruvate elimination mechanisms. Of the 6 residues that differ between the MbtI and AS-sm active sites, none have polar side chains directly contacting the ligand

and only MbtI Lys205 and Leu268 are likely to be directly involved in catalysis (12). By analogy to our studies on MenF, we propose that Lys205 activates a water molecule for attack at the C2 of chorismate and the proximity of the backbone carbonyl of Leu268 to the essential Glu252 and C4 hydroxyl suggests that Leu268 is involved in recognition and elimination of the C4 hydroxyl. MbtI Arg417 is the only other nonidentical polar residue within 6 Å of the substrate and directly precedes a conserved XAGAG sequence that recognizes both the C1 ring carboxylate and the pyruvate in the AS-sm structure. Salicylate synthases conserve either an Arg or Gln at this position and the homologous AS-sm residue is Gln481. In contrast, isochorismate synthases have a preference for a conserved aromatic residue at this position, and thus variability in this motif may correlate with pyruvate elimination. During the preparation of this manuscript, the structure of the salicylate synthase, Irp9, from *Yersinia enterocolitica*, was reported (14). MbtI is 36% identical and 56% similar to Irp9. The Irp9 structure was solved in complex with Mg<sup>2+</sup>, salicylate, and pyruvate, and 27 of 28 residues within 6 Å of the bound product are conserved in MbtI. MbtI Arg417 is replaced by Gln402 in Irp9 (14-15).

```

TrpE  NGEAYRQQVARAVAEIRRGEYVYKIVSRAIPLPSR--IDMPATLLVGRQANTPVRSFMFR QEGREALGFSPELVMSVTGN-KVVTPELAGTRDRMG-----NPEHNKAKEAELLHDSKE 284
MbtI  DPSGFRRRVAVAVDEIAAGRYHKVILSRCEVEVPPFA--IDPFLTYRLGRRHNTPVRSFLLQ LGGTRALGYSPELVAVRADGVVITEPLAGTRALGR-----GPAIDRLARDDLESNSKE 294
MenF  DKTGWTLQLELATKTAEGELDKVWLRARATDLHFASPVNAAWMAASRRNLNLCYHFYMA FDCGENIFLGSSPERLWRRRDKALRTEALACTVANNP-----DDKQMQQLGEVLMDDKN 281
PabB  TRECYGKFRQVQYLYHSQDCYQNLAQRFHATYSG-DEWQAFLLQANRAPPFAFLRL EQG--AITSLSPERFIFLCDSNEIQTRPIKGTLPRLP-----DPQEDSKQAVKLANSARD 299
TrpE  SDEEFGGVVRLLOKAIATRAGEIFQVWPSRFRSFLPCPS--PLAAYVYVKKSNPSPYMFMMQD NDFTLFGASPESSLKYDATSRLIEIYPIAGTRPGRGRADGSLDRDLDRLSRIELEMRITDHE 358
      : . : * : * : : : : * : : : : ** : . : : * :
TrpE  VLEHILSVKEAIAELEAVCLPGSVVVEDLMSVVRGRGSVQLGSGVSGQLAENKDAWDAFT VLFPSTASGIPNNAALNAIMQIEKTPPELYSGAILLLDDTR FDAALVLRVSVQDSQRC 403
MbtI  IVEHAIYSRSLLEEITDIAEPGSAVIDFMTVRERGSYQLGSTIRARLDFSSDRMAALE ALFPAVTASGIPKAAVGEAIFRLDECPGLYSGAVVMLSADGGGLDAALTLRAAYQVGRT 414
MenF  QRENMLVVEDIQRLQADTQLDVLFPQVLRLR--KVVQLRRCIWTSLN-KADDVICLH QLQPTAAVAGLPPDLARQFARIEPFTHEWYAGSAGYLSLQ--SEFCYLSRSGAKISGNV 396
PabB  RAENLMTVDLMRNDIGRVAVAGSVKVPPELVVEPPAVRHLVSTITAQLPEQLHASDLLR AAFPGGSTGAPKVRAMEIIDELEPQRINAWGSGYLSFGNMDTSITIRILTAINQTI 419
TrpE  LSEHMLVLDLARNDLARICTPGSRVYADLTKVDRYSYVMHLVSRVWVGLRFDLDAHAYR ACMNIGTISGAPKVRAMQLAAEAGRRGSGYGGAGVYFTAHGDLDTIVIRSALENGIA 478
      * : * : : . . : : ** : * . . : * : : * : * : : : : : * :
TrpE  WIQAGAGILAGSTPERELTETREKLASIAPYLMV----- 437
MbtI  WLRAGAGILIEESEPEREFETCEKSLSTLTPYLVARQ----- 450
MenF  RLYAGAGTVRGSDPPEQEWGETDNKAAGLRLLQME----- 431
PabB  FCSAGGGTVADSQEAEVGETFDKVNRIKQLEK----- 453
TrpE  TVQAGAGVVLDSVPQSEADETRNKRARAVLRAIATAHHAQETF 520
      ** : : * : * * : * : :

```

**Figure 4- 15: The alignment above explores sequence conservation in the TrpE *Serratia marcescens* 117Q structure with bound Mg<sup>2+</sup>, benzoate and pyruvate. Residues in or homologous to those in the TrpE structure are highlighted by colors. The coloring of residues takes place according to the different physiochemical criteria according to manufacturer’s instruction.**

#### *Pyruvate Elimination Selectivity*

In MbtI there were no obvious active site functional residues poised to act in pyruvate elimination. This supports against a mechanism in which pyruvate elimination is initiated by proton abstraction by a base. Hilvert and coworkers investigated pyruvate elimination by isochorismate pyruvate lyase (IPL) PchB from *Psuedomonas aeruginosa* (16). They proposed an intramolecular reaction in which the C2 proton was transferred to the enolpyruvate leading to a breaking of the carbon ether oxygen bond in a reaction similar to the chorismate mutase reaction (Fig. 4-16). The isotopically labeled chorismate

was designed by Hilvert and coworkers and incubated with PchB as isochorismate pyruvate lyase. The characterization of products supported the intramolecular mechanism. This model was extended to MbtI which is carried out the formation of salicylate from chorismate via the elimination of pyruvate from intermediate isochorismate. The analysis of the structural data reveals that the  $Mg^{2+}$  is coordinated by two conserved acidic residues, Glu297 and Glu434, as well as the C1 carboxylate of chorismate. The structural data also shows that Lys205 is appropriately positioned to assist in the attack of water at the chorismate C2 carbon for the isomerization reaction and that Glu252 could provide acid catalysis for the elimination of the hydroxyl group from C4 carbon (Fig. 4-16).

The stereochemistry of the reaction catalyzed by anthranilate synthase TrpE has been previously investigated by Asano et al. Using selectively deuterated and tritiated chorismate, it was shown that the pyruvate side chain is stereospecifically protonated on its re-face during the synthesis of anthranilate by AS-sm. Assuming that the stereochemistry of the MbtI reaction mirrors that observed for AS-sm, then intramolecular proton transfer within the isochorismate molecule requires that the re face of the enolpyruvyl group faces C2. From the model built by PyMOL, the substrate can adopt a twisted boat conformation in which the re face of the enolpyruvyl side chain is oriented towards the isochorismate C2 carbon. In this conformation, the only labile proton accessible to the re face of the pyruvate side chain, apart from that of



the substrate, corresponds to the hydroxyl group of Tyr385, which is already hydrogen bonded to the pyruvate carboxylate (**Fig. 4-17**) (17-20). This tyrosine is highly conserved throughout the MST family in both pyruvate retaining and eliminating enzymes.

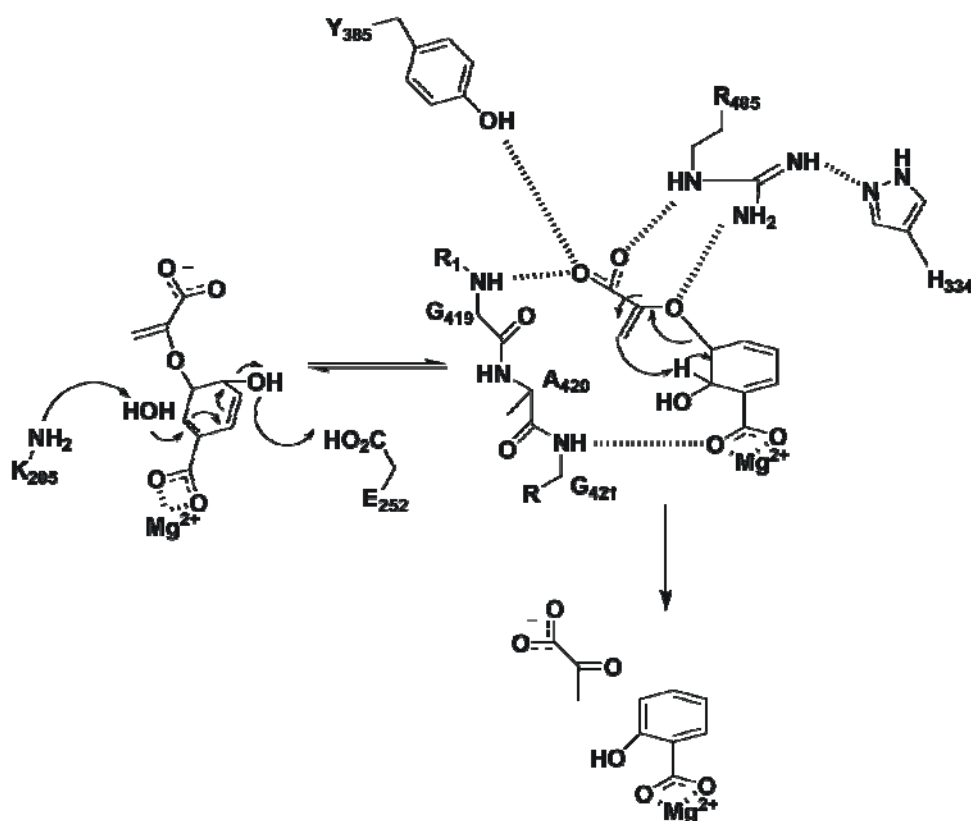


**Figure 4- 16: Proposed intramolecular mechanism catalyzed elimination mechanism for MbtI**

$Mg^{2+}$  is coordinated by two conserved acidic residues, Glu297 and Glu434, as well as the C1 carboxylate of chorismate. Lys205 is appropriately positioned to assist in the attack of water at the chorismate C2 carbon for the isomerization reaction and that Glu252 could provide acid catalysis for the elimination of the hydroxyl group from C4 carbon. Arg405 is coordinated by His334 to assist in position pyruvate side chain

for elimination.

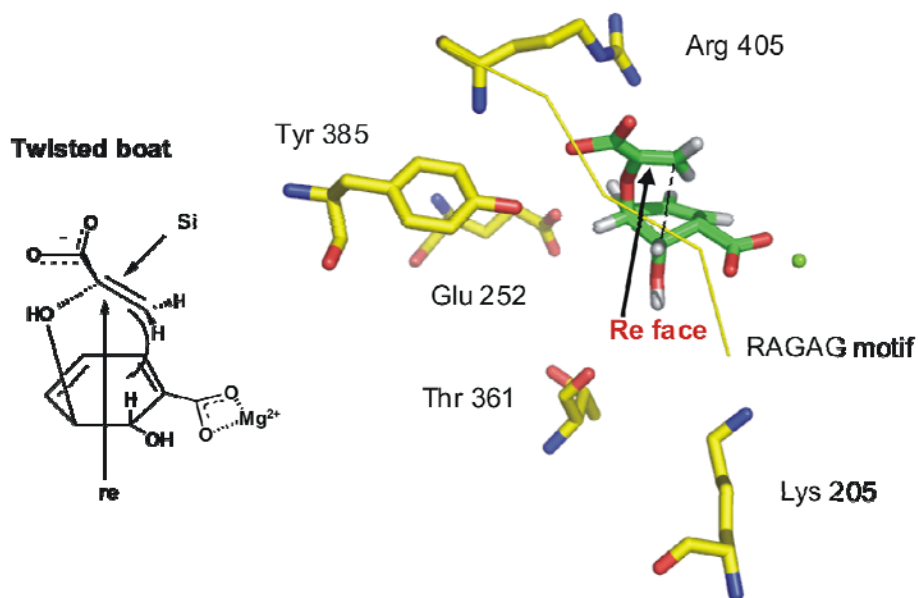


Figure 4- 17: The model of twisted boat conformation built by PyMOL

The pyruvate side chain was protonated on its re-face in studies with TrpE from *Serratia marcesans*. This requires isochorismate to be bound in a twisted diaxial boat conformation.

*Enzyme Activities Affecting End Product Distribution in Response to Changes in Ion Concentration*

The initial step in the biosynthesis of mycobactin is the conversion of chorismate to salicylate. In general, this is accomplished either by a single salicylate synthase enzyme or by a pair of enzymes, an isochorismate synthase and an isochorismate pyruvate lyase sequentially. Our work

indicated that MbtI catalyzes the  $Mg^{2+}$  dependent formation of salicylate from chorismate, consistent with the observation that *M. tuberculosis* lacks homologues of the isochorismate pyruvate lyase enzyme that would be required for the subsequent conversion of isochorismate to salicylate. Thus MbtI catalyzes both the isomerization of chorismate to isochorismate and the subsequent elimination of pyruvate from isochorismate under certain pH region.

MbtI is a member of a family of chorismate-binding enzymes that catalyze distinct reactions on a conserved structural template. A mechanism for isomerization and substitution within this enzyme family has recently been proposed, while pyruvate elimination has generally been thought to occur via acid/base catalysis utilizing one or more active site residues, which discussed previously. With the observation that MbtI catalyzes the formation of prephenate, as well as isochorismate and salicylate, we propose a mechanism for pyruvate elimination applicable to the entire MST family.

Interestingly, besides as a salicylate synthase, MbtI is also the chorismate mutase in the absence of  $Mg^{2+}$ . Generally speaking, Chorismate has to be bound in a conformation such that the enolpyruvyl group can approach the C1 substrate carbon. This can occur by slight changes in the orientation of the side chain in the diaxial twisted boat conformation in which the enolpyruvyl side chain forms hydrogen bonds with Tyr372, Arg391, and Gly405. With the exception of the  $Mg^{2+}$  dependent enzyme family including MenF and MbtI all

chorismate binding enzymes use Arg to coordinate the 1' CO<sup>2-</sup> of chorismate. This suggests Mg<sup>2+</sup> has a role unique to the product distribution. As MenF and MbtI catalysis proceeds via nucleophilic attack at the C2 carbon, Mg<sup>2+</sup> can be imagined to promote catalysis by generation of a partial positive charge on C2 carbon. This hypothesis can be investigated experimentally using NMR with a stable chorismate analogue labeled at C2 position. The chemical shift of the labeled position can be compared free in solution, bound to MenF/MbtI, and bound to MenF/MbtI in the presence of Mg<sup>2+</sup>. A candidate analogue is the fluorochorismate reported by Abell and coworkers (14). It is unknown if this molecule is a substrate for MenF/ MbtI. If the 2 fluoro compound turns over MenF K190A/ MbtI K205A mutants could be used to form a stable enzyme analogue complex. Binding of the compound to either the WT or mutant enzyme both with and without Mg<sup>2+</sup> would first have to be demonstrated before NMR experiments could be performed.

Hence, in the MST enzymes Mg<sup>2+</sup> could potentially be involved in ligand activation. He et al.'s general mechanism for the MST family involves attack at the C2 carbon of chorismate by an exogenous or main chain nucleophile. Ligand polarization by Mg<sup>2+</sup>, as shown in **Figure 4-18**, would generate a partial positive charge at the C2 position, facilitating nucleophilic attack at that position. This is similar to the proposal by Walsh et al. in which positively charged active site residues perform an analogous role to the Mg<sup>2+</sup> as part of a S<sub>N</sub>2 Michael addition/elimination sequence (8). We propose that chorismate is

bound to MbtI in a conformation that can partition either to isochorismate or prephenate. In the wild type enzyme activation of C2 by  $Mg^{2+}$  results in isochorismate formation while in the absence of  $Mg^{2+}$  prephenate is the preferred product. The two reaction pathways are finely balanced and thus mutations that perturb isomerization.

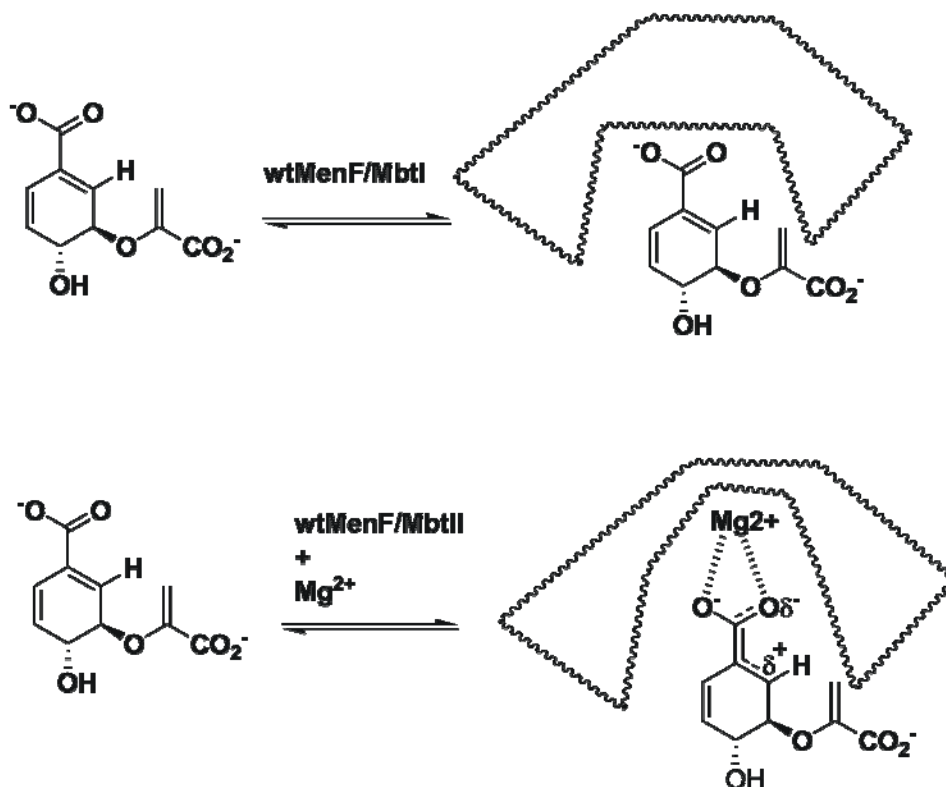


Figure 4- 18: The proposed mechanism for substrate activation via  $Mg^{2+}$

$Mg^{2+}$  can be imagined to promote catalysis by generation of a partial positive charge on C2 carbon, facilitating nucleophilic attack at that position

#### **4.5 Conclusion**

Siderophores are essential for bacteria, which require iron for growth and consequently produce iron-chelating molecules. Siderophores can very efficiently scavenge iron from the environment. In *M. tuberculosis* the siderophore is mycobactin and the biosynthesis of this molecule is under the transcriptional control of the iron-dependent regulator IdeR.

Isochorismate and Salicylate Synthase Activities MbtI (Rv2386c) is annotated in the *M. tuberculosis* genome as an isochorismate synthase and is 28% identical and 46% similar to MenF the isochorismate synthase from *E. coli*. At pH 7 MbtI demonstrates isochorismate synthase activity but as the pH is raised above 7.5 salicylate becomes the primary product. In addition, at pH 8 MbtI can utilize isochorismate as a substrate for salicylate production and the kinetic data show that isochorismate is a kinetically competent intermediate on the reaction pathway. As observed for other homologues in the MST enzyme family, the isochorismate and salicylate synthase activity of MbtI is Mg<sup>2+</sup> dependent and analysis of the structural data reveals that the Mg<sup>2+</sup> is coordinated by two conserved acidic residues, Glu297 and Glu434, as well as the C1 carboxylate of chorismate. The structural data also shows that Lys205 is appropriately positioned to assist in the attack of water at the chorismate C2 carbon for the isomerization reaction and that Glu252 could provide acid catalysis for the elimination of the hydroxyl group from C4 carbon.

Accumulation of isochorismate at pH below 7.5 can be explained by the

ionization of an active site residue required for the subsequent elimination of pyruvate from isochorismate. The corresponding ionizable residue is still under investigation, although His334 may be a key role in positioning the isochorismate pyruvate side chain in the active site. Another big question mark is that since the intracellular pH of the bacterium is thought to be around 7.0, it is not consistent with the *in vitro* observation that in pH values under 7.5, MbtI acts as an isochorismate synthase but not salicylate synthase as expected. One possible explanation could be that the next enzyme MbtA in the mycobactin biosynthetic pathway controls whether isochorismate or salicylate is the product of the MbtI reaction. One indirect support is that the incubation assay of MbtA with isochorismate didn't generate salicylate-AMP as product, which indicated that isochorismate is not a stable substrate for MbtA. entC is annotated as the isochorismate synthase in menaquinone biosynthetic pathway in *M. tuberculosis*. Although we have obtained the soluble EntC protein, so far we have been unable to demonstrate that EntC is able to synthesize isochorismate.

In almost every case, the MbtI mutants and wild-type MbtI displayed chorismate mutase activity in the absence of  $Mg^{2+}$ . In order to explain this observation, we propose that chorismate is bound to MbtI in a diaxial conformation that is optimized for isomerization and elimination, and from which prephenate can be also formed. Hilvert and coworkers have extensively studied the nonenzymatical rearrangement of chorismate and isochorismate

by using labeling compounds, and demonstrated that the nonenzymatic rearrangements of the molecules depend upon the orientation of their enolpyruvyl side chains. Specifically, it was shown that the elimination of pyruvate from chorismate and isochorismate to give p-hydroxybenzoate and salicylate, respectively, proceeded via a concerted pericyclic mechanism in which the respective C4 and C2 protons are transferred to the enolpyruvyl side chain. A similar mechanism was subsequently proposed for the isochorismate pyruvate lyase, PchB. PchB, which is a pyruvate lyase, also has chorismate mutase activity suggesting that chorismate can bind to the enzyme in an orientation that dominates an intramolecular rearrangement (16). Hilvert and coworkers demonstrated that PchB catalyzed the elimination of pyruvate from isochorismate via an intramolecular mechanism in which the C2 proton of isochorismate is transferred to the pyruvate (16). Here we proposed a similar reaction mechanism utilized by MbtI and considered the stereochemistry of the reaction.



## Reference

1. Ratledge, C. (2004) Iron, mycobacteria and tuberculosis, *Tuberculosis (Edinb)* 84, 110-130.
2. Gobin, J., Moore, C. H., Reeve, J. R., Jr., Wong, D. K., Gibson, B. W., and Horwitz, M. A. (1995) Iron acquisition by *Mycobacterium tuberculosis*: isolation and characterization of a family of iron-binding exochelins, *Proc Natl Acad Sci U S A* 92, 5189-5193.
3. Wong, D. K., Gobin, J., Horwitz, M. A., and Gibson, B. W. (1996) Characterization of exochelins of *Mycobacterium avium*: evidence for saturated and unsaturated and for acid and ester forms, *J Bacteriol* 178, 6394-6398.
4. Gobin, J., and Horwitz, M. A. (1996) Exochelins of *Mycobacterium tuberculosis* remove iron from human iron-binding proteins and donate iron to mycobactins in the *M. tuberculosis* cell wall, *J Exp Med* 183, 1527-1532.
5. Brosch, R., Gordon, S. V., Billault, A., Garnier, T., Eiglmeier, K., Soravito, C., Barrell, B. G., and Cole, S. T. (1998) Use of a *Mycobacterium tuberculosis* H37Rv bacterial artificial chromosome library for genome mapping, sequencing, and comparative genomics, *Infect Immun* 66, 2221-2229.
6. De Voss, J. J., Rutter, K., Schroeder, B. G., and Barry, C. E., 3rd. (1999) Iron acquisition and metabolism by mycobacteria, *J Bacteriol* 181,

4443-4451.

7. Crosa, J. H., and Walsh, C. T. (2002) Genetics and assembly line enzymology of siderophore biosynthesis in bacteria, *Microbiol Mol Biol Rev* 66, 223-249.
8. Liu, J., Quinn, N., Berchtold, G. A., and Walsh, C. T. (1990) Overexpression, purification, and characterization of isochorismate synthase (EntC), the first enzyme involved in the biosynthesis of enterobactin from chorismate, *Biochemistry* 29, 1417-1425.
9. Romero, R. M., Roberts, M. F., and Phillipson, J. D. (1995) Anthranilate synthase in microorganisms and plants, *Phytochemistry* 39, 263-276.
10. Viswanathan, V. K., Green, J. M., and Nichols, B. P. (1995) Kinetic characterization of 4-amino 4-deoxychorismate synthase from *Escherichia coli*, *J Bacteriol* 177, 5918-5923.
11. Davidson, B. E., and Hudson, G. S. (1987) Chorismate mutase-prephenate dehydrogenase from *Escherichia coli*, *Methods Enzymol* 142, 440-450.
12. Spraggon, G., Kim, C., Nguyen-Huu, X., Yee, M. C., Yanofsky, C., and Mills, S. E. (2001) The structures of anthranilate synthase of *Serratia marcescens* crystallized in the presence of (i) its substrates, chorismate and glutamine, and a product, glutamate, and (ii) its end-product inhibitor, L-tryptophan, *Proc Natl Acad Sci U S A* 98, 6021-6026.

13. Parsons, J. F., Jensen, P. Y., Pachikara, A. S., Howard, A. J., Eisenstein, E., and Ladner, J. E. (2002) Structure of *Escherichia coli* aminodeoxychorismate synthase: architectural conservation and diversity in chorismate-utilizing enzymes, *Biochemistry* 41, 2198-2208.
14. Kerbarh, O., Ciulli, A., Howard, N. I., and Abell, C. (2005) Salicylate biosynthesis: overexpression, purification, and characterization of Irp9, a bifunctional salicylate synthase from *Yersinia enterocolitica*, *J Bacteriol* 187, 5061-5066.
15. Kerbarh, O., Chirgadze, D. Y., Blundell, T. L., and Abell, C. (2006) Crystal structures of *Yersinia enterocolitica* salicylate synthase and its complex with the reaction products salicylate and pyruvate, *J Mol Biol* 357, 524-534.
16. Kunzler, D. E., Sasso, S., Gamper, M., Hilvert, D., and Kast, P. (2005) Mechanistic insights into the isochorismate pyruvate lyase activity of the catalytically promiscuous PchB from combinatorial mutagenesis and selection, *J Biol Chem* 280, 32827-32834.
17. Aberhart, D. J., Ghoshal, P. K., Cotting, J. A., and Russell, D. J. (1985) Coenzyme A biosynthesis: steric course of 4'-phosphopantothenoyl-L-cysteine decarboxylase, *Biochemistry* 24, 7178-7182.
18. Cook, A. G., and Knowles, J. R. (1985) Phosphoenolpyruvate synthetase and pyruvate, orthophosphate dikinase: stereochemical

consequences at both the beta-phospho and gamma-phospho groups of ATP, *Biochemistry* 24, 51-58.

19. Guo, H., Cui, Q., Lipscomb, W. N., and Karplus, M. (2001) Substrate conformational transitions in the active site of chorismate mutase: their role in the catalytic mechanism, *Proc Natl Acad Sci U S A* 98, 9032-9037.
20. Kerbarh, O., Campopiano, D. J., and Baxter, R. L. (2006) Mechanism of alpha-oxoamine synthases: identification of the intermediate Claisen product in the 8-amino-7-oxononanoate synthase reaction, *Chem Commun (Camb)*, 60-62.

## **Bibliography**

### **Chapter I**

1. Grenet, K., Guillemot, D., Jarlier, V., Moreau, B., Dubourdiou, S., Ruimy, R., Armand-Lefevre, L., Bau, P., and Andremont, A. (2004) Antibacterial resistance, Wayampis Amerindians, French Guyana, *Emerg Infect Dis* 10, 1150-1153.
2. Zarocostas, J. (2008) WHO urges action on drug resistant tuberculosis, *BMJ* 336, 465.
3. N'Guessan J, D., Coulibaly, A., Ramanou, A. A., Okou, O. C., Djaman, A. J., and Guede-Guina, F. (2007) Antibacterial activity of *Thonningia sanguinea* against some multi-drug resistant strains of *Salmonella enterica*, *Afr Health Sci* 7, 155-158.
4. Haddadin, A. S., Fappiano, S. A., and Lipsett, P. A. (2002) Methicillin resistant *Staphylococcus aureus* (MRSA) in the intensive care unit, *Postgrad Med J* 78, 385-392.
5. Wright, G. D. (2007) The antibiotic resistome: the nexus of chemical and genetic diversity, *Nat Rev Microbiol* 5, 175-186.
6. Corbett, E. L. (2003) HIV and tuberculosis: surveillance revisited, *Int J Tuberc Lung Dis* 7, 709.
7. Corbett, E. L., Watt, C. J., Walker, N., Maher, D., Williams, B. G., Raviglione, M. C., and Dye, C. (2003) The growing burden of tuberculosis: global trends and interactions with the HIV epidemic,

*Arch Intern Med* 163, 1009-1021.

8. Gutierrez, M. C., Brisse, S., Brosch, R., Fabre, M., Omais, B., Marmiesse, M., Supply, P., and Vincent, V. (2005) Ancient origin and gene mosaicism of the progenitor of *Mycobacterium tuberculosis*, *PLoS Pathog* 1, e5.
9. (2010) Global tuberculosis control: key findings from the December 2009 WHO report, *Wkly Epidemiol Rec* 85, 69-80.
10. Tonge, P. J. (2000) Another brick in the wall, *Nat Struct Biol* 7, 94-96.
11. Tupasi, T. E., Radhakrishna, S., Quelapio, M. I., Villa, M. L., Pascual, M. L., Rivera, A. B., Sarmiento, A., Co, V. M., Sarol, J. N., Beltran, G., Legaspi, J. D., Mangubat, N. V., Reyes, A. C., Solon, M., Solon, F. S., Burton, L., and Mantala, M. J. (2000) Tuberculosis in the urban poor settlements in the Philippines, *Int J Tuberc Lung Dis* 4, 4-11.
12. Rose, C., Auxenfant, E., Noel, M. P., Mahieu, M., Demory, J. L., Croxo, C., Wallaert, B., and Bauters, F. (1997) [Tuberculosis, mycobacterium infection and hairy cell leukemia], *Presse Med* 26, 110-114.
13. Parrish, N. M., Dick, J. D., and Bishai, W. R. (1998) Mechanisms of latency in *Mycobacterium tuberculosis*, *Trends Microbiol* 6, 107-112.
14. Bishai, W. R., Dannenberg, A. M., Jr., Parrish, N., Ruiz, R., Chen, P., Zook, B. C., Johnson, W., Boles, J. W., and Pitt, M. L. (1999) Virulence of *Mycobacterium tuberculosis* CDC1551 and H37Rv in rabbits evaluated by Lurie's pulmonary tubercle count method, *Infect Immun*

67, 4931-4934.

15. Tufariello, J. M., Chan, J., and Flynn, J. L. (2003) Latent tuberculosis: mechanisms of host and bacillus that contribute to persistent infection, *Lancet Infect Dis* 3, 578-590.
16. Gardam, M., and Iverson, K. (2003) Rheumatoid arthritis and tuberculosis: time to take notice, *J Rheumatol* 30, 1397-1399.
17. Long, R., and Gardam, M. (2003) Tumour necrosis factor-alpha inhibitors and the reactivation of latent tuberculosis infection, *CMAJ* 168, 1153-1156.
18. Gardam, M. A., Keystone, E. C., Menzies, R., Manners, S., Skamene, E., Long, R., and Vinh, D. C. (2003) Anti-tumour necrosis factor agents and tuberculosis risk: mechanisms of action and clinical management, *Lancet Infect Dis* 3, 148-155.
19. Amaral, L., Viveiros, M., and Kristiansen, J. E. (2001) Phenothiazines: potential alternatives for the management of antibiotic resistant infections of tuberculosis and malaria in developing countries, *Trop Med Int Health* 6, 1016-1022.
20. Amaral, L., Kristiansen, J. E., Viveiros, M., and Atouguia, J. (2001) Activity of phenothiazines against antibiotic-resistant *Mycobacterium tuberculosis*: a review supporting further studies that may elucidate the potential use of thioridazine as anti-tuberculosis therapy, *J Antimicrob Chemother* 47, 505-511.

21. Viveiros, M., and Amaral, L. (2001) Enhancement of antibiotic activity against poly-drug resistant *Mycobacterium tuberculosis* by phenothiazines, *Int J Antimicrob Agents* 17, 225-228.
22. Bonhoeffer, S., Lipsitch, M., and Levin, B. R. (1997) Evaluating treatment protocols to prevent antibiotic resistance, *Proc Natl Acad Sci U S A* 94, 12106-12111.
23. Bonhoeffer, S., Coffin, J. M., and Nowak, M. A. (1997) Human immunodeficiency virus drug therapy and virus load, *J Virol* 71, 3275-3278.
24. Nowak, M. A., Bonhoeffer, S., Shaw, G. M., and May, R. M. (1997) Anti-viral drug treatment: dynamics of resistance in free virus and infected cell populations, *J Theor Biol* 184, 203-217.
25. Gandhi, N. R., Moll, A., Sturm, A. W., Pawinski, R., Govender, T., Lalloo, U., Zeller, K., Andrews, J., and Friedland, G. (2006) Extensively drug-resistant tuberculosis as a cause of death in patients co-infected with tuberculosis and HIV in a rural area of South Africa, *Lancet* 368, 1575-1580.
26. Frieden, T. R. (1996) The phylogeny of *Mycobacterium tuberculosis*, *Tuber Lung Dis* 77, 291.
27. Washko, R. M., and Frieden, T. R. (1996) Tuberculosis surveillance using death certificate data, New York City, 1992, *Public Health Rep* 111, 251-255.



28. Kaye, K., and Frieden, T. R. (1996) Tuberculosis control: the relevance of classic principles in an era of acquired immunodeficiency syndrome and multidrug resistance, *Epidemiol Rev* 18, 52-63.
29. Frieden, T. R. (1996) Clarifying the issues in tuberculosis control, *Am J Public Health* 86, 267-268.
30. Boshoff, H. I., Myers, T. G., Copp, B. R., McNeil, M. R., Wilson, M. A., and Barry, C. E., 3rd. (2004) The transcriptional responses of *Mycobacterium tuberculosis* to inhibitors of metabolism: novel insights into drug mechanisms of action, *J Biol Chem* 279, 40174-40184.
31. Barczak, A. K., Domenech, P., Boshoff, H. I., Reed, M. B., Manca, C., Kaplan, G., and Barry, C. E., 3rd. (2005) In vivo phenotypic dominance in mouse mixed infections with *Mycobacterium tuberculosis* clinical isolates, *J Infect Dis* 192, 600-606.
32. (1984) Classics in infectious diseases. "On abscesses". Alexander Ogston (1844-1929), *Rev Infect Dis* 6, 122-128.
33. McGregor, J. C., Dumyati, G., Casiano-Colon, A. E., Chang, P. J., and Klevens, R. M. (2009) Usefulness of antibiogram surveillance for methicillin-resistant *Staphylococcus aureus* in outpatient pediatric populations, *Diagn Microbiol Infect Dis* 64, 70-75.
34. Panlilio, A. L., Culver, D. H., Gaynes, R. P., Banerjee, S., Henderson, T. S., Tolson, J. S., and Martone, W. J. (1992) Methicillin-resistant *Staphylococcus aureus* in U.S. hospitals, 1975-1991, *Infect Control*

*Hosp Epidemiol* 13, 582-586.

35. Eady, E. A., and Cove, J. H. (2003) Staphylococcal resistance revisited: community-acquired methicillin resistant *Staphylococcus aureus*--an emerging problem for the management of skin and soft tissue infections, *Curr Opin Infect Dis* 16, 103-124.
36. Baumert, N., von Eiff, C., Schaaff, F., Peters, G., Proctor, R. A., and Sahl, H. G. (2002) Physiology and antibiotic susceptibility of *Staphylococcus aureus* small colony variants, *Microb Drug Resist* 8, 253-260.
37. Brouillette, E., Martinez, A., Boyll, B. J., Allen, N. E., and Malouin, F. (2004) Persistence of a *Staphylococcus aureus* small-colony variant under antibiotic pressure in vivo, *FEMS Immunol Med Microbiol* 41, 35-41.
38. Ma, Z., Lienhardt, C., McIlleron, H., Nunn, A. J., and Wang, X. (2010) Global tuberculosis drug development pipeline: the need and the reality, *Lancet* 375, 2100-2109.
39. Lienhardt, C., Vernon, A., and Raviglione, M. C. (2010) New drugs and new regimens for the treatment of tuberculosis: review of the drug development pipeline and implications for national programmes, *Curr Opin Pulm Med* 16, 186-193.
40. Thompson, D. (2010) Hospital infection control and the reduction in intensive care unit-acquired MRSA between 1996 and 2009, *J Hosp*

*Infect.*

41. Cavaco, L. M., Hasman, H., Stegger, M., Andersen, P. S., Skov, R., Fluit, A. C., Ito, T., and Aarestrup, F. M. (2010) Cloning and occurrence of *czrC*, a gene conferring cadmium and zinc resistance in MRSA CC398, *Antimicrob Agents Chemother.*
42. Naimi, T. S., LeDell, K. H., Como-Sabetti, K., Borchardt, S. M., Boxrud, D. J., Etienne, J., Johnson, S. K., Vandenesch, F., Fridkin, S., O'Boyle, C., Danila, R. N., and Lynfield, R. (2003) Comparison of community- and health care-associated methicillin-resistant *Staphylococcus aureus* infection, *JAMA* 290, 2976-2984.
43. Perencevich, E. N., and Diekema, D. J. (2010) Decline in invasive MRSA infection: where to go from here?, *JAMA* 304, 687-689.
44. Skiest, D., Brown, K., Hester, J., Moore, T., Crosby, C., Mussa, H. R., Hoffman-Roberts, H., and Cooper, T. (2006) Community-onset methicillin-resistant *Staphylococcus aureus* in an urban HIV clinic, *HIV Med* 7, 361-368.
45. Cohen, P. R., and Grossman, M. E. (2004) Management of cutaneous lesions associated with an emerging epidemic: community-acquired methicillin-resistant *Staphylococcus aureus* skin infections, *J Am Acad Dermatol* 51, 132-135.
46. Shaw, D. J., Guest, J. R., Meganathan, R., and Bentley, R. (1982) Characterization of *Escherichia coli* men mutants defective in

conversion of o-succinylbenzoate to 1,4-dihydroxy-2-naphthoate, *J Bacteriol* 152, 1132-1137.

47. Bentley, R., and Meganathan, R. (1982) Biosynthesis of vitamin K (menaquinone) in bacteria, *Microbiol Rev* 46, 241-280.
48. Kolappan, S., Zwahlen, J., Zhou, R., Truglio, J. J., Tonge, P. J., and Kisker, C. (2007) Lysine 190 is the catalytic base in MenF, the menaquinone-specific isochorismate synthase from *Escherichia coli*: implications for an enzyme family, *Biochemistry* 46, 946-953.
49. Zwahlen, J., Kolappan, S., Zhou, R., Kisker, C., and Tonge, P. J. (2007) Structure and mechanism of MbtI, the salicylate synthase from *Mycobacterium tuberculosis*, *Biochemistry* 46, 954-964.
50. Truglio, J. J., Theis, K., Feng, Y., Gajda, R., Machutta, C., Tonge, P. J., and Kisker, C. (2003) Crystal structure of *Mycobacterium tuberculosis* MenB, a key enzyme in vitamin K2 biosynthesis, *J Biol Chem* 278, 42352-42360.
51. Kurosu, M., Narayanasamy, P., Biswas, K., Dhiman, R., and Crick, D. C. (2007) Discovery of 1,4-dihydroxy-2-naphthoate [corrected] prenyltransferase inhibitors: new drug leads for multidrug-resistant gram-positive pathogens, *J Med Chem* 50, 3973-3975.
52. Kurosu, M., and Begari, E. (2010) Vitamin K2 in electron transport system: are enzymes involved in vitamin K2 biosynthesis promising drug targets?, *Molecules* 15, 1531-1553.

53. Dhungana, S., Ratledge, C., and Crumbliss, A. L. (2004) Iron chelation properties of an extracellular siderophore exochelin MS, *Inorg Chem* 43, 6274-6283.
54. Ratledge, C. (2004) Iron, mycobacteria and tuberculosis, *Tuberculosis (Edinb)* 84, 110-130.
55. Ferreras, J. A., Ryu, J. S., Di Lello, F., Tan, D. S., and Quadri, L. E. (2005) Small-molecule inhibition of siderophore biosynthesis in *Mycobacterium tuberculosis* and *Yersinia pestis*, *Nat Chem Biol* 1, 29-32.
56. Crosa, J. H., and Walsh, C. T. (2002) Genetics and assembly line enzymology of siderophore biosynthesis in bacteria, *Microbiol Mol Biol Rev* 66, 223-249.

## Chapter II

1. Babbitt, P. C., Kenyon, G. L., Martin, B. M., Charest, H., Slyvestre, M., Scholten, J. D., Chang, K. H., Liang, P. H., and Dunaway-Mariano, D. (1992) Ancestry of the 4-chlorobenzoate dehalogenase: analysis of amino acid sequence identities among families of acyl:adenyl ligases, enoyl-CoA hydratases/isomerases, and acyl-CoA thioesterases, *Biochemistry* 31, 5594-5604.
2. Bentley, R., and Meganathan, R. (1982) Biosynthesis of vitamin K (menaquinone) in bacteria, *Microbiol Rev* 46, 241-280.
3. Hiratsuka, T., Furihata, K., Ishikawa, J., Yamashita, H., Itoh, N., Seto, H., and Dairi, T. (2008) An alternative menaquinone biosynthetic pathway operating in microorganisms, *Science* 321, 1670-1673.
4. Reger, A. S., Wu, R., Dunaway-Mariano, D., and Gulick, A. M. (2008) Structural characterization of a 140 degrees domain movement in the two-step reaction catalyzed by 4-chlorobenzoate:CoA ligase, *Biochemistry* 47, 8016-8025.
5. Cole, S. T., Brosch, R., Parkhill, J., Garnier, T., Churcher, C., Harris, D., Gordon, S. V., Eiglmeier, K., Gas, S., Barry, C. E., 3rd, Tekaia, F., Badcock, K., Basham, D., Brown, D., Chillingworth, T., Connor, R., Davies, R., Devlin, K., Feltwell, T., Gentles, S., Hamlin, N., Holroyd, S., Hornsby, T., Jagels, K., Krogh, A., McLean, J., Moule, S., Murphy, L., Oliver, K., Osborne, J., Quail, M. A., Rajandream, M. A., Rogers, J.,

- Rutter, S., Seeger, K., Skelton, J., Squares, R., Squares, S., Sulston, J. E., Taylor, K., Whitehead, S., and Barrell, B. G. (1998) Deciphering the biology of *Mycobacterium tuberculosis* from the complete genome sequence, *Nature* 393, 537-544.
6. Meganathan, R., and Bentley, R. (1979) Menaquinone (vitamin K2) biosynthesis: conversion of o-succinylbenzoic acid to 1,4-dihydroxy-2-naphthoic acid by *Mycobacterium phlei* enzymes, *J Bacteriol* 140, 92-98.
  7. Kwon, O., Bhattacharyya, D. K., and Meganathan, R. (1996) Menaquinone (vitamin K2) biosynthesis: overexpression, purification, and properties of o-succinylbenzoyl-coenzyme A synthetase from *Escherichia coli*, *J Bacteriol* 178, 6778-6781.
  8. Curran, J. P., and Al-Salihi, F. L. (1980) Neonatal staphylococcal scalded skin syndrome: massive outbreak due to an unusual phage type, *Pediatrics* 66, 285-290.
  9. Lodise, T. P., Jr., McKinnon, P. S., and Rybak, M. (2003) Prediction model to identify patients with *Staphylococcus aureus* bacteremia at risk for methicillin resistance, *Infect Control Hosp Epidemiol* 24, 655-661.
  10. Lodise, T. P., McKinnon, P. S., Swiderski, L., and Rybak, M. J. (2003) Outcomes analysis of delayed antibiotic treatment for hospital-acquired *Staphylococcus aureus* bacteremia, *Clin Infect Dis* 36, 1418-1423.

11. Hiramatsu, K., Hanaki, H., Ino, T., Yabuta, K., Oguri, T., and Tenover, F. C. (1997) Methicillin-resistant *Staphylococcus aureus* clinical strain with reduced vancomycin susceptibility, *J Antimicrob Chemother* 40, 135-136.
12. Menichetti, F. (2005) Current and emerging serious Gram-positive infections, *Clin Microbiol Infect* 11 Suppl 3, 22-28.
13. Moran, G. J., Krishnadasan, A., Gorwitz, R. J., Fosheim, G. E., McDougal, L. K., Carey, R. B., and Talan, D. A. (2006) Methicillin-resistant *S. aureus* infections among patients in the emergency department, *N Engl J Med* 355, 666-674.
14. Klevens, R. M., Edwards, J. R., Tenover, F. C., McDonald, L. C., Horan, T., and Gaynes, R. (2006) Changes in the epidemiology of methicillin-resistant *Staphylococcus aureus* in intensive care units in US hospitals, 1992-2003, *Clin Infect Dis* 42, 389-391.
15. Luo, L., Taylor, K. L., Xiang, H., Wei, Y., Zhang, W., and Dunaway-Mariano, D. (2001) Role of active site binding interactions in 4-chlorobenzoyl-coenzyme A dehalogenase catalysis, *Biochemistry* 40, 15684-15692.
16. Martinez-Blanco, H., Reglero, A., Fernandez-Valverde, M., Ferrero, M. A., Moreno, M. A., Penalva, M. A., and Luengo, J. M. (1992) Isolation and characterization of the acetyl-CoA synthetase from *Penicillium chrysogenum*. Involvement of this enzyme in the biosynthesis of



- penicillins, *J Biol Chem* 267, 5474-5481.
17. May, J. J., Kessler, N., Marahiel, M. A., and Stubbs, M. T. (2002) Crystal structure of DhbE, an archetype for aryl acid activating domains of modular nonribosomal peptide synthetases, *Proc Natl Acad Sci U S A* 99, 12120-12125.
  18. Lu, X., Zhang, H., Tonge, P. J., and Tan, D. S. (2008) Mechanism-based inhibitors of MenE, an acyl-CoA synthetase involved in bacterial menaquinone biosynthesis, *Bioorg Med Chem Lett* 18, 5963-5966.
  19. Zheng, R., and Blanchard, J. S. (2001) Steady-state and pre-steady-state kinetic analysis of *Mycobacterium tuberculosis* pantothenate synthetase, *Biochemistry* 40, 12904-12912.
  20. Wu, R., Cao, J., Lu, X., Reger, A. S., Gulick, A. M., and Dunaway-Mariano, D. (2008) Mechanism of 4-chlorobenzoate:coenzyme a ligase catalysis, *Biochemistry* 47, 8026-8039.
  21. Branchini, B. R., Magyar, R. A., Murtiashaw, M. H., Anderson, S. M., Helgerson, L. C., and Zimmer, M. (1999) Site-directed mutagenesis of firefly luciferase active site amino acids: a proposed model for bioluminescence color, *Biochemistry* 38, 13223-13230.
  22. Wisplinghoff, H., Bischoff, T., Tallent, S. M., Seifert, H., Wenzel, R. P., and Edmond, M. B. (2004) Nosocomial bloodstream infections in US

- hospitals: analysis of 24,179 cases from a prospective nationwide surveillance study, *Clin Infect Dis* 39, 309-317.
23. Reger, A. S., Carney, J. M., and Gulick, A. M. (2007) Biochemical and crystallographic analysis of substrate binding and conformational changes in acetyl-CoA synthetase, *Biochemistry* 46, 6536-6546.
  24. Hisanaga, Y., Ago, H., Nakagawa, N., Hamada, K., Ida, K., Yamamoto, M., Hori, T., Aii, Y., Sugahara, M., Kuramitsu, S., Yokoyama, S., and Miyano, M. (2004) Structural basis of the substrate-specific two-step catalysis of long chain fatty acyl-CoA synthetase dimer, *J Biol Chem* 279, 31717-31726.
  25. Horswill, A. R., and Escalante-Semerena, J. C. (2002) Characterization of the propionyl-CoA synthetase (PrpE) enzyme of *Salmonella enterica*: residue Lys592 is required for propionyl-AMP synthesis, *Biochemistry* 41, 2379-2387.
  26. Kaneko, M., Ohnishi, Y., and Horinouchi, S. (2003) Cinnamate:coenzyme A ligase from the filamentous bacterium *Streptomyces coelicolor* A3(2), *J Bacteriol* 185, 20-27.
  27. Lindermayr, C., Fliegmann, J., and Ebel, J. (2003) Deletion of a single amino acid residue from different 4-coumarate:CoA ligases from soybean results in the generation of new substrate specificities, *J Biol Chem* 278, 2781-2786.
  28. Gulick, A. M., Starai, V. J., Horswill, A. R., Homick, K. M., and

- Escalante-Semerena, J. C. (2003) The 1.75 Å crystal structure of acetyl-CoA synthetase bound to adenosine-5'-propylphosphate and coenzyme A, *Biochemistry* 42, 2866-2873.
29. Jogl, G., and Tong, L. (2004) Crystal structure of yeast acetyl-coenzyme A synthetase in complex with AMP, *Biochemistry* 43, 1425-1431.
30. Yonus, H., Neumann, P., Zimmermann, S., May, J. J., Marahiel, M. A., and Stubbs, M. T. (2008) Crystal structure of DltA. Implications for the reaction mechanism of non-ribosomal peptide synthetase adenylation domains, *J Biol Chem* 283, 32484-32491.

### Chapter III

1. Lodise, T. P., McKinnon, P. S., Swiderski, L., and Rybak, M. J. (2003) Outcomes analysis of delayed antibiotic treatment for hospital-acquired *Staphylococcus aureus* bacteremia, *Clin Infect Dis* 36, 1418-1423.
2. Luo, L., Taylor, K. L., Xiang, H., Wei, Y., Zhang, W., and Dunaway-Mariano, D. (2001) Role of active site binding interactions in 4-chlorobenzoyl-coenzyme A dehalogenase catalysis, *Biochemistry* 40, 15684-15692.
3. Martinez-Blanco, H., Reglero, A., Fernandez-Valverde, M., Ferrero, M. A., Moreno, M. A., Penalva, M. A., and Luengo, J. M. (1992) Isolation and characterization of the acetyl-CoA synthetase from *Penicillium chrysogenum*. Involvement of this enzyme in the biosynthesis of penicillins, *J Biol Chem* 267, 5474-5481.
4. May, J. J., Kessler, N., Marahiel, M. A., and Stubbs, M. T. (2002) Crystal structure of DhbE, an archetype for aryl acid activating domains of modular nonribosomal peptide synthetases, *Proc Natl Acad Sci U S A* 99, 12120-12125.
5. Qiao, C., Gupte, A., Boshoff, H. I., Wilson, D. J., Bennett, E. M., Somu, R. V., Barry, C. E., 3rd, and Aldrich, C. C. (2007) 5'-O-[(N-acyl)sulfamoyl]adenosines as antitubercular agents that inhibit MbtA: an adenylation enzyme required for siderophore biosynthesis of the mycobactins, *J Med Chem* 50, 6080-6094.

6. Kane, J. F. (1995) Effects of rare codon clusters on high-level expression of heterologous proteins in *Escherichia coli*, *Curr Opin Biotechnol* 6, 494-500.
7. Lu, X., Zhang, H., Tonge, P. J., and Tan, D. S. (2008) Mechanism-based inhibitors of MenE, an acyl-CoA synthetase involved in bacterial menaquinone biosynthesis, *Bioorg Med Chem Lett* 18, 5963-5966.
8. Page, M. I., and Jencks, W. P. (1971) Entropic contributions to rate accelerations in enzymic and intramolecular reactions and the chelate effect, *Proc Natl Acad Sci U S A* 68, 1678-1683.
9. Isono, K., Uramoto, M., Kusakabe, H., Miyata, N., Koyama, T., Ubukata, M., Sethi, S. K., and McCloskey, J. A. (1984) Ascamycin and dealanylascamycin, nucleoside antibiotics from *Streptomyces* sp, *J Antibiot (Tokyo)* 37, 670-672.
10. Somu, R. V., Boshoff, H., Qiao, C., Bennett, E. M., Barry, C. E., 3rd, and Aldrich, C. C. (2006) Rationally designed nucleoside antibiotics that inhibit siderophore biosynthesis of *Mycobacterium tuberculosis*, *J Med Chem* 49, 31-34.
11. Ferreras, J. A., Ryu, J. S., Di Lello, F., Tan, D. S., and Quadri, L. E. (2005) Small-molecule inhibition of siderophore biosynthesis in *Mycobacterium tuberculosis* and *Yersinia pestis*, *Nat Chem Biol* 1, 29-32.

12. Arora, P., Goyal, A., Natarajan, V. T., Rajakumara, E., Verma, P., Gupta, R., Yousuf, M., Trivedi, O. A., Mohanty, D., Tyagi, A., Sankaranarayanan, R., and Gokhale, R. S. (2009) Mechanistic and functional insights into fatty acid activation in *Mycobacterium tuberculosis*, *Nat Chem Biol* 5, 166-173.
13. Neres, J., Labello, N. P., Somu, R. V., Boshoff, H. I., Wilson, D. J., Vannada, J., Chen, L., Barry, C. E., 3rd, Bennett, E. M., and Aldrich, C. C. (2008) Inhibition of siderophore biosynthesis in *Mycobacterium tuberculosis* with nucleoside bisubstrate analogues: structure-activity relationships of the nucleobase domain of 5'-O-[N-(salicyl)sulfamoyl]adenosine, *J Med Chem* 51, 5349-5370.
14. Faergeman, N. J., and Knudsen, J. (1997) Role of long-chain fatty acyl-CoA esters in the regulation of metabolism and in cell signalling, *Biochem J* 323 ( Pt 1), 1-12.
15. Fan, F., Luxenburger, A., Painter, G. F., and Blanchard, J. S. (2007) Steady-state and pre-steady-state kinetic analysis of *Mycobacterium smegmatis* cysteine ligase (MshC), *Biochemistry* 46, 11421-11429.
16. Tian, Y., Suk, D. H., Cai, F., Crich, D., and Mesecar, A. D. (2008) *Bacillus anthracis* o-succinylbenzoyl-CoA synthetase: reaction kinetics and a novel inhibitor mimicking its reaction intermediate, *Biochemistry* 47, 12434-12447.
17. Farrar, W. W., and Plowman, K. M. (1979) Kinetics of acetyl-CoA

- synthetase-II. Products inhibition studies, *Int J Biochem* 10, 583-588.
18. Kim, Y. S., and Kang, S. W. (1994) Steady-state kinetics of malonyl-CoA synthetase from *Bradyrhizobium japonicum* and evidence for malonyl-AMP formation in the reaction, *Biochem J* 297 ( Pt 2), 327-333.
  19. Vessey, D. A., and Kelley, M. (2001) Characterization of the reaction mechanism for the XL-I form of bovine liver xenobiotic/medium-chain fatty acid:CoA ligase, *Biochem J* 357, 283-288.
  20. Gupte, A., Boshoff, H. I., Wilson, D. J., Neres, J., Labello, N. P., Somu, R. V., Xing, C., Barry, C. E., and Aldrich, C. C. (2008) Inhibition of siderophore biosynthesis by 2-triazole substituted analogues of 5'-O-[N-(salicyl)sulfamoyl]adenosine: antibacterial nucleosides effective against *Mycobacterium tuberculosis*, *J Med Chem* 51, 7495-7507.
  21. Miethke, M., Bisseret, P., Beckering, C. L., Vignard, D., Eustache, J., and Marahiel, M. A. (2006) Inhibition of aryl acid adenylation domains involved in bacterial siderophore synthesis, *FEBS J* 273, 409-419.
  22. Sikora, A. L., Cahill, S. M., and Blanchard, J. S. (2009) Enterobactin synthetase-catalyzed formation of P(1),P(3)-diadenosine-5'-tetrphosphate, *Biochemistry* 48, 10827-10829.

## Chapter V

1. Ratledge, C. (2004) Iron, mycobacteria and tuberculosis, *Tuberculosis (Edinb)* 84, 110-130.
2. Gobin, J., Moore, C. H., Reeve, J. R., Jr., Wong, D. K., Gibson, B. W., and Horwitz, M. A. (1995) Iron acquisition by *Mycobacterium tuberculosis*: isolation and characterization of a family of iron-binding exochelins, *Proc Natl Acad Sci U S A* 92, 5189-5193.
3. Wong, D. K., Gobin, J., Horwitz, M. A., and Gibson, B. W. (1996) Characterization of exochelins of *Mycobacterium avium*: evidence for saturated and unsaturated and for acid and ester forms, *J Bacteriol* 178, 6394-6398.
4. Gobin, J., and Horwitz, M. A. (1996) Exochelins of *Mycobacterium tuberculosis* remove iron from human iron-binding proteins and donate iron to mycobactins in the *M. tuberculosis* cell wall, *J Exp Med* 183, 1527-1532.
5. Brosch, R., Gordon, S. V., Billault, A., Garnier, T., Eiglmeier, K., Soravito, C., Barrell, B. G., and Cole, S. T. (1998) Use of a *Mycobacterium tuberculosis* H37Rv bacterial artificial chromosome library for genome mapping, sequencing, and comparative genomics, *Infect Immun* 66, 2221-2229.
6. De Voss, J. J., Rutter, K., Schroeder, B. G., and Barry, C. E., 3rd. (1999) Iron acquisition and metabolism by mycobacteria, *J Bacteriol* 181,



4443-4451.

7. Crosa, J. H., and Walsh, C. T. (2002) Genetics and assembly line enzymology of siderophore biosynthesis in bacteria, *Microbiol Mol Biol Rev* 66, 223-249.
8. Liu, J., Quinn, N., Berchtold, G. A., and Walsh, C. T. (1990) Overexpression, purification, and characterization of isochorismate synthase (EntC), the first enzyme involved in the biosynthesis of enterobactin from chorismate, *Biochemistry* 29, 1417-1425.
9. Romero, R. M., Roberts, M. F., and Phillipson, J. D. (1995) Anthranilate synthase in microorganisms and plants, *Phytochemistry* 39, 263-276.
10. Viswanathan, V. K., Green, J. M., and Nichols, B. P. (1995) Kinetic characterization of 4-amino 4-deoxychorismate synthase from *Escherichia coli*, *J Bacteriol* 177, 5918-5923.
11. Davidson, B. E., and Hudson, G. S. (1987) Chorismate mutase-prephenate dehydrogenase from *Escherichia coli*, *Methods Enzymol* 142, 440-450.
12. Spraggon, G., Kim, C., Nguyen-Huu, X., Yee, M. C., Yanofsky, C., and Mills, S. E. (2001) The structures of anthranilate synthase of *Serratia marcescens* crystallized in the presence of (i) its substrates, chorismate and glutamine, and a product, glutamate, and (ii) its end-product inhibitor, L-tryptophan, *Proc Natl Acad Sci U S A* 98, 6021-6026.

13. Parsons, J. F., Jensen, P. Y., Pachikara, A. S., Howard, A. J., Eisenstein, E., and Ladner, J. E. (2002) Structure of *Escherichia coli* aminodeoxychorismate synthase: architectural conservation and diversity in chorismate-utilizing enzymes, *Biochemistry* 41, 2198-2208.
14. Kerbarh, O., Ciulli, A., Howard, N. I., and Abell, C. (2005) Salicylate biosynthesis: overexpression, purification, and characterization of Irp9, a bifunctional salicylate synthase from *Yersinia enterocolitica*, *J Bacteriol* 187, 5061-5066.
15. Kerbarh, O., Chirgadze, D. Y., Blundell, T. L., and Abell, C. (2006) Crystal structures of *Yersinia enterocolitica* salicylate synthase and its complex with the reaction products salicylate and pyruvate, *J Mol Biol* 357, 524-534.
16. Kunzler, D. E., Sasso, S., Gamper, M., Hilvert, D., and Kast, P. (2005) Mechanistic insights into the isochorismate pyruvate lyase activity of the catalytically promiscuous PchB from combinatorial mutagenesis and selection, *J Biol Chem* 280, 32827-32834.
17. Aberhart, D. J., Ghoshal, P. K., Cotting, J. A., and Russell, D. J. (1985) Coenzyme A biosynthesis: steric course of 4'-phosphopantothenoyl-L-cysteine decarboxylase, *Biochemistry* 24, 7178-7182.
18. Cook, A. G., and Knowles, J. R. (1985) Phosphoenolpyruvate synthetase and pyruvate, orthophosphate dikinase: stereochemical

consequences at both the beta-phospho and gamma-phospho groups of ATP, *Biochemistry* 24, 51-58.

19. Guo, H., Cui, Q., Lipscomb, W. N., and Karplus, M. (2001) Substrate conformational transitions in the active site of chorismate mutase: their role in the catalytic mechanism, *Proc Natl Acad Sci U S A* 98, 9032-9037.
20. Kerbarh, O., Campopiano, D. J., and Baxter, R. L. (2006) Mechanism of alpha-oxoamine synthases: identification of the intermediate Claisen product in the 8-amino-7-oxononanoate synthase reaction, *Chem Commun (Camb)*, 60-62.

